COMPUTATIONAL METHODS FOR THE ONE-PARTICLE GREEN'S FUNCTION

W. von NIESSEN

Technische Universität Braunschweig, D-3300 Braunschweig, Fed. Rep. Germany

J. SCHIRMER and L.S. CEDERBAUM

Universität Heidelberg, D-6900 Heidelberg, Fed. Rep. Germany

1984

NORTH-HOLLAND PHYSICS PUBLISHING – AMSTERDAM

Contents

1. Introduction 60
2. The one-particle Green's function 62
2.1. The relation to physical observables 62
2.2. Self-energy and diagrammatic perturbation theory 65
2.3. ADC approximation for the dynamic self-energy 69
2.4. Extended two-particle–hole Tamm–Dancoff approximation 71
2.5. A simple geometric approximation for the outer-valence region 74
3. Computational procedures 76
3.1. SCF-calculations and handling of Coulomb matrix elements 76
3.2. Numerical aspects of the extended 2ph-TDA 80
3.2.1. Diagonalization of the 2p–1h and 2h–1p parts 81
3.2.2. Solution of the Dyson equation 82
3.2.3. Evaluation of the static self-energy part 83
3.3. Numerical aspects of the OVGF method 84
4. The eigenvalue problem for arrow matrices 85
4.1. The one-dimensional case $N = 1$ 86
4.2. The multi-dimensional case $N > 1$ 88
4.3. A pole search algorithm for solving the eigenvalue problem of Hermitian arrow matrices 94
5. Applications 95
5.1. N_2 103
5.2. s-tetrazine 108
5.3. Zinc dichloride 110
5.4. Electron affinities of C_2, P_2, SO_2 and O_3 111
6. Concluding remarks 113
Appendix A. Spin-free working equations of the extended 2ph-TDA 114
Appendix B. A linear equation for the static self-energy part 117
Appendix C. Formulae for the OVGF method including terms up to third order 119
References 122

Computer Physics Reports 1 (1984) 57–125
North-Holland, Amsterdam

COMPUTATIONAL METHODS FOR THE ONE-PARTICLE GREEN'S FUNCTION

W. von NIESSEN

Institut für Physikalische und Theoretische Chemie, Technische Universität Braunschweig, D-3300 Braunschweig, Fed. Rep. Germany

J. SCHIRMER and L.S. CEDERBAUM

Institut für Physikalische Chemie, Universität Heidelberg, D-6900 Heidelberg, Fed. Rep. Germany

Received 30 June 1983; in final form 28 October 1983

A review is given of computational methods for the one-particle Green's function of finite electronic systems. Two distinct approximation schemes are considered which are based on the diagrammatic perturbation expansions of the Green's function **G** and of the self-energy part Σ related to **G** via the Dyson equation. The first scheme referred to as the extended two-particle hole Tamm–Dancoff approximation (extended 2ph-TDA) is derived as an infinite partial summation for Σ and **G** being complete through third-order in the electronic repulsion. The essential numerical problem is the diagonalization of a symmetric matrix defined in the space of a special class of ionic configurations. The structure of this matrix allows for an efficient two-step diagonalization procedure where a special diagonalization algorithm for matrices with an arrow-type structure is employed. The second approximation scheme discussed here is the outer-valence Green's function method (OVGF) based on a finite perturbation expansion of the self-energy part (it is exact to third order in the electronic repulsion and is supplemented by a geometrical approximation to higher orders). The OVGF is much simpler than the extended 2ph-TDA, since no matrices are to be diagonalized. The range of applicability of the OVGF is, however, restricted. For both approximation schemes spin-free formulations of the working equations are presented. Aspects of an optimal implementation in computer codes are discussed. The numerical performance of the methods is demonstrated by application to the ionization spectra and electron affinities of selected molecules.

1. Introduction

Since the first ab initio applications to atoms and molecules over a decade ago, the method of the one-particle Green's function [1–4] and related many-body methods have developed to a viable means of quantum-chemical calculations. The conceptual advantage of these methods over the conventional wave function approach such as the configuration interaction (CI) treatment stems from the fact that relevant physical entities, e.g., ionization energies and transition moments are calculated directly without resorting to separate calculations for the initial ground state and the final (parent) ionic states. Hereby one circumvents from the outset one source of errors, which is immanent to approximations within the wave function approach, namely the possibly unbalanced treatment of ground and ionic states. A further advantage is that the Green's function methods permit sophisticated approximation schemes due to non-trivial combination of perturbation theory and full diagonalization which have no analogue in the wave function approach. Moreover, the Green's function approach leads in a natural way to "size-consistent" approximations which have the correct scaling behaviour with respect to the number of electrons. This may be essential for the treatment of large systems.

The use of the one-particle Green's function and of the related methods in atomic and molecular physics is the subject of several previous review articles [5–8]. For a detailed discussion of the various specific approaches which have been developed and applied so far we refer to these articles and to the references therein. However, a few remarks on the main theoretical developments are in order.

One such development is the diagrammatical approach. Here approximations are based on the use of the well-known perturbation expansions of the one-particle Green's function $\mathbf{G}$ and of the related self-energy part $\mathbf{\Sigma}$ which can be formulated in terms of the Feynman diagrams [1–4]. A previous review on diagrammatical methods aimed at atomic and molecular applications has been given by Cederbaum and Domcke [6]. Another concept is the equation-of-motion approach (EOM) which – originally formulated for the (electronic) excitation problem [9,10] – has been adopted for the treatment of ionization and attachment processes [11–14]. The basic EOM equations appear to be quite different from the one-particle Green's function, since they are formulated in terms of ground-state expectation values of exact excitation operators for $N \pm 1$ particles. There is, however, a close relationship as is apparent from a propagator formalism [15–16] in which the so-called super-operator representation of the one-particle Green's function is approximated by inner-projection techniques. For an overview of these propagator techniques the reader may consult the review article by Öhrn and Born [8]. The theory and applications of the EOM approach are documented in the review article by Herman et al. [7].

The present article reviews two Green's function methods that have developed within the diagrammatic approach namely the outer valence Green's function method (OVGF) [6,17] and the extended two-particle–hole Tamm–Dancoff approximation (extended 2ph-TDA) [18,19]. It is intended to complement and to continue the previous review article by Cederbaum and Domcke [6] in two respects: to present the advances which in the meantime have been achieved in the development of diagrammatic approximation schemes and to give a thorough discussion of the numerical procedures required in the application of these methods. However, the presentation in the present article is largely self-contained and does not presuppose the previous article.

Within the diagrammatic approach one obvious way to obtain an approximation for the

one-particle Green's function is to employ a finite expansion of the self-energy part Σ. The OVGF method is based on the full third-order expansion of Σ and introduces in addition a simple geometrical approximation for higher order contributions. It has been demonstrated by many applications (see table 1 to be discussed below) that the OVGF provides very accurate results for the ionization potentials of the outer valence orbitals and for electron affinities. Owing to the simplicity of the method one may apply this method to large systems without additional approximations. This also applies to the use of large basis sets. The applicability, however, is restricted to the energy range of the outer valence orbitals, where the ionization (attachment) is well described within the quasi-particle picture. In this region the self-energy part is a smooth function of the energy variable and a finite expansion is a good means to approximate Σ. For energy regions where higher excited (shake-up) configurations are important the self-energy part has poles and thus cannot properly be described by any finite expansion.

The correct analytical form is maintained by approximations which represent infinite (though partial) summations of the perturbation series for Σ. Well-known examples are the random phase approximation (RPA) and the ladder summation for the self-energy part (see e.g. Mattuck [3]). In spite of their success in treating infinite fermion systems (electron gas, nuclear matter), these approximations are not always adequate for finite electronic systems [6]. A basic infinite partial summation which combines the contributions of special RPA and ladder diagrams is the 2ph-TDA [6,20]. Although this approximation does not provide very accurate results, it enables a useful qualitative description of the entire valence-shell ionization spectrum and gives, in particular, access to the inner-valence regime, where in general, the single-particle picture of ionization is not adequate. For applications of the 2ph-TDA we refer to table 1 given in section 5.

A simple extension of the 2ph-TDA leads to an infinite partial summation for the self-energy part and the one-particle Green's function which is complete through third order. This extended 2ph-TDA [18,19] represents a distinctly improved approximation scheme combining the virtues of the OVGF and of the previous 2ph-TDA. A closely related third-order approximation has been derived within the EOM approach [11–14]. The systematic derivation of the extended 2ph-TDA follows from a new diagrammatic approach [19,21] which has been termed algebraic diagrammatic construction (ADC). The ADC represents an exact resummation of the perturbation series for e.g., the self-energy part, in terms of a simple algebraic form introducing effective (higher-order) quantities. There exists a unique method for constructing successively the effective terms by comparing the original diagrammatic perturbation series with the perturbation expansion of the ADC form. This defines in a natural way a set of systematic approximation schemes for the self-energy part representing infinite partial summations complete through nth order of perturbation theory. The resulting mathematical procedures involve hermitian eigenvalue problems within a space of physical excitations of $N \pm 1$ particles. Explicit expressions for the first three ADC schemes $n = 2$, 3 and 4 have been presented recently [19]. The case $n = 2$ is trivial and reproduces the second-order approximation for Σ. The third-order scheme (ADC(3)) yields the extended 2ph-TDA which will be considered in this article. The fourth-order ADC scheme will only be mentioned here. Its numerical requirements are considerably higher than those of the extended 2ph-TDA and prevent, at the present stage, application to other than rather small systems.

The essential numerical elements which have to be dealt with in actual applications are the

diagonalization of (in general large) Hermitian matrices and the evaluation of terms which are familiar from perturbation theory. Although, in principle, both tasks represent standard problems in quantum chemical calculations, they appear in modifications which are specific to the Green's function approach and which require special numerical strategies. A thorough presentation and discussion is attempted here of all the numerical steps which are encountered in the computational implementation of the present Green's function methods.

2. The one-particle Green's function

2.1. The relation to physical observables

In this section a brief review is given of the one-particle Green's function and of its relevance in the theoretical description of finite electronic systems. For definiteness we consider a N-electron system with a non-degenerate normalized ground state $|\psi_0^N\rangle$ and energy E_0^N. In the case of a molecule a fixed nuclear geometry is assumed and rotational and vibrational degrees of freedom are suppressed. The (electronic) Hamiltonian of the considered system consists of a one-particle part $\hat{T}$ and of the two-particle (Coulomb) interaction $\hat{V}$. In the notation of second-quantization we may write

$$\hat{H} = \hat{T} + \hat{V} = \sum T_{ij} c_i^\dagger c_j + \tfrac{1}{2} \sum V_{ijkl} c_i^\dagger c_j^\dagger c_l c_k , \tag{2.1}$$

where $c_j^\dagger$ (c_j) denote creation (destruction) operators for the one-particle states $|\varphi_j\rangle$ of a suitably chosen basis, in general, the Hartree–Fock (HF) basis for the ground state. The Coulomb matrix elements in (2.2) are defined according to

$$V_{ijkl} = \langle \varphi_i(1)\varphi_j(2)|V(1,2)|\varphi_k(1)\varphi_l(2)\rangle \tag{2.2}$$

and T_{ij} denote the matrix elements of the one-particle part $\hat{T}$.

In a representation spanned by the one-particle states $|\varphi_j>$ the one-particle Green's function [1] becomes a matrix $\mathbf{G}(t, t')$ with components

$$G_{pq}(t, t') = -\mathrm{i}\langle \psi_0^N | c_p(t) c_q^\dagger(t') | \psi_0^N \rangle \Theta(t - t') + \mathrm{i}\langle \psi_0^N | c_q^\dagger(t') c_p(t) | \psi_0^N \rangle \Theta(t' - t). \tag{2.3}$$

Here

$$c_p(t) = \mathrm{e}^{\mathrm{i}\hat{H}t} c_p \mathrm{e}^{-\mathrm{i}\hat{H}t} \tag{2.4}$$

denotes the Heisenberg representation of c_p and $\Theta(\tau)$ is the Heaviside step function.

For a time-independent Hamiltonian $\mathbf{G}(t, t')$ depends only on the time difference $t - t'$ and we may introduce the Fourier transform of $\mathbf{G}(t, t')$ according to

$$\mathbf{G}(\omega) = \int \mathrm{e}^{\mathrm{i}\omega(t-t')} \mathbf{G}(t, t') \mathrm{d}(t - t'). \tag{2.5}$$

By inserting in (2.3) complete sets of $(N \pm 1)$-particle eigenstates $|\psi_n^{N\pm1}\rangle$ of $\hat{H}$ (with energies $E_n^{N\pm1}$) one arrives at the spectral representation [1] for $\mathbf{G}(\omega)$:

$$G_{pq}(\omega) = \sum_n \frac{\langle\psi_0^N|c_p|\psi_n^{N+1}\rangle\langle\psi_n^{N+1}|c_q^\dagger|\psi_0^N\rangle}{\omega + E_0^N - E_n^{N+1} + i\eta} + \sum_n \frac{\langle\psi_0^N|c_q^\dagger|\psi_n^{N-1}\rangle\langle\psi_n^{N-1}|c_p|\psi_0^N\rangle}{\omega + E_n^{N-1} - E_0^N - i\eta}. \tag{2.6}$$

Here, η is a positive infinitesimal introduced to guarantee the convergence of the Fourier transform (2.5).

The one-particle Green's function contains physical information on the N-particle ground state and the ionic $(N \pm 1)$-particle states. The ground-state expectation value of any one-particle operator

$$\hat{A} = \sum A_{pq} c_p^\dagger c_q \tag{2.7}$$

may be extracted from $\mathbf{G}$ according to the expression [1–4]

$$\langle\psi_0^N|\hat{A}|\psi_0^N\rangle = -i\sum_{p,q} A_{pq} G_{qp}(t, t^+) \tag{2.8a}$$

$$= \sum_{p,q} A_{pq} \frac{1}{2\pi i} \oint G_{qp}(\omega)\mathrm{d}\omega. \tag{2.8b}$$

In (2.8a) the time argument $t' = t^+$ is infinitesimally larger than t, which means that one has to insert the second contribution on the right-hand side of the definition (2.3). The contour integration in (2.8b) must be performed over the upper complex ω-plane and, thus, encloses all poles of $\mathbf{G}$ located above the real axis, i.e., all $(N-1)$-particle poles of the second sum in (2.6). Moreover, also the ground state energy E_0^N can be obtained [1–4] from $\mathbf{G}$:

$$E_0^N = \sum_{p,q} \frac{1}{4\pi i} \oint (\omega\delta_{pq} + T_{pq}) G_{qp}(\omega)\mathrm{d}\omega. \tag{2.9}$$

Here, the contour is as in (2.8b), T_{pq} are the matrix elements of the one-particle part $\hat{T}$ of the Hamiltonian (2.1), and δ_{pq} is the Kronecker symbol. The contour integrations required in (2.8b) and (2.9) are readily performed once the spectral representation of the form (2.6) is available. It should be noted that alternative integration procedures based on modified contour paths have been investigated [22,23].

The physical relevance of the one-particle Green's function is mainly based on its relation to the ionization and electron attachment spectra. As is apparent from the spectral representation (2.6) the (vertical-electronic) ionization energies

$$I_n = E_n^{N-1} - E_0^N \tag{2.10a}$$

and the electron affinities

$$A_n = E_0^N - E_n^{N+1} \tag{2.10b}$$

are given by the negative pole positions in $G_{pq}(\omega)$. The residue corresponding to a pole n

$$Q_{pq}^{(n)} = x_p^{(n)} x_q^{(n)*} \tag{2.11}$$

is given by the product of two transition amplitudes

$$x_p^{(n)} = \begin{cases} \langle \psi_0^N | c_p | \psi_n^{N+1} \rangle & n \in \{N+1\}, \\ \langle \psi_n^{N-1} | c_p | \psi_0^N \rangle & n \in \{N-1\}. \end{cases} \tag{2.12}$$

In the following we show how these amplitudes are related to the spectral intensities of the ionization experiment. Let us consider the case of photoelectron spectroscopy. If the photon energy ω_0 is sufficiently above the threshold for production of ions in the state $|\psi_n^{N-1}\rangle$, then the corresponding partial-channel photoionization cross section is given by the expression [6,24]

$$\sigma_n(\epsilon) = \tfrac{2}{3}\epsilon |\sum_p \tau_{\epsilon p} x_p^{(n)}|^2. \tag{2.13}$$

Here,

$$\tau_{\epsilon p} = \langle \psi_\epsilon | \hat{d} | \varphi_p \rangle \tag{2.14}$$

denotes the matrix-element of the dipole operator $\hat{d}$ taken between the one-particle state $|\varphi_p\rangle$ and the one-particle scattering state $|\psi_\epsilon\rangle$ with kinetic energy $\epsilon = \omega_0 - I_n$. It should be mentioned that the derivation of eq. (2.13) involves two assumptions. First, the N-electron scattering states can be represented in the form (apart from appropriate spin and symmetry coupling)

$$|\psi_{\epsilon,n}^N\rangle = c_\epsilon^\dagger |\psi_n^{N-1}\rangle, \tag{2.15}$$

where $c_\epsilon^\dagger$ denotes the creation operator for the scattering state $|\psi_\epsilon\rangle$. Second, the scattering state $|\psi_\epsilon\rangle$ does not contribute to ground and ionic state correlation, i.e.,

$$c_\epsilon |\psi_0^N\rangle \equiv 0, \quad c_\epsilon |\psi_n^{N-1}\rangle \equiv 0. \tag{2.16}$$

According to eq. (2.13) the calculation of the spectral intensities consists of two separate parts. On one hand, one has to determine the dipole matrix-elements $\tau_{\epsilon p}$ containing the information on the specific scattering process, e.g., the energy dependence of the cross section. The spectroscopic amplitudes $x_p^{(n)}$ of eq. (2.12), on the other hand, depend only on the electronic properties of the (initial) ground state and of the parent ionic state. In general, the sum over orbitals p in eq. (2.13) runs over all (occupied and unoccupied) orbitals. Often, however, to a good approximation only

one term gives a non-vanishing contribution. Then eq. (2.13) simplifies to

$$\sigma_n(\epsilon) = \tfrac{2}{3}\epsilon|\tau_{\epsilon p}|^2|x_p^{(n)}|^2. \tag{2.17a}$$

The pole strength

$$P_n = |x_p^{(n)}|^2 \tag{2.17b}$$

is called the relative intensity, since it provides a measure for the relative intensities of the states n which derive their intensity from the same orbital p (in the sense of eq. (2.17a)). Of course, this supposes that $|\tau_{\epsilon p}|^2$ is only weakly energy-dependent. For a more thorough discussion of the intensity problem the reader is referred to refs. [6,24].

Finally, we mention that the one-particle Green's function also represents an approach to the elastic scattering of electrons off atoms and molecules. For a discussion of this subject we refer to ref. [5]. Recent applications are cited in section 5.

2.2. Self-energy and diagrammatic perturbation theory

The perturbation expansion of the one-particle Green's function $\mathbf{G}(\omega)$ and of the related self-energy part $\mathbf{\Sigma}(\omega)$ introduced below is based on the usual decomposition of the full Hamiltonian $\hat{H}$ into an "unperturbed" diagonal one-particle Hamiltonian $\hat{H}_0$ and a perturbation part $\hat{H}_1$:

$$\begin{aligned} &\hat{H} = \hat{T} + \hat{V} = \hat{H}_0 + \hat{H}_1, \quad \hat{H}_0 = \sum \epsilon_i c_i^\dagger c_i, \\ &\hat{H}_I = \hat{W} + \hat{V} = \sum W_{ij} c_i^\dagger c_j + \tfrac{1}{2}\sum V_{ijkl} c_i^\dagger c_j^\dagger c_l c_k. \end{aligned} \tag{2.18}$$

Here, we use the second-quantized representation based on ground-state Hartree–Fock (HF) one-particle states $|\varphi_j\rangle$, ϵ_i denote HF orbital energies, and W_{ij} denote the matrix elements of the non-diagonal one-particle perturbation contribution $\hat{W}$. In the HF case they are given by

$$W_{ij} = -\sum_k V_{ik[jk]} n_k. \tag{2.19}$$

Here and in the following we use the notation $V_{ij[kl]} = V_{ijkl} - V_{ijlk}$ for the antisymmetrized Coulomb matrix elements, and $n_k = 1 - \bar{n}_k$ denote orbital occupation numbers in the N-electron HF ground state $|\phi_0^N\rangle$. The choice $\hat{H}_0 = \hat{H}_{\mathrm{HF}}$ reduces considerably the number of terms in the perturbation series of $\mathbf{G}$ and $\mathbf{\Sigma}$. The formulation for a general unperturbed part $\hat{H}_0$ is more lengthy, but a straightforward extension of the HF case.The one-particle Green's function $\mathbf{G}(\omega)$ is related to the self-energy part $\mathbf{\Sigma}(\omega)$ by the Dyson equation [1]

$$\mathbf{G}(\omega) = \mathbf{G}^0(\omega) + \mathbf{G}^0(\omega)\mathbf{\Sigma}(\omega)\mathbf{G}(\omega) \tag{2.20}$$

allowing for the (formal) solution

$$\mathbf{G}(\omega) = \left[\mathbf{G}^0(\omega)^{-1} - \mathbf{\Sigma}(\omega)\right]^{-1}. \tag{2.21}$$

The "free" Green's function $\mathbf{G}^0(\omega)$ introduced here is given by

$$G^{(0)}_{pq}(\omega) = \delta_{pq}\left(\frac{n_p}{\omega - \epsilon_p - i\eta} + \frac{\bar{n}_p}{\omega - \epsilon_p + i\eta}\right). \tag{2.22}$$

This expression results from the definition (2.3) and (2.5) in the unperturbed case $\hat{H} - \hat{H}_0$. The self-energy part $\Sigma(\omega)$ can be expanded in a well-defined perturbation series in terms of Feynmann diagrams which is simpler than the one for $\mathbf{G}(\omega)$. The rules for drawing and evaluating these diagrams are found in several textbooks [1–4] and review articles [6]. We confine ourselves to a few remarks which are intended to clarify the notions used in the following. A nth order Feynman diagram for $\Sigma(\omega)$ has two outer and $n-2$ inner vertices (wiggly lines) representing Coulomb matrix elements and $2n-1$ straight G^0-lines. A more compact notation is obtained by combining the wiggly lines for the direct and exchange matrix elements to a dot. This is referred to as the Abrikosov or Hugenholtz [1,86] notation. Each nth order Feynman diagram requires $n-2$ integrations over internal energy variables (or time variables). The results of these integrations can directly be evaluated by special rules concerning the $n!$ time orderings (or Goldstone diagrams) which are generated by each Feynman diagram. The second- and third-order Goldstone diagrams for $\Sigma(\omega)$ in Abrikosov notation are shown in figs. 1 and 2, respectively.

Several important properties of the self-energy part $\Sigma(\omega)$ can be derived either by an inspection of the diagrammatic representation or by resorting to exact relations which relate Σ to higher Green's functions [25,26]. The self-energy $\Sigma(\omega)$ can be written as a sum of a static (ω-independent) part $\Sigma(\infty)$ considered further below and a dynamic (ω-dependent) part $\mathbf{M}(\omega)$

$$\Sigma(\omega) = \Sigma(\infty) + \mathbf{M}(\omega). \tag{2.23}$$

The dynamic part has a spectral representation

$$M_{pq}(\omega) = \sum_n \frac{m_p^{(n)} m_q^{(n)*}}{\omega - \omega_n + i\eta\sigma_n} \tag{2.24}$$

similar to the one of $\mathbf{G}(\omega)$. According to $\sigma_n = \pm 1$ the poles of $\mathbf{M}(\omega)$ are located in the lower ($\sigma_n = +1$) or upper ($\sigma_n = -1$) complex ω plane. Thus the dynamic self-energy part $\mathbf{M}(\omega)$ can be written as a sum

$$\mathbf{M}(\omega) = \mathbf{M}^{\mathrm{I}}(\omega) + \mathbf{M}^{\mathrm{II}}(\omega) \tag{2.25}$$

of two parts I and II being analytic in the upper and lower complex ω plane, respectively. Physically these parts are associated with excitations of $N+1$ (I) and of $N-1$ particles (II), respectively. In general, the energies ω_n do not yet correspond to energies of physical states. These result from the coupling to the space of one-particle (1p) and one-hole (1h) configurations via the Dyson equation.

The decomposition of $\mathbf{M}(\omega)$ into the parts I and II is directly reflected in the diagrammatic perturbation expansion. The $n!$ Goldstone diagrams for a given nth-order Feynman diagram can be divided into two distinct classes according to the time ordering $t > t'$ and $t < t'$ of the external

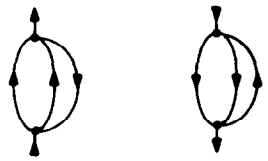

Fig. 1. Second order time-ordered (Goldstone) diagrams for the self-energy part $\mathbf{M}(\omega)$.

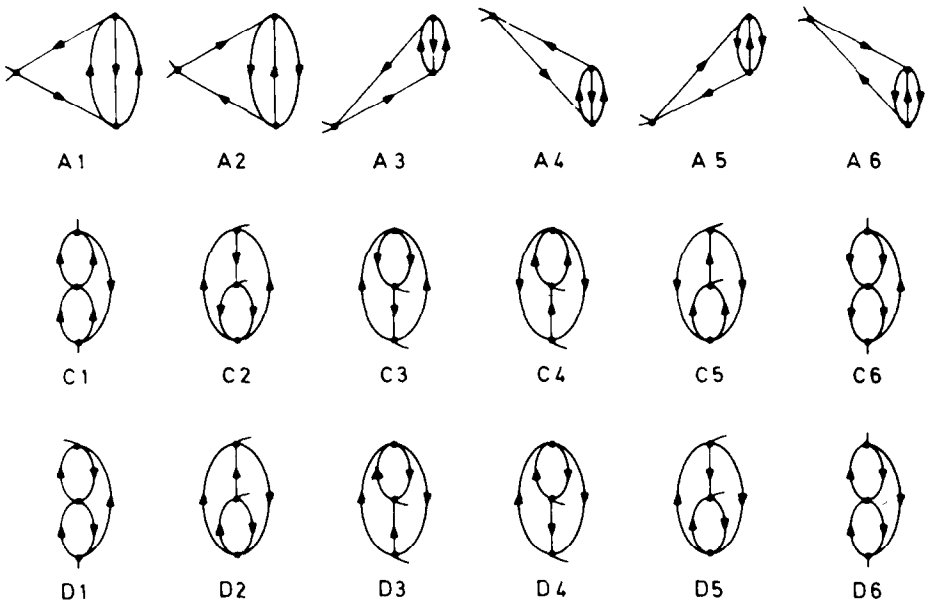

Fig. 2. Time-ordered (Goldstone) diagrams in third order. The diagrams C1 to C3 and D1 to D3 contribute to $\mathbf{M}^{\mathrm{I}}(\omega)$, C4 to C6 and D4 to D6 to $\mathbf{M}^{\mathrm{II}}(\omega)$ and A1 to A6 are the diagrams of the static self-energy part.

vertices. The first class ($t > t'$) contributes exclusively to $\mathbf{M}^{\mathrm{I}}(\omega)$, whereas the second class ($t < t'$) contributes to $\mathbf{M}^{\mathrm{II}}(\omega)$ only. There are no mixed terms and $\mathbf{M}^{\mathrm{I}}(\omega)$ and $\mathbf{M}^{\mathrm{II}}(\omega)$ may be calculated separately from their respective diagrammatic expansions.

The static self-energy part $\Sigma(\infty)$ can be expressed by the one-particle Green's function according to [6,25,26]

$$\Sigma_{pq}(\infty) = \sum_{k,l} V_{pk[ql]} \left\{ -\delta_{kl} n_k + \frac{1}{2\pi \mathrm{i}} \oint G_{lk}(\omega) \mathrm{d}\omega \right\}. \tag{2.26}$$

Here, the contour integration is closed in the upper complex plane. Thus,

$$\frac{1}{2\pi \mathrm{i}} \oint G_{lk}(\omega) \mathrm{d}\omega = \sum_{n \in \{N-1\}} x_l^{(n)} x_k^{(n)*}, \tag{2.27}$$

where the summation is over all $(N-1)$-particle states n. Replacing $\mathbf{G}(\omega)$ in eq. (2.26) with the

right-hand side of eq. (2.21) one obtains the implicit equation

$$\Sigma_{pq}(\epsilon) = \sum_{k,l} V_{pk[ql]} \left\{ -\delta_{kl} n_k + \frac{1}{2\pi i} \oint \left(\mathbf{G}^0(\omega)^{-1} - \Sigma(\infty) - \mathbf{M}(\omega) \right)^{-1}_{lk} d\omega \right. \tag{2.28}$$

by which the static part $\Sigma(\infty)$ can be determined self-consistently when $\mathbf{M}(\omega)$ or an approximation for it is given. As a consequence of eq. (2.28) and of the Dyson equation (2.21) the calculation of $\mathbf{G}(\omega)$ can be reduced to the problem of calculating the dynamic self-energy part $\mathbf{M}(\omega)$. The evaluation of the contour integration according to (2.27) requires the knowledge of all cationic residues. Alternatively, one may attempt a direct numerical evaluation along a modified contour path [22,23].

Instead of the iterative procedure suggested by eq. (2.28) one obtains a direct determination of $\Sigma(\infty)$ by inserting the expansion

$$\mathbf{G} = \mathbf{G}^0 + \mathbf{G}^0 \Sigma(\omega) \mathbf{G}^0 + \ldots \tag{2.29}$$

on the right-hand side of eq. (2.26). Retaining the first two terms of this expansion for $\mathbf{G}$, eq. (2.26) becomes

$$\Sigma_{pq}(\infty) = \sum_{k,l} V_{pk[ql]} \frac{1}{2\pi i} \oint d\omega \, G^0_{ll}(\omega) \left(\Sigma_{lk}(\infty) + M_{lk}(\omega) \right) G^0_{kk}(\omega). \tag{2.30}$$

For a given dynamic self-energy part $\mathbf{M}(\omega)$ the contour integration in eq. (2.30) can be performed yielding a linear equation for the components $\Sigma_{pq}(\infty)$ of the static self-energy part. The error introduced by the truncation of the expansion (2.29) is at least of fifth order and, as a consequence, $\Sigma(\infty)$ is obtained complete through fourth order, if the dynamic self-energy part $\mathbf{M}(\omega)$ of the extended 2ph-TDA (ADC(3)) is employed. In general, one obtains by eq. (2.30) an excellent approximation to the fully iterated result of eq. (2.28). In appendix B the explicit linear equations resulting from eq. (2.30) are presented.

The representation of the self-energy according to eqs. (2.23)–(2.25) allows to reformulate the Dyson equation (2.21) as the diagonalization problem

$$\mathbf{AX} = \mathbf{XE}, \quad \mathbf{XX}^\dagger = 1, \tag{2.31a}$$

$$\mathbf{A} = \begin{pmatrix} \epsilon + \Sigma(\infty) & \mathbf{m}^{\mathrm{I}} & \mathbf{m}^{\mathrm{II}} \\ (\mathbf{m}^{\mathrm{I}})^\dagger & \Omega^{\mathrm{I}} & \mathbf{0} \\ (\mathbf{m}^{\mathrm{II}})^\dagger & \mathbf{0} & \Omega^{\mathrm{II}} \end{pmatrix}. \tag{2.31b}$$

Here ϵ denotes the diagonal matrix of one-particle energies, $\Omega^{\mathrm{I,II}}$ are the diagonal matrices of the energies ω_n of $\mathbf{M}^{\mathrm{I,II}}(\omega)$ and $\mathbf{m}^{\mathrm{I,II}}$ are the corresponding matrices of the coupling (Dyson) amplitudes $m_p^{(n)}$. The one-particle Green's function is obtained as

$$G_{pq}(\omega) = \sum_n x_p^{(n)} x_q^{(n)*} / (\omega - e_n) \tag{2.32}$$

in terms of the eigenvalues $e_n = E_{nn}$ and the corresponding eigenvector components $x_p^{(n)} = X_{pn}$. In these algebraic equations (devised for a finite discrete basis) the infinitesimal $\pm i\eta$ is unessential and has been dropped. For numerical applications it is advantageous to resort to the original form (2.21) of the Dyson equation and to use the special algorithm described in section 4. We finally mention the sum rules

$$\sum_n x_p^{(n)} x_q^{(n)*} = \delta_{pq}, \tag{2.33}$$

$$\sum_n e_n x_p^{(n)} x_q^{(n)*} = \epsilon_p \delta_{pq} + \Sigma_{pq}(\infty) \tag{2.34}$$

which are readily derived from the eigenvalue problem (2.31). Here the summation runs over all cationic and anionic states n.

2.3. ADC approximation for the dynamic self-energy part

As is discussed further below (section 2.5), a finite expansion of the self-energy part, say to third-order, may provide a good approximation in special cases. In general, however, one has to resort to approximations that are derived as infinite partial summations of the perturbation series. A general construction scheme referred to as algebraic diagrammatic construction (ADC) has been presented recently [19]. This scheme is designed to derive systematically infinite partial summations for $\mathbf{M}(\omega)$ complete through a finite (nth) order of perturbation theory. In the following we present the essentials of the ADC concept and discuss the second- and third-order ADC equations. A more comprehensive discussion of the ADC approach and the derivation of the complete fourth order equations is given in ref. [19].

The basic point of the ADC is that the exact self-energy parts $\mathbf{M}^{\mathrm{I}}(\omega)$ and $\mathbf{M}^{\mathrm{II}}(\omega)$ can be obtained by the simple algebraic form

$$M_{pq}(\omega) = \mathbf{U}_p^{\dagger}(\omega\mathbf{1} - \mathbf{K} - \mathbf{C})^{-1}\mathbf{U}_q. \tag{2.35}$$

For notational brevity the superscripts I, II are omitted whenever they are unessential. In eq. (2.35) $\mathbf{U}_p$ denotes a constant (ω-independent) vector of modified (effective) coupling amplitudes for the orbital p and $\mathbf{K}$ and $\mathbf{C}$ are constant, Hermitian matrices, the latter being referred to as the matrix of modified (effective) interaction. The configuration space for these matrices is given by the physical excitations of $N \pm 1$ particles excluding the 1h and 1p configurations. More precisely, the configuration space for the $N+1$ particle case $\mathbf{M}^{\mathrm{I}}(\omega)$ is given by the 2p–1h, 3p–2h,..., configurations (with respect to the HF ground state $|\phi_0^N\rangle$), whereas the 2h–1p, 3h–2p,... excitations are required in the $(N-1)$-particle case $\mathbf{M}^{\mathrm{II}}(\omega)$.

The effective quantities $\mathbf{U}_p$ and $\mathbf{C}$ are determined by perturbation expansions

$$\mathbf{U}_p = \mathbf{U}_p^{(1)} + \mathbf{U}_p^{(2)} + \ldots, \tag{2.36a}$$

$$\mathbf{C} = \mathbf{C}^{(1)} + \mathbf{C}^{(2)} + \ldots, \tag{2.36b}$$

each series starting with a first-order contribution. The matrix **K** is the diagonal matrix of the zeroth-order (HF) excitation energies, e.g.,

$$\begin{aligned} K_{jkl,jkl} &= -\epsilon_j + \epsilon_k + \epsilon_l, \quad n_j \bar{n}_k \bar{n}_l = 1, \\ K_{ijklm,ijklm} &= -\epsilon_i - \epsilon_j + \epsilon_k + \epsilon_l + \epsilon_m, \quad n_i n_j \bar{n}_k \bar{n}_l \bar{n}_m = 1, \end{aligned} \tag{2.37}$$

for the 2p–1h and 3p–2h space, respectively.

Now a well-defined approximation $\mathbf{M}(\omega; n)$ is obtained which is complete to nth order of perturbation theory, $n = 2, 3, \ldots$, by comparing the ADC form

$$M_{pq}(\omega; n) = \mathbf{U}_p^\dagger(n)(\omega \mathbf{1} - \mathbf{K} - \mathbf{C}(n))^{-1} \mathbf{U}_q(n) \tag{2.38}$$

with the (diagrammatic) perturbation series up to nth order and by requiring that $M_{pq}(\omega; n)$ is exact up to nth order:

$$M_{pq}(\omega; n) = \sum_{\nu=2}^{n} M_{pq}^{(\nu)}(\omega) + \mathcal{O}(n+1). \tag{2.39}$$

It is demonstrated in ref. [19] that this requirement enables a unique construction of the quantities $\mathbf{U}_p(n)$ and $\mathbf{C}(n)$ in the nth order ADC form.

The required configuration space in the nth order scheme depends on the order n. For $n = 2$ and 3 the space is restricted to 2p–1h and 2h–1p configurations in the case I and II, respectively. At each even order the space has to be increased by the next higher class of excitations, e.g., by 3p–2h (I) and 3h–2p (II) excitations for $n = 4$ and 5.

For given ADC expression for $\mathbf{U}_p$ and $\mathbf{C}$ the matrix inversion problem of eq. (2.35) can be solved in form of the eigenvalue problem

$$(\mathbf{K} + \mathbf{C})\mathbf{Y} = \mathbf{Y}\Omega, \quad \mathbf{Y}\mathbf{Y}^\dagger = \mathbf{1}, \tag{2.40}$$

where Ω and $\mathbf{Y}$ denote the diagonal matrix of eigenvalues and the eigenvector matrix, respectively. The eigenvalues represent the poles of the self-energy parts $\mathbf{M}^{\mathrm{I,II}}(\omega)$ and the corresponding Dyson amplitudes are obtained according to

$$m_p^{(\nu)} = \mathbf{U}_p^\dagger Y^{(\nu)}, \tag{2.41}$$

where $Y^{(\nu)}$ denotes the νth eigenvector. In the next step the Dyson equation can be solved either by resorting to the form (2.21) or by the diagonalization according to eq. (2.31). Obviously, the latter is equivalent to the following diagonalization problem

$$\mathbf{B}\mathbf{X}' = \mathbf{X}'\mathbf{E}, \quad \mathbf{X}'\mathbf{X}'^\dagger = \mathbf{1}, \tag{2.42a}$$

$$\mathbf{B} = \begin{pmatrix} \epsilon + \Sigma(\infty) & (\mathbf{U}^{\mathrm{I}})^\dagger & (\mathbf{U}^{\mathrm{II}})^\dagger \\ \mathbf{U}^{\mathrm{I}} & \mathbf{K}^{\mathrm{I}} + \mathbf{C}^{\mathrm{I}} & \mathbf{0} \\ \mathbf{U}^{\mathrm{II}} & \mathbf{0} & \mathbf{K}^{\mathrm{II}} + \mathbf{C}^{\mathrm{II}} \end{pmatrix}. \tag{2.42b}$$

The Green's function is again given in the form (2.32) where $e_n = E_{nn}$ and $x_p^{(n)} = X'_{pn}$. By arranging the submatrices of **B** in the order 1p, 1h, 2p–1h, 2h–1p, 3p–2h,... one obtains a structure shown in fig. 3.

2.4. Extended two-particle–hole Tamm–Dancoff approximation

Following the general ADC concept presented above we now construct explicitly the effective coupling amplitudes $\mathbf{U}_p$ and the effective interaction matrices **C** for the second- and third-order schemes.

The second-order contribution to the self-energy part $\mathbf{M}^{\mathrm{I}}(\omega)$ represented by the diagram (1) in fig. 1 reads

$$M_{pq}^{\mathrm{I}(2)}(\omega) = \sum_{j,k<l} \frac{V_{pj[kl]} V^*_{qj[kl]}}{\omega + \epsilon_j - \epsilon_k - \epsilon_l} n_j \bar{n}_k \bar{n}_l . \tag{2.43}$$

Obviously, this expression has the form (2.35) where (case I)

$$U^{\mathrm{I}}_{p,jkl} = U^{(1)}_{p,jkl} = V^*_{pj[kl]}, \tag{2.44a}$$

$$K^{\mathrm{I}}_{jkl,j'k'l'} = (-\epsilon_j + \epsilon_k + \epsilon_l)\delta_{jj'}\delta_{kk'}\delta_{ll'}, \tag{2.44b}$$

$$C^{\mathrm{I}}_{jkl,j'k'l'} = 0. \tag{2.44c}$$

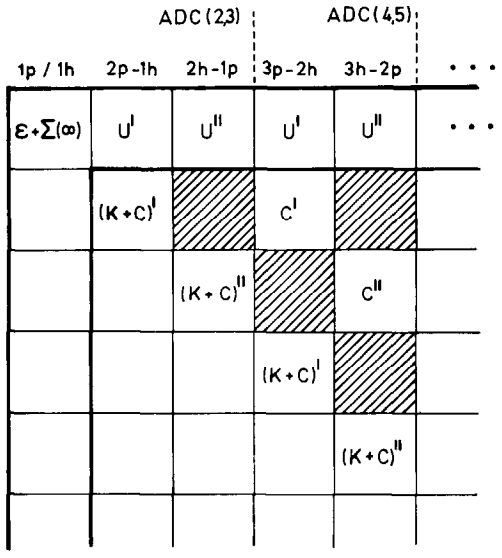

Fig. 3. Structure of the eigenvalue problem (eq. (2.42)) for the one-particle Green's function in the ADC approach.

The configuration space is spanned by the 2p–1h excitations

$$\text{I: } (j,k,l), \quad n_j \bar{n}_k \bar{n}_l = 1, \quad k < l. \tag{2.45a}$$

For the case II the expressions for $\mathbf{K}$, $\mathbf{U}_p$ and $\mathbf{C}$ are formally identical; however, the configuration space is defined by all 2h–1p excitations

$$\text{II: } (j,k,l), \quad \bar{n}_j n_k n_l = 1, \quad k < l. \tag{2.45b}$$

We note that in the strict second-order ADC scheme given by eqs. (2.35), (2.44) and (2.45) the effective interaction matrix $\mathbf{C}$ vanishes and the resulting approximation for $\mathbf{M}(\omega)$ is just the (trivial) second-order contribution (2.43). A simple extension can be obtained by employing the first-order expression for $\mathbf{C}$ which, strictly speaking, is only derived within the third-order scheme considered below:

$$C_{jkl,j'k'l'} = C^{(1)}_{jkl,j'k'l'} \quad \text{case I}, \tag{2.46a}$$

$$C_{jkl,j'k'l'} = -C^{(1)}_{jkl,j'k'l'} \quad \text{case II}, \tag{2.46b}$$

where

$$C^{(1)}_{jkl,j'k'l'} = \delta_{jj'} V_{kl[k'l']} - (\delta_{kk'} V_{j'l[jl']} + \delta_{ll'} V_{j'k[jk']}) + (k' \leftrightarrow l'). \tag{2.46c}$$

The resulting approximation scheme for $\mathbf{M}(\omega)$ is readily identified as the two-particle–hole Tamm–Dancoff approximation (2ph-TDA) [6,20]. Obviously, the 2ph-TDA represents an infinite summation for $\mathbf{M}(\omega)$ which is consistent through second order, but incomplete in third and higher orders of perturbation theory.

A consistent third-order approximation is the third-order (ADC(3)) scheme also referred to as extended 2ph-TDA [18,19]. In order to derive the corresponding effective matrix elements of $\mathbf{U}_p(3)$ and $\mathbf{C}(3)$ we expand the algebraic form (2.38) to third order:

$$\begin{aligned} M_{pq}(\omega;3) = {} & \mathbf{U}_p^{(1)\dagger}(\omega\mathbf{1}-\mathbf{K})^{-1}\mathbf{U}_q^{(1)} + \mathbf{U}_p^{(2)\dagger}(\omega\mathbf{1}-\mathbf{K})^{-1}\mathbf{U}_q^{(1)} + \mathbf{U}_p^{(1)\dagger}(\omega\mathbf{1}-\mathbf{K})^{-1}\mathbf{U}_q^{(2)} \\ & + \mathbf{U}_p^{(1)\dagger}(\omega\mathbf{1}-\mathbf{K})^{-1}\mathbf{C}^{(1)}(\omega\mathbf{1}-\mathbf{K})^{-1}\mathbf{U}_q^{(1)} + \mathcal{O}(4). \end{aligned} \tag{2.47}$$

This expansion starts with the second-order contribution which has already been considered. Since $\mathbf{U}_p$ is at least of first order, the three third-order contributions on the right-hand side of (2.47) involve the new factors $\mathbf{U}_p^{(2)}$ and $\mathbf{C}^{(1)}$ which are of the second and first order, respectively. These quantities have to be determined by comparison with the third-order contribution in the diagrammatic perturbation expansion for $\mathbf{M}^{\mathrm{I}}(\omega)$ ($\mathbf{M}^{\mathrm{II}}(\omega)$). In fig. 2 the third-order diagrams (C1, C2, C3, D1, D2, D3) contributing to $\mathbf{M}^{\mathrm{I}}(\omega)$ are shown. The corresponding analytical expressions have been given elsewhere [6]. They are also given in appendix C. The diagrams C1, D1 are readily identified with the last third-order term of (2.47). Hereby $\mathbf{C}^{(1)}$ can be determined. The diagrams C3, D3 and C2, D2 correspond to the first and second third-order term in (2.47). Thus,

we can evaluate $\mathbf{U}_p^{(2)}$. The resulting expressions for case I read

$$U^{\mathrm{I}}_{p,jkl} = U^{(1)}_{p,jkl} + U^{(2)}_{p,jkl}, \tag{2.48a}$$

$$U^{(2)}_{p,jkl} = -\tfrac{1}{2}\sum_{u,v}\frac{V_{kl[uv]}}{\epsilon_k+\epsilon_l-\epsilon_u-\epsilon_v}V^*_{pj[uv]}n_u n_v + \left(\sum_{r,v}\frac{V_{kr[vj]}}{\epsilon_k+\epsilon_r-\epsilon_v-\epsilon_j}V^*_{pr[vl]}\bar{n}_r n_v\right) - (k\leftrightarrow l), \tag{2.48b}$$

$$C^{\mathrm{I}}_{jkl,j'k'l'} = C^{(1)}_{jkl,j'k'l'}. \tag{2.48c}$$

Here, $U^{(1)}_{p,jkl}$ and $C^{(1)}_{jkl,j'k'l'}$ are given by eqs. (2.44a) and (2.46), respectively. The configuration space is defined by (2.45a). For the case of $\mathbf{M}^{\mathrm{II}}(\omega)$ the configuration space is defined by (2.45b) and the results are

$$U^{\mathrm{II}}_{p,jkl} = U^{(1)}_{p,jkl} - \bar{U}^{(2)}_{p,jkl}, \tag{2.49a}$$

$$\bar{U}^{(2)}_{p,jkl} = -\tfrac{1}{2}\sum_{u,v}\frac{V_{kl[uv]}V^*_{pj[uv]}}{\epsilon_k+\epsilon_l-\epsilon_u-\epsilon_v}\bar{n}_u\bar{n}_v + \left(\sum_{r,v}\frac{V_{kr[vj]}V^*_{pr[vl]}}{\epsilon_k+\epsilon_r-\epsilon_v-\epsilon_j}n_r\bar{n}_v\right) - (k\leftrightarrow l), \tag{2.49b}$$

$$C^{\mathrm{II}}_{jkl,j'k'l'} = -C^{(1)}_{jkl,j'k'l'}, \tag{2.49c}$$

where $U^{(1)}_{p,jkl}$ and $C^{(1)}_{jkl,j'k'l'}$ are (formally) given by eqs. (2.44a) and (2.46).

The algebraic form of eq. (2.35) implemented with the effective coupling amplitudes $\mathbf{U}_p$ and the effective interaction matrix $\mathbf{C}$ as given by eqs. (2.48) and (2.49) constitutes the third-order ADC approximation (ADC(3)) for the dynamic self-energy part $\mathbf{M}(\omega)$. Via the Dyson equation (2.21) and eq. (2.26) one obtains the ADC(3) approximation for the one-particle Green's function $\mathbf{G}(\omega)$, also referred to as extended 2ph-TDA (see refs. [18,19]). It should be noted that closely related third-order equations have been derived within the equation-of-motion (EOM) approach [11–14].

The ADC schemes reflect the symmetry properties of the Hamiltonian. For a spin-independent Hamiltonian one easily arrives at a spin-free formulation of the ADC equations. In appendix A we present the spin-free working equations for the extended 2ph-TDA (ADC(3)) approximation. A formulation exploiting the full rotation symmetry in the atomic case has been given elsewhere [18].

In the extended 2ph-TDA (ADC(3)) the ionization energies, electron attachment energies, and the transition amplitudes of the ionic main states are treated consistently through third order. Within a wave function approach the consistency requires the consideration of 2p–2h double excitations for the ground state and of 1h (1p), 2h–1p (2p–1h) and 3h–2p (3p–2h) excitations for the ionic states on the other hand. The explicit space employed in the extended 2ph-TDA is spanned by the 1h and 2h–1p excitations of $N-1$ particles and by the 1p and 2p–1h excitations of $N+1$ particles. This shows that in the Green's function approach both the ground-state

correlation and the higher ionic excitations (here 3h–2p (or 3p–2h) excitations) are implicitly taken into account by means of the coupling of the $(N-1)$- and $(N+1)$-particle spaces in the Dyson equation and by the use of higher-order (effective) coupling amplitudes $\mathbf{U}_p$. The extended 2ph-TDA also calculates explicitly the higher excited (2h–1p, 2p–1h) ionic states. Their energies and transition amplitudes are treated consistently through first and second order, respectively.

2.5. *A simple geometric approximation for the outer-valence region*

In the preceding sections we have discussed a systematic scheme (ADC scheme) to determine the ionization potentials and electron affinities of an atom or molecule. The ADC scheme includes an infinite partial summation of Feynman diagrams and is exact through nth order perturbation theory. The $n=2$ (2ph-TDA) and $n=3$ (extended 2ph-TDA) schemes have been given explicitly, the $n=4$ scheme is discussed in detail elsewhere [19]. The 2ph-TDA and its extended version aim at the calculation of all (valence) ionization potentials and electron affinities. For this purpose large matrices have to be diagonalized. The computational details of these methods are given in section 4.

In many cases we are not interested in the whole valence ionization spectrum, but rather in the first few ionization potentials of the system. The assignment of the ionization potentials of these outer-valence electrons of a molecule is essential for interpreting its photoelectron spectrum. The outer-valence ionization potentials are characteristic of the molecule and provide direct information about the chemical bonding. However, several of the outer-valence ionization potentials fall into a narrow energy range, making their assignment a severe theoretical problem. It is thus desirable to have a relatively simple method for their accurate calculation. If we restrict ourselves to the evaluation of the Green's function in the outer-valence region of closed-shell atoms and molecules, we may take advantage of the fact that usually no poles of the self-energy part $\mathbf{\Sigma}(\omega)$ lie in the energy (ω) range of the outer-valence electrons. Consequently, $\mathbf{\Sigma}(\omega)$ will be a smooth function with a small slope $(\partial\mathbf{\Sigma}/\partial\omega \leq 0.1)$ in the neighbourhood of the outer-valence ionization potentials. This simplifies the calculation considerably, especially because it is not necessary to calculate the poles of $\mathbf{\Sigma}(\omega)$ accurately.

In the following we discuss a simple method to calculate the outer-valence ionization potentials (and electron affinities), the OVGF method. Since this method has been investigated elsewhere in detail [6,17,27], we discuss it here only briefly. It should be mentioned that his method has been successful in the calculation of the outer-valence ionization potentials of more than 250 molecules [28,29].

In the OVGF method it is assumed that the Green's function is diagonal for those orbital indices which characterize outer-valence electrons and for ω-values which are far away from poles of the self-energy

$$G_{pq}(\omega) \approx G_{pp}(\omega)\delta_{pq}. \tag{2.50}$$

This central assumption can easily be checked, e.g., by carrying out a fast second order or 2ph-TDA calculation using a small basis set. For nearly all molecules we have calculated the approximation (2.50) has been found to be very satisfactory. Since $\mathbf{G}$ is diagonal, the self-energy

$\mathbf{\Sigma}(\omega)$ is also diagonal. The energy dependent part of the self-energy can be written as

$$M_{pp}(\omega) = \sum_n |m_p^{(n)}|^2/(\omega - \omega_n). \tag{2.51}$$

where the superscripts I and II in eq. (2.25) have been omitted for brevity. In the (extended) 2ph-TDA all poles ω_n develop from poles of the second-order self-energy $M^{(2)}(\omega)$. We may, therefore, write

$$M_{pp}(\omega) = \sum_n |m_{pn}^{(2)}|^2 (1 - A_{pn})/(\omega - \omega_n^{(0)} - x_n), \tag{2.52}$$

where $\omega_n^{(0)}$ is a pole of the second-order self-energy, i.e. it is just a linear combination of three orbital energies, and $|m_{pn}^{(2)}|^2$ is the second-order residue of this pole. (Here we write m_{pn} for the terms $m_p^{(n)}$ of eq. (2.24).) The quantities x_n and A_{pn} are defined such that their inclusion in eq. (2.52) reproduces the self-energy in eq. (2.51). The corrections x_n and A_{pn} are assumed to be small, or more precisely:

$$|A_{pn}| < 1, \quad |x_n/(\epsilon_p - \omega_n^{(0)})| < 1. \tag{2.53}$$

We may now expand $M_{pp}(\omega)$

$$M_{pp}(\omega) = \sum_n \frac{|m_{pn}^{(2)}|^2}{\omega - \omega_n^{(0)}} \left\{1 + \frac{x_n}{\omega - \omega_n^{(0)}} + \ldots\right\} - \sum_n \frac{A_{pn}|m_{pn}^{(2)}|^2}{\omega - \omega_n^{(0)}} \left\{1 + \frac{x_n}{\omega - \omega_n^{(0)}} + \ldots\right\}. \tag{2.54}$$

Each term appearing in this expansion can be assigned to groups of distinct diagrams [6,17]. We define an average quantity A_p by

$$A_p \sum_n \frac{|m_{pn}^{(2)}|^2}{\omega - \omega_n^{(0)} - x_n} = \sum_n \frac{A_{pn}|m_{pn}^{(2)}|^2}{\omega - \omega_n^{(0)} - x_n}. \tag{2.55}$$

A_p actually depends on ω, but due to the fact that we are interested here in energies ω far away from the poles of the self-energy we may consider A_p to be a constant for $\omega \approx \epsilon_p$ (ϵ_p is the orbital energy of the orbital in question). To lowest order A (the index p is dropped for simplicity) is determined by

$$A = -\sum_{I=2}^{5} (CI + DI)/M^{(2)}, \tag{2.56}$$

where the diagrams C2 to D5 of third order are shown in fig. 2. The analysis of terms in eq. (2.54) leads to our final result

$$\Sigma(\omega) \approx \Sigma^{(2)}(\omega) + (1 + A)^{-1}\Sigma^{(3)}(\omega) \tag{2.57}$$

which constitutes the OVGF self-energy part. From eq. (2.53) we find that the "screening parameter" A should be smaller than 1. It may happen, however, that the self-energy part in second order is very small leading to a too large value of A (see eq. (2.56)). We encounter such situations, e.g. in those rare cases where Koopmans' theorem accidentally leads to excellent results. We may overcome the difficulty by dividing the self-energy into its two natural terms, $\mathbf{M}^{\mathrm{I}}$ and $\mathbf{M}^{\mathrm{II}}$, and repeat the above analysis for these individual terms by defining two screening parameters. These screening parameters then enter an expression similar to the one in eq. (2.57) (for more details see ref. [17]). In the extreme situation where $\Sigma^{(2)}(\omega)$ nearly vanishes eq. (2.57) is again the final result, but the parameter A has to be defined somewhat differently (for more details see ref. [6]). The formulae for all three possibilities are given in appendix C.

As already mentioned, the simple formula (2.57) leads to surprisingly good results. It involves the calculation of the second- and third-order terms of the self-energy part only. Consequently, the OVGF method is a very practical and easy to handle method: no matrices have to be diagonalized and extended basis sets can be used. As is usually the case with practical methods, the OVGF method has some obvious shortcomings: It can only be applied to outer-valence electrons (see also next section) and – in contrast to the 2ph-TDA method – it is difficult to improve systematically by an extension to next (fourth) order. Here we should mention that the OVGF method is exact up to third order and the "renormalization" procedure we have introduced to obtain eq. (2.57) is a geometric approximation to fourth and higher orders.

3. Computational procedures

In this section we describe the computational procedures which are used in the extended 2ph-TDA (section 3.2) and OVGF (section 3.3) Green's function calculations. The input data for these calculations are the HF one-particle energies and the corresponding Coulomb matrix elements. We begin with a few comments on these preliminaries.

3.1. SCF-calculations and handling of Coulomb matrix elements

The standard formulation of the Green's function methods presented in section 2 is based on the one-particle data of a SCF calculation for the initial N-particle ground state and applies only to systems where this state is a closed-shell state. The latter requirement is a restriction of the Green's function method which has not been fully overcome yet. As has been mentioned it is not necessary to employ the ground-state Hartree–Fock basis. However, this basis certainly represents the natural and preferable choice within the Green's function approach.

The Green's function methods considered here require discrete one-particle states which are obtained by standard LCAO–MO–SCF procedures. Most applications presented in section 5 employ the program system MUNICH [30]. The problem of constructing adequate basis sets is similar to the one encountered in the conventional CI treatments and we do not enter a discussion of this subject here. A few comments regarding the basis sets are given in section 5.

The quantities which enter the Green's function calculation are the orbital energies ϵ_k and the Coulomb matrix elements V_{ijkl}, where the indices denote spatial one-particle quantum numbers. Since the number of Coulomb matrix elements can be very large their handling in an actual

computation, that is, the storage and retrieval, is an important point and a few considerations on this problem are in order.

Part of the problem of handling the Coulomb matrix elements is common to the CI-type and Green's function type approaches. These problems are associated with the large number of these matrix elements, their storage and addressing. Other problems are different. In the CI-type approaches one forms from the V_{ijkl} matrix elements the Hamiltonian matrix elements or directly the contributions to the eigenvectors and eigenvalues. The Coulomb matrix elements enter linearly into the expressions. In the Green's function approaches, on the other hand, multiple products of V_{ijkl} matrix elements enter the expression for the self-energy. In particular we have to deal with this latter problem. In the handling of the V_{ijkl} matrix elements the use of symmetry is very essential for reducing their number to the number of unique non-zero matrix elements. Two types of symmetry are of importance, the permutational symmetry according to which we have (for real orbitals)

$$V_{ijkl} = V_{kjil} = V_{ilkj} = V_{klij} = V_{jilk} = V_{lijk} = V_{jkli} = V_{lkji} \tag{3.1}$$

and the point group symmetry of the nuclear framework according to which an integral V_{ijkl} is only different from zero, if the direct product of the irreducible representations Γ_i of orbitals i contains the totally symmetric representation Γ_a i.e.

$$V_{ijkl} \neq 0 \quad \text{if } \Gamma_i \times \Gamma_j \times \Gamma_k \times \Gamma_l \supset \Gamma_a. \tag{3.2}$$

Our list of integrals is thus unique by permutational symmetry and we keep only non-zero integrals by the point group symmetry. This procedure is advantageous for symmetric molecules (for molecules with very low symmetry (C_s, C_2) or no symmetry it would be preferable to drop the point group symmetry and store only non-zero integrals together with their indices). At present we are not using symmetry groups with degenerate representations directly but use Abelian subgroups e.g. C_{2v} for T_d and $C_{\infty v}$, D_{2h} for $D_{\infty h}$ and O_h, etc. In these cases we still keep a number of integrals which are actually zero by symmetry and others which are equal (within a phase factor) due to symmetry. In working with Abelian subgroups of groups containing degenerate representations one has to pay attention in the four index transformation of the two-electron integrals from the basis of atomic (Gaussian) functions to molecular orbitals that the molecular orbitals belonging to a degenerate representation all refer to the same axis system (i.e. the components of e-type orbitals all transform as e_x, e_y and not some as e_x, e_y others as e'_x, e'_y, similarly for triply degenerate representations). Prior to the transformation a rotation in the space of degenerate orbitals has to be performed to achieve the proper symmetry behaviour.

Multiple products of V_{ijkl} matrix elements appear in the expression for the self-energy in two distinct contexts. In the OVGF method the self-energy matrix elements consist of sums of diagrams and these diagrams are sums of products of V_{ijkl} matrix elements. In the extended 2ph-TDA method the coupling matrix elements $m_p^{(n)}$ contain sums of Coulomb matrix elements and sums of products of these. Both expressions are of the form

$$T_{pq} = \sum_{a,\ldots,l} C_{a\ldots l} V_{abcd} V_{efgh} V_{ijkl}, \tag{3.3}$$

where the last factor would be missing in the case of the second-order diagrams or the coupling matrix elements. C is a numerical constant containing the orbital energies and purely numerical constants. Some of the indices $a,\ldots,l$ are equal. Some of these indices are also equal to the indices p and q in which case these indices are not summed over. In the case the Coulomb matrix elements enter the expressions for the matrix elements to be calculated in a linear form the same methods as used in CI-type approaches could be used. We will only discuss the methods used to deal with products of V_{ijkl} matrix elements. Three methods which can be used for the evaluation of such products are known in the literature. Which one is used depends on the computer situation with respect to core and disk space available. In the first method we keep all integrals unique by permutational symmetry and non-zero by spatial symmetry in fast core as a linear array. The addressing is done by a set of three index arrays. Given the indices i, j, k, l of an integral V_{ijkl} the first of these index vectors gives the address of the integral V_{i111}, the second one for given i the address of the integral V_{ijk1}, the third one the address of the integral V_{ijkl}. These index vectors can themselves be symmetry reduced. The numerical procedures used in this method to deal with the second-order diagrams and the coupling matrix elements $m_p^{(n)}$ (products of Coulomb matrix elements) on the one hand and the third-order diagrams (triple products of Coulomb matrix elements) on the other hand are essentially identical, but the complexity of the third-order diagrams is certainly larger. The constant diagrams which do not contain the ω-variable in the denominator can be simplified by extracting one combination of integrals and separating the summations. For the A1 diagram (see appendix C), e.g., this takes the following form

$$\mathrm{A1}_{pp} = -\sum_{\substack{i,j\\a,b}} \frac{(2V_{abji} - V_{abij})}{(\epsilon_j + \epsilon_i - \epsilon_a - \epsilon_b)} \sum_k \frac{B_{kj} V_{abki}}{(\epsilon_k + \epsilon_i - \epsilon_a - \epsilon_b)}, \tag{3.4}$$

where $B_{kj} = 2V_{pkpj} - V_{ppkj}$. This procedure is possible for all A-type diagrams. Similar factorization of the summations can be implemented for all third-order diagrams.

In the second method which has been described by Silver and Wilson [31], we start from the assumption that a considerable percentage of the integrals can be kept in core but not all so that external storage on disk must be used too. Typically tens of thousand to a few hundred thousand integrals are kept in fast core. This method is described in detail elsewhere [31] and we thus describe it only very shortly. The diagrams or matrix elements to be evaluated contain integrals of the type V_{ijkl}, V_{ijka}, V_{ijab}, V_{iabc}, V_{abcd}, where i, j, k, l refer to occupied orbitals and a, b, c, d to virtual ones. In general the number of occupied orbitals is considerably smaller than the number of virtual ones. Thus, the first blocks at least for some range of index pairs can be kept in core, but the block V_{abcd}, for instance, not. The blocks in core are stored in individual linear arrays with suitable addressing vectors. The block V_{abcd} is read into fast core in individual loads. The storage sequence of these integrals and/or the DO loops have to be arranged in such a way as to minimize data transfer.

If we can keep only a small fraction of the integrals in core or if we do not wish to keep them in core, then a method devised by Diercksen [32] can be used to evaluate the required matrix elements. This method is similar to the algorithm of Yoshimine [33] for the four index transformation of the integrals. It has been implemented by Diercksen and Grüner [34] in the

framework of the polarization propagator method of Oddershede [35] and also for the one particle Green's function. It will be described in detail in another article [36] and we thus give only the essential outline of the procedure.

In this method the two-electron integrals V_{ijkl} are subdivided into coreloads. A coreload is the number of integrals which will be kept in core in the process of evaluating the self-energy diagrams, e.g. 20000. Thus, if there are 2×10^6 integrals there will be 100 coreloads. The four indices of the integrals will rarely be used to identify them, instead a linear index m will be used. Integrals as well as the matrix elements are referred to by two indices (n, m), the first one (n) is the coreload, it is going to appear in, the second one (m) is the sequence number of the integral in the coreload,

$$(ijkl) \rightarrow (n, m). \tag{3.5}$$

The matrix elements which we wish to compute consist of quantities – which we shall call terms – of the structure

$$\underset{\text{I } (n_1,m_1)}{(p, q)\, C\ \underbrace{(abcd)}} \qquad \underbrace{(efgh)}_{\text{II } (n_2,m_2)} \qquad \underbrace{(ijkl)}_{\text{III } (n_3,m_3)}, \tag{3.6}$$

where (p, q) denotes the matrix element of the self-energy or the matrix element of the coupling matrix **m** of eq. (2.31b). C is a numerical constant and the three sets of indices, I, II and III,denote the two-electron integrals. Terms which contain integrals zero by symmetry will be dropped from the outset. For a second-order diagram or for the coupling matrix elements the set III of indices will be missing as has been mentioned above. Some of the indices $p, q, a, \ldots, l$, can be equal. Thus, the terms written as symbolic matrix elements consists of one real word and 8 integers. The quantity ω and the orbital energies have been omitted, but as these are kept in core they can be inserted at any stage in the computation. We will step by step evaluate these terms starting with the index group III which we will replace by the numerical value of the integral. As the integrals cannot be kept in core we have to order the terms with respect to the indices of III such that all terms in a given group can be filled with the numerical values of the integrals once a coreload of integrals has been read into core. In this procedure we have to minimize input/output. The procedure is as follows. To each coreload n we assign a box n, thus if we have 100 coreloads there will be 100 boxes. The terms will be put into these boxes such that all terms will be put into box n if the integral defined by III will appear in coreload n. The sequence number m of this integral in the coreload n will be assigned to the term in box n. Thus the terms in box n will be

$$(p, q) C \text{ I II } (n, m). \tag{3.7}$$

There may be no terms in box n if the corresponding integrals are not required, there may also be more terms than the size of the coreload in box n if some of the integrals appear several times with different indices in I and II. The size of the boxes requires some comment. We have to keep M boxes in core if there are M coreloads of integrals. If we do not want to keep all integrals in core we have to subdivide the boxes into subparts and write a given subpart of box n onto a

direct access file once it is filled and then start with the next subpart of this box. The size of the boxes should be computed iteratively given a certain core size. At start the box is chosen equal to the track length of the direct access device. It is reduced in size if not all M boxes fit into core until this is the case. As mentioned the terms are created and distributed into the M boxes such that all terms in box n require only integrals from coreload n. If a given subpart of box n is filled, it is written on a direct access file. Its address on the direct access file is written on an identification section which is the first part of the next subpart. Thus starting with the last subpart of any given box whose address must be noted for each box we always have the address of the previous subpart belonging to this box. The boxes (subparts) are written in the arbitrary order in which they are filled on the direct access file. Thus, the subparts of box n may be in position 3, 8, 21, 22 and 44 on the direct access file. After this sorting procedure is finished and the addresses of the last subpart of each box noted we start reading in the integrals by coreloads. If coreload n has been read we start reading the subparts of box n starting with the last one. If a box is empty one can immediately jump over the entire coreload. Each subpart of box n is scanned and the sequence number of the integral in the term is used to identify the integral. This reference is then resolved by replacing the index set III by the numerical value of the integral and multiplying it by the constant C. The resulting terms

$$(p, q)\, C'\, \mathrm{I}\, \mathrm{II} \tag{3.8}$$

are then written on disk. The procedure is repeated for the new terms and the index set II and later I is replaced by the numerical value of the integral and combined with the constant. At the end we arrive at a list of terms

$$\begin{aligned} &(p, p)\, T_1, (p, p)\, T_2, \cdots, \\ &(q, q)\, T_k, \cdots, (p, q)\, T_s, \cdots. \end{aligned} \tag{3.9}$$

All terms having the same index pair (p, q) are combined. (Their sum gives the matrix element $\Sigma_{pq}(\omega)$ or $m_p^{(q)}$, respectively, which is then used for solving the Dyson equation.)

The results which are going to be discussed below in section 5 have been obtained using the first method, where all integrals are kept in core.

3.2. Numerical aspects of the extended 2ph-TDA

As is discussed in section 2 the extended 2ph-TDA calculations require the following steps

(1) Diagonalization of the matrices $(\mathbf{K} + \mathbf{C})^{\mathrm{I,II}}$ of the 2p–1h-part I and of the 2h–1p-part II according to eq. (2.40).
(2) The solution of the Dyson equation (2.21) in form of the eigenvalue problem for the special matrix $\mathbf{A}$ specified in eq. (2.31).
(3) The self-consistent or direct evaluation of the constant self-energy part $\Sigma(\infty)$.

In the following we shall discuss in some detail the numerical aspects of these steps. As we shall see the major numerical problem arises from the size of the configuration spaces I and II and,

thus, from the size of the matrices which have to be diagonalized. In the eigenvalue problem of step (2) one can take advantage of the special "arrow-type" structure of the matrix **A**. Here a new diagonalization algorithm has been developed [37] which can handle effectively very large dimensions of the spaces I and II. This algorithm is presented and discussed at length in section 4. The actual bottlenecks are the eigenvalue problems of step (1). Here the full diagonalization, i.e., the determination of all eigenvalues and eigenvectors, is required to generate the input data of the matrix **A** of step (2).

It should be kept in mind that instead of the two-step diagonalization procedure suggested above one could also proceed via the direct diagonalization of the matrix **B** specified in eq. (2.42). As long as one is interested in a few well-defined roots, e.g., those of the outer valence ionic main states, one could employ one of the diagonalization procedures which are used in the extended CI schemes, such as the Davidson procedure [38]. If, however, the aim is to calculate the full valence ionization spectrum including all satellite states and the inner valence region where the single-particle picture of ionization may break down [39–41], one has to determine all roots of **B** (at least in a given energy interval). In this situation, especially when the density of cationic states is large, the two-step diagonalization procedure is advantageous. The use of direct diagonalization procedures has been investigated by Baker and Pickup [42].

3.2.1. Step (1): Diagonalization of the 2p–1h and 2h–1p parts

The explicit spin-free expressions for the matrix elements of the matrices $(\mathbf{K}+\mathbf{C})^{\mathrm{I,II}}$ are given in appendix A. As we will show in appendix A, there are two independent submatrices, one for the doublet states and one for quartet states. The latter do not couple to the one-hole (particle) configurations (in the matrix **A** of step (2)) and thus do not appear in the one-particle Green's function. For completeness appendix A also lists the **C** matrix corresponding to the quartet states eq. (A.7). In the following we refer to the doublet case only. Here for each set (j, k, l), $k \leqslant l$, of spatial one-particle quantum numbers, there arise one or two configurations depending on whether $k = l$ or $k < l$, respectively. Since in the matrix $(\mathbf{K}+\mathbf{C})^{\mathrm{I}}$ the quantum numbers j and k, l correspond to the occupied and unoccupied one-particle states, respectively, the number of configurations, i.e. the dimension of $\mathbf{K}+\mathbf{C}$, is $N^{\mathrm{I}} = N_{\mathrm{h}} N_{\mathrm{p}}^2$ where N_{h} and N_{p} denote the number of occupied and unoccupied (spatial) orbitals, respectively, which are taken into account. Similarly, $N^{\mathrm{II}} = N_{\mathrm{p}} N_{\mathrm{h}}^2$ is the dimension of $\mathbf{K}+\mathbf{C}$ in the case II.

The spatial symmetry can be exploited to achieve a further reduction of the dimension of the diagonalization problems. In principle, one can construct configurations which transform according to irreducible representations of the spatial symmetry group. Such a formulation of the extended 2ph-TDA equation has been worked out for the case of atoms [18] where one can use the apparatus of tensor analysis. For molecules, on the other hand, each symmetry group requires a special treatment. Thus, it is more convenient to confine oneself to the largest one-dimensional (Abelian) subgroup of the considered symmetry group, e.g. D_{2h} in the case of $D_{\infty h}$. Since here all irreducible representations are one-dimensional it is a trivial task to classify the spatial configurations (j, k, l) with respect to their transformation properties. For each irreducible representation there results a decoupled submatrix of $\mathbf{K}+\mathbf{C}$ which is subject of a separate diagonalisation procedure. We note that the eigenstates which are obtained as the result of these diagonalizations can, of course, be classified according to the irreducible representations of the full spatial symmetry groups.

It is apparent that already for moderate systems and basis sets the dimension of the matrices I and II may prevent the full standard diagonalisation, which is required to generate the input data for step (2). As an example consider the extended 2ph-TDA calculation for N_2 reported in section 5. Here the largest dimension is 146 for the 2h–1p space II, and 1028 for the 2p–1h space (I). Since for most large computers the dimension of 500 represents the limit for the standard diagonalization routines, only the smaller diagonalization can be performed fully.

A situation like this requires additional technical approximations. One possibility for reducing the dimensions of the configuration spaces I and II is the truncation of the HF basis set, in particular, of the virtual (unoccupied) orbitals. If one is interested in the valence ionization, for example, one may omit to a good approximation the core orbitals and thus all configurations involving a core orbital. Similarly, one may discard high-lying virtual orbitals. However, the truncation of orbitals reaches soon the limits where the reliability of the results is seriously affected. Thus, one should, as a rule, try to exhaust the underlying basis as completely as possible.

A simple approximation for the diagonalization of a matrix with dimension larger than 500 (or the limit of the standard diagonalization) is to select a submatrix of the maximum dimension, which then is subjected to a full diagonalization, and to approximate the remaining eigenvalues by their first-order (diagonal) expressions

$$\omega_{jkl} = -\epsilon_j + \epsilon_k + \epsilon_l + C_{jkl,jkl}. \tag{3.10}$$

The corresponding eigenvectors are taken in the zeroth-order approximation

$$x^{(jkl)}_{j'k'l'} = \delta_{jj'}\delta_{kk'}\delta_{ll'}. \tag{3.11}$$

As selection criterion (e.g. in the case of the calculation of ionization potentials) one may take the coupling strength

$$S_{jkl} = \sum_p \frac{|U_{p,jkl}|n_p}{|\epsilon_p + \epsilon_j - \epsilon_k - \epsilon_l - C_{jkl,jkl}|} \tag{3.12}$$

between the configuration (j, k, l) and all one-hole configurations. Often, as in the mentioned example of N_2, the 2h–1p matrix can be diagonalized without any approximation and the selection procedure has only to be employed for the 2p–1h part. Since the approximated 2p–1h levels are energetically far apart from the cationic solutions this technical approximation will affect the final results very little. If a selection is required also in the space of the 2h–1p configurations it has been found to be advantageous to use directly the quantities ω_{jkl} of eq. (3.10) instead of eq. (3.12) as selection criterion. We note that in the case of degenerate first-order energies ω_{jkl} all configurations (j, k, l) have to be included on the same footing either in the full diagonalization or in the diagonal approximation. Otherwise the spatial symmetry of the eigenvalue problem will be destroyed.

3.2.2. Step (2): solution of the Dyson equation

Once the diagonalization procedures of step (1) are completed one can generate the matrix

elements of the matrix **A** (eq. (2.31)) whose eigenvalues and eigenvectors determine the one-particle Green's function (eq. (2.32)). The matrix **A** has the structure

$$\mathbf{A} = \begin{pmatrix} \mathbf{a} & \mathbf{b} \\ \mathbf{b}^{\dagger} & \mathbf{c} \end{pmatrix}, \tag{3.13}$$

where the block $\mathbf{a} = \boldsymbol{\epsilon} + \boldsymbol{\Sigma}(\infty)$ corresponds to the space of one-hole and one-particle configurations and is small (dimension $N_p + N_h$). The block **c** is the large (dimension $N^{I} + N^{II}$), but diagonal matrix of the eigenvalues Ω_n of the eigenvalue problems I and II of step (1). The matrix **b** represents the coupling (matrix elements $m_p^{(n)}$) between the 2p–1h and 2h–1p block **c** and the 1h and 1p block **a** (eq. (2.41)). The spin-free expressions for the coupling matrix elements are specified in eqs. (A.9)–(A.13) of appendix A. As has been mentioned above only the doublet states of I and II have non-vanishing coupling matrix elements.

The eigenvalue problem for **A** decouples with respect to the spatial symmetry properties in a simple way. Since the one-hole and one-particle states (as solutions of a SCF calculation) reflect the symmetry properties of the full point group and since this also applies for the solutions of the diagonalization in step (1), the coupling matrix elements between states of a different symmetry species vanish. Thus, one can simply by inspection discard the coupling matrix elements of all configurations which belong to a different symmetry species.

The special structure of the matrix **A** is called an "arrow-type" structure. The eigenvalue problem for such a matrix can be treated very effectively by the special algorithm [37] to which section 4 is devoted. There also the requirements on storage and computer time of this algorithm are discussed.

3.2.3. Step (3): evaluation of the static self-energy part

The static self-energy part $\boldsymbol{\Sigma}(\infty)$ which appears as a part of the small block **a** of the matrix **A** in step (2) can be determined iteratively, as has been outlined in section 2. For this purpose one repeatedly performs step (2). One starts by setting $\boldsymbol{\Sigma}(\infty) = 0$ and solves the eigenvalue problem of step (2). In eq. (A.15) of appendix A the spin-free equations for the components of $\boldsymbol{\Sigma}(\infty)$ are given. These expressions require the first (1-h and 1-p) eigenvector components of all $(N-1)$-particle eigenstates. The $(N+1)$-particle eigenstates do not contribute and need not be considered. Usually, the $(N-1)$- and $(N+1)$-particle solutions of the eigenvalue problem in step (2) are separated by a large energy interval, so that the identification of the $(N-1)$-particle solutions does not render a problem. Another criterion is the magnitude of the coefficients of the $(N-1)$- and $(N+1)$-particle configurations within a given eigenvector of **A**. The fact that only the $(N-1)$-particle solutions have to be calculated can directly be exploited by the special diagonalization algorithm described in section 4. It should be noted that the evaluation of the components $\Sigma_{pq}(\infty)$ according to eq. (A.15) involves, in general, all spatial symmetry species of the eigenstates of **A**. The resulting expression for $\boldsymbol{\Sigma}(\infty)$ exhibits the symmetry properties of the full spatial symmetry group. The next iteration step follows by inserting the previous expression for $\boldsymbol{\Sigma}(\infty)$ into **A** and by repeating step (2). Usually only a few iterations are needed to obtain convergence.

Another possibility is to use the direct determination of $\boldsymbol{\Sigma}(\infty)$ according to eq. (2.30)). This leads to a set of linear equations for the components $\Sigma_{pq}(\infty)$. The spin-free formulation of these

equations is presented in appendix B. The input data which are required here are the eigenvalue ω_n and the coupling matrix elements $m_p^{(n)}$ resulting from the doublet eigenvalue problems I and II of step (1). Again, all spatial symmetry species are involved. As is shown in appendix B, the solution of the linear equations is obtained by the inversion of a relatively small matrix defined with respect to configurations (k, l) where k and l are particle and hole quantum numbers, respectively.

3.3. Numerical aspects of the OVGF method

As briefly discussed in section 2.5 the ionic ground and the ionic first few excited states are of special interest. Of course we can use the extended 2ph-TDA to calculate the corresponding energies. In this case it is unnecessary to follow the diagonalization procedure described in section 3.2 which has been devised to be especially efficient when many eigenvalues should be computed. Rather being interested in a few eigenvalues only, we may use instead the Davidson diagonalization procedure [38] or related procedures. The fact that the pole strengths corresponding to the outer valence levels are close to unity helps in achieving convergence of these diagonalization procedures. The drawback in using the 2ph-TDA for calculating only a few eigenvalues is that the static self-energy part cannot any more be calculated self-consistently from the dynamic self-energy part as described in section 3.2.3, since this procedure requires knowledge of all eigenvalues. Instead one has to resort to a straightforward perturbation evaluation of the static self-energy part by including all expansion terms of $\boldsymbol{\Sigma}(\infty)$ up to a given order (third order in our case). This strategy has been recently used by Baker and Pickup [42]. The approach is useful as long as $|\boldsymbol{\Sigma}(\infty)|$ is small.

In section 2.5 it has been shown that the extended 2ph-TDA self-energy part can be approximated by a simplified form as long as only outer valence levels are of interest. The underlying method – named the OVGF method – is based on a geometric type of approximation to the self-energy part, is correct up to third-order perturbation theory and requires only the straightforward evaluation of terms in the perturbation expansion of $\boldsymbol{\Sigma}(\omega)$. No matrices need to be diagonalized. The working equations are given in section 2.5 and the handling of the perturbation terms has been described in section 3.1. Once the self-energy part has been calculated, the relevant pole of the Green's function $G_{pq}(\omega)$ is determined as a root of the following Dyson equation

$$\omega - \epsilon_q = \Sigma_{qq}(\omega). \tag{3.14}$$

The relevant pole, i.e. the pole which corresponds to an outer valence cationic state when q is an occupied outer valence orbital in the HF ground state or to the electron affinity when q is a virtual orbital, is characterized by a pole strength close to unity. The pole strength is given by

$$P_q \equiv |x_q^{(q)}|^2 = \left[1 - \frac{\partial \Sigma_{qq}(e_q)}{\partial \omega}\right]^{-1}, \tag{3.15}$$

where e_q is the solution of eq. (3.14). It should be noted that $0 \leq P_q \leq 1$.

The OVGF method is restricted to poles for which $P_q \approx 1$ (in practice $p_q > 0.9$). For these poles

eq. (3.14) can be solved iteratively by defining the series $\omega_q^{(\nu)}$, $\nu = 0, 1, \ldots$

$$\omega_q^{(\nu+1)} = \omega_q^{(\nu)} + \left[\epsilon_q + \Sigma_{qq}\left(\omega_q^{(\nu)}\right) - \omega_q^{(\nu)}\right] P_q^{(\nu)}, \tag{3.16a}$$

$$\omega_q^{(0)} = \epsilon_q \tag{3.16b}$$

which converges rapidly to e_q. The auxiliary series $P_q^{(\nu)}$, $\nu = 0, 1, \ldots$, where

$$P_q^{(\nu)} = \left[1 - \frac{\partial \Sigma_{qq}\left(\omega_q^{(\nu)}\right)}{\partial \omega}\right]^{-1} \tag{3.16c}$$

converges to the pole strength P_q. The simplicity of the equations for determining the self-energy part and for solving the Dyson equation makes the OVGF method applicable to larger molecules and enables the use of extended basis sets. The necessary formulae for the OVGF method (diagrams, and expressions for the renormalization) are given in appendix C.

4. The eigenvalue problem for arrow matrices

In section 2.2 it has been demonstrated how the solution of the Dyson equation reduces to the diagonalization of an arrow matrix. The computational details of the construction of this matrix have been given in sections 3.1 and 3.2. In the following we discuss the eigenvalue problem of a general Hermitian arrow matrix and present an efficient algorithm for obtaining its eigenvalues and eigenvectors. We adopt the numerical procedure of Walter et al. [37]. We consider a general Hermitian arrow matrix **Y** of the form

$$\mathbf{Y} = \begin{pmatrix} \mathbf{A} & \mathbf{B} \\ \mathbf{B}^\dagger & \mathbf{C} \end{pmatrix}, \tag{4.1}$$

where **A** is an $N \times N$ Hermitian matrix with elements a_{ij} coupled to the real $M \times M$ *diagonal* matrix $\mathbf{C} = \{c_i \delta_{ij}\}$ by the $N \times M$ matrix $\boldsymbol{B}$ with elements b_{ij}. Without loss of generality one may take the c_i to be ordered such that

$$c_1 \leq c_2 \leq c_3 \leq \ldots \leq c_M. \tag{4.2}$$

Hermitian arrow matrices have been studied, e.g., for determining the changes of the unperturbed energies caused by adding additional states to the hamiltonian matrix [43,44].

To make contact with the preceding sections we note that the arrow matrix **Y** in eq. (4.1) is identical with the matrix **A** in eq. (3.4). It is convenient to introduce a matrix $\mathbf{L}(\omega)$ which is – apart from the diagonal matrix of the orbital energies – identical to the self-energy part $\boldsymbol{\Sigma}(\omega)$

$$\mathbf{L}(\omega) = \boldsymbol{\epsilon} + \boldsymbol{\Sigma}(\omega). \tag{4.3}$$

Whenever unambiguously defined, **L** is also called the self-energy part. In the present notation

the elements of this matrix read

$$L_{ij} = a_{ij} + \sum_{m=1}^{M} \frac{b_{im} b_{jm}^*}{\omega - c_m}, \quad 1 \le i, j \le N. \tag{4.4}$$

For completeness we recall that the Green's function is closely related to **L** via the Dyson equation

$$\mathbf{G}(\omega) = [\omega \mathbf{1} - \mathbf{L}(\omega)]^{-1}. \tag{4.5}$$

We can express the Green's function in terms of the eigenvalues and eigenvectors of **Y**:

$$\mathbf{YX} = \mathbf{XE}, \quad \mathbf{XX}^{\dagger} = \mathbf{1}. \tag{4.6}$$

Here **E** is the diagonal matrix of eigenvalues e_n and $\mathbf{X} = \{x_{ij}\}$ is the unitary matrix of eigenvectors. The Green's function now reads

$$G_{ij}(\omega) = \sum_{n=1}^{N+M} \frac{x_{in} x_{jn}^*}{\omega - e_n}, \quad 1 \le i, j \le N. \tag{4.7}$$

Eqs. (4.1) to (4.7) constitute our working equations. The Dyson equation (4.5) has the essential advantage that the eigenvalue problem of **Y** can be studied by investigating the pole structure of the ω-dependent Green's function. From a numerical point of view the attractive feature of this approach is the fact that the poles of $\mathbf{G}(\omega)$ can be obtained by "graphical" methods and that the matrices to be dealt with are of order N only. This last attribute is of particular importance because for all applications $M \gg N$.

If the dimension N of the submatrix **A** is equal to 1, the structure of **Y** is particularly simple: only the first row, the first column and the diagonal are different from zero. This one-dimensional case has been considered by many authors [43,45]. The eigenvalues can be obtained by a straightforward graphical procedure. The multidimensional case $N > 1$, however, has found less attention and has only recently been treated by Walter et al. [37]. We follow here their "graphical" procedure for obtaining the eigenvalues and eigenvectors of Hermitian arrow matrices. For the sake of completeness and clarity we first discuss the one-dimensional case.

4.1. The one-dimensional case N = 1

As an illustrative example we first consider the one-dimensional case. If the dimension of **A** is equal to 1, **Y** has the form

$$\mathbf{Y} = \begin{pmatrix} a & b_1 & b_2 & b_3 & \dots \\ b_1^* & c_1 & 0 & 0 & \dots \\ b_2^* & 0 & c_2 & 0 & \dots \\ b_3^* & 0 & 0 & c_3 & \dots \\ \vdots & \vdots & \vdots & \vdots & \end{pmatrix} \tag{4.8}$$

and the corresponding Green's function matrix is one dimensional and reads

$$G(\omega) = 1/[\omega - l(\omega)], \tag{4.9a}$$

$$l(\omega) = a + \sum_{m=1}^{M} |b_m|^2/(\omega - c_m). \tag{4.9b}$$

The analytic properties of the solutions of eq. (4.9) are well-known [43,45]. Here we restrict ourselves to a brief summary of the essential results.

The $(M+1)$ eigenvalues of **Y** are obtained as the solutions e_n of the implicit equation for ω

$$\omega = l(\omega). \tag{4.10}$$

These solutions can easily be found by a graphical method. Let us first assume that all c_m are different, i.e., $c_1 < c_2 < c_3 < \ldots < c_M$. In this case the eigenvalues e_n are all distinct. Fig. 4 shows a graph of $l(\omega)$ for a particular set of parameters a, b_m and c_m. The poles of $l(\omega)$ are indicated by vertical dotted lines and the intervals $(-\infty, c_1)$, $(c_1, c_2), \ldots, (c_M, \infty)$ are specified by the index $h = 1, 2, \ldots, M+1$, respectively. As can be seen from this graph the solutions e_n of eq. (4.16) are obtained as the values of ω at the intersections of $l(\omega)$ with the dashed line $y = \omega$. Since $l(\omega)$ is monotonically decreasing in each interval h, there is exactly one eigenvalue of **Y** in each of these intervals. This property of the eigenvalues of **Y** is often referred to as the separation theorem [43]. Numerically, eq. (4.10) can be solved separately for each interval using well-known algorithms [46], e.g. the Newton–Raphson method.

Let us now consider the case when K diagonal elements of **C** are equal, say

$$c_m = c_{m+1} = \ldots = c_{m+K-1}. \tag{4.11}$$

From the explicit expression of $l(\omega)$ in eq. (4.9b) we see immediately that this is equivalent to replacing **Y** by a matrix $\tilde{\mathbf{Y}}$, where K coupling matrix elements $b_m, b_{m+1}, \ldots, b_{m+K-1}$ are replaced by modified quantities $\tilde{b}_m, \tilde{b}_{m+1}, \ldots, \tilde{b}_{m+K-1}$

$$\begin{aligned} \tilde{b}_m &= \left[\sum_{i=0}^{K-1} |b_{mi}|^2 \right]^{1/2}, \\ \tilde{b}_{m+1} &= \tilde{b}_{m+2} = \ldots = \tilde{b}_{m+K-1} = 0. \end{aligned} \tag{4.12}$$

Now $(K-1)$ diagonal elements of $\tilde{\mathbf{Y}}$ decouple and one finds that c_m is a $(K-1)$-fold degenerate eigenvalue of Y. The residues of the corresponding poles of the Green's function vanish and the $(K-1)$-fold degenerate eigenvalues $e_n = c_m$ do not occur as poles of $G(\omega)$.

Finally, we turn to the problem of determining the eigenvector matrix. It is easily seen that

$$x_{i+1,n} = b_i^* x_{i,n}/(e_n - c_i), \quad 1 \le i \le M. \tag{4.13}$$

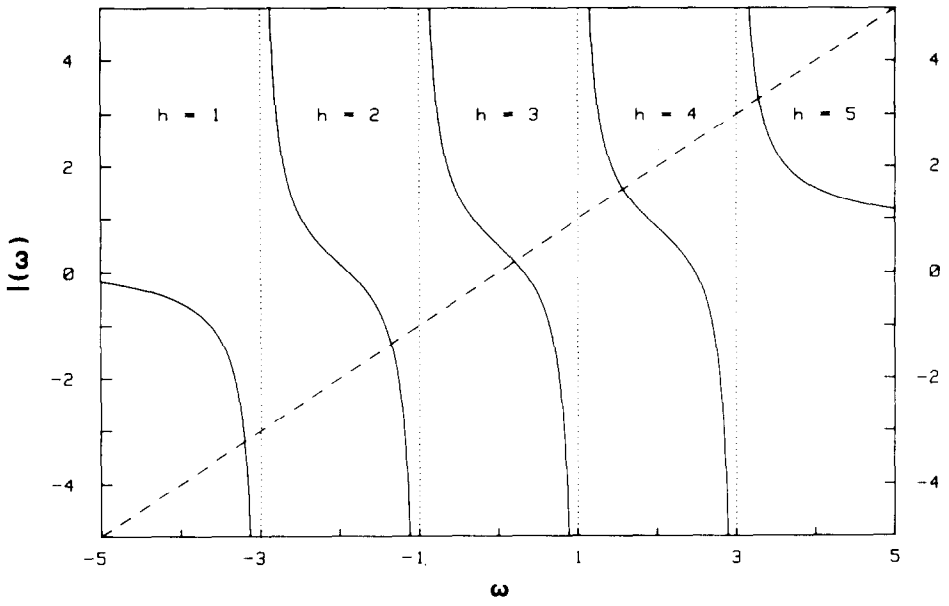

Fig. 4. Graphical determination of the eigenvalues of an arrow matrix **Y** for the one-dimensional case $N = 1$ ($M = 4$). The full lines represent the function $l(\omega)$, the poles of $l(\omega)$ are indicated by vertical dotted lines. The eigenvalues of **Y** are obtained as the values of ω at the intersections of $l(\omega)$ with the dashed line $y = \omega$.

The normalization condition $\mathbf{X}^{+}\mathbf{X} = \mathbf{1}$ fixes the remaining first eigenvector component to be

$$x_{1,n} = \left[1 + \sum_{m=1}^{M} \frac{|b_m|^2}{(e_n - c_m)^2}\right]^{-1/2}. \tag{4.14}$$

The sum within the brackets is easily identified with the slope of $l(\omega)$ at the intersection point of the straight line $y = \omega$ with $l(\omega)$, i.e., at the pole $\omega = e_n$ of the Green's function

$$x_{1,n} = \left[1 - \partial l(e_n)/\partial\omega\right]^{-1/2}. \tag{4.15}$$

The graphical method of computing the poles and residues of $\mathbf{G}(\omega)$ is extremely fast. Furthermore it has the advantage that there is exactly one pole of $G(\omega)$ in each interval h. Each of these poles can be computed in a separate calculation.

4.2. The multi-dimensional case $N > 1$

For the general case $N > 1$ the arrow matrix **Y** is of order $N + M$ and the Green's function matrix **G** as well as **L** are of order N. The function $l(\omega)$ in eq. (4.9) is replaced by a set of N functions $l_i(\omega)$ which are defined by diagonalizing $\mathbf{L}(\omega)$ at every value of ω ($\omega \neq c_m$, $m =$

$1, 2, \ldots, M$):

$$l_i(\omega) = \left[\mathbf{F}^\dagger(\omega)\mathbf{L}(\omega)\mathbf{F}(\omega)\right]_{ii}, \quad \mathbf{F}(\omega)\mathbf{F}^\dagger(\omega) = \mathbf{1}. \tag{4.16}$$

The matrix $\mathbf{F}(\omega)$ of eigenvectors is unitary. In the following we discuss the analytic properties of this set of functions and subsequently we present a pole search algorithm built upon these analytic properties.

The poles of the Green's function are obtained again – as in the one-dimensional case – as the solutions of the implicit equations

$$\omega = l_i(\omega), \quad i = 1, 2, \ldots, N. \tag{4.17}$$

While the function $l(\omega)$ in the one-dimensional case has simple poles at $\omega = c_m$ ($m = 1, 2, \ldots, M$), the $l_i(\omega)$ are of a more complex form. To study the behaviour of the $l_i(\omega)$ at the poles c_m of $\mathbf{L}(\omega)$, we first discuss the case where all c_m are different. Let us consider the structure of the $l_i(\omega)$ around a particular pole of $\mathbf{L}(\omega)$, say c_k. For $c_{k-1} < \omega < c_{k+1}$, we divide $\mathbf{L}(\omega)$ into two parts

$$\mathbf{L}(\omega) = \tilde{\mathbf{L}}(\omega) + \frac{1}{\omega - c_k}\mathbf{B}_k\mathbf{B}_k^\dagger, \tag{4.18}$$

where $\tilde{\mathbf{L}}(\omega)$ is identical to $\mathbf{L}(\omega)$ except that it does not contain the pole at c_k, i.e. the summation in eq. (4.4) is restricted to $m \neq k$. $\mathbf{B}_k$ is a column vector of length N and elements b_{ik}. We now diagonalize the Hermitian matrix $\mathbf{B}_k\mathbf{B}_k^\dagger$:

$$(\mathbf{B}_k\mathbf{B}_k^\dagger)\mathbf{S} = \mathbf{S}\beta^{(k)}. \tag{4.19}$$

The eigenvalues are simply given by

$$\beta_1^{(k)} = \sum_{n=1}^{N} |b_{nk}|^2, \quad \beta_2^{(k)} = \beta_3^{(k)} = \ldots = \beta_N^{(k)} = 0 \tag{4.20}$$

and the N components s_{i1} of the eigenvector $\mathbf{S}_1$ corresponding to the eigenvalue $\beta_1^{(k)}$ are explicitly obtained as

$$s_{i1} = \left[\sum_{n=1}^{N} |b_{nk}|^2\right]^{-1/2} b_{ik} \tag{4.21}$$

and the remaining $(N-1)$ eigenvectors corresponding to the eigenvalues 0 span the orthogonal complement of $\mathbf{S}_1$. If N is a power of 2 this orthogonal complement is determined straightforwardly by permutations of the elements b_{ik}.

With the aid of the unitary transformation $\mathbf{S}$ which diagonalizes $\mathbf{B}_k\mathbf{B}_k^\dagger$ we arrive at

$$\mathbf{S}^\dagger\mathbf{L}(\omega)\mathbf{S} = \begin{pmatrix} H_{11}(\omega) & \mathbf{I}(\omega) \\ \mathbf{I}^\dagger(\omega) & \mathbf{D}(\omega) \end{pmatrix} + \begin{pmatrix} \dfrac{\beta_1^{(k)}}{\omega - c_k} & \mathbf{0} \\ \mathbf{0} & \mathbf{0} \end{pmatrix}, \tag{4.22}$$

where $\mathbf{0}$ is either a matrix or a vector containing only zeros and the other quantities arise from the diagonalization of $\tilde{\mathbf{L}}(\omega)$:

$$\begin{aligned} &\mathbf{S}^\dagger\tilde{\mathbf{L}}(\omega)\mathbf{S} = \mathbf{H}(\omega), \\ &I_{ij}(\omega) = H_{ij}(\omega), \quad i = 1, j = 2, 3, \ldots, N, \\ &D_{ij}(\omega) = H_{ij}(\omega), \quad i, j = 2, 3, \ldots, N. \end{aligned} \tag{4.23}$$

For $c_{k-1} < \omega < c_{k+1}$ the elements of the matrix $\tilde{\mathbf{L}}(\omega)$ are continuous by construction and, therefore, also the $H_{ij}(\omega)$ are continuous. Consequently [37], one function $l_i(\omega)$ has a simple pole at $\omega = c_k$ and the other $(N-1)$ functions $l_i(\omega)$ are continuous for $c_{k-1} < \omega < c_{k+1}$. Furthermore, one obtains for the value of these functions at $\omega = c_k$

$$l_i(c_k) = d_i(c_k), \tag{4.24}$$

where the $d_i(c_k)$ are the eigenvalues of the matrix $\mathbf{D}(c_k)$ defined above in eqs. (4.22) and (4.23).

Two additional properties of the functions $l_i(\omega)$ should be mentioned: (a) each $l_i(\omega)$ is a monotonically decreasing function between any two of its successive poles and (b) when $|\omega|$ approaches infinity, $l_i(\omega)$ approaches a constant α_i which is an eigenvalue of the submatrix $\mathbf{A}$ in eq. (4.1).

We note that in the one-dimensional case the number of poles of the function $l(\omega)$ is M, whereas for $N > 1$ the number of poles I_i of the particular function $l_i(\omega)$ is less than M. If we denote by $l_1(\omega)$ the function which has a pole at $\omega = c_1$, the next poles of $l_1(\omega)$ occur at c_{1+N}, $c_{1+2N}, \ldots, c_{1+(I_1-1)N}$. Similarly, the poles of $l_2(\omega)$ occur at c_2, $c_{2+N}, \ldots, c_{2+(I_2-1)N}$, etc. It follows that the number of poles is given by

$$I_i = 1 + \left[\frac{M-i}{N}\right], \quad M, N \geq i, \tag{4.25}$$

where $[a]$ denotes the largest integer number which is $\leq a$. It should be noted that this formula for the number of poles is valid only if all c_m are different.

The analytic properties of the functions $l_i(\omega)$ can best be visualized by a graphical analysis. Fig. 5 shows a graph of the functions $l_i(\omega)$ for $N = 3$, the dimension of $\mathbf{C}$ being $M = 4$. The positions of the poles c_m of $\mathbf{L}(\omega)$ ($c_1 = -3$, $c_2 = -1$, $c_3 = 1$, $c_4 = 3$) are marked by vertical dotted lines. At $\omega = -3$ the function $l_1(\omega)$ has a simple pole, but is continuous at $\omega = -1$ and $\omega = 1$. The second ($I_1 = 2$ according to eq. (4.25)) pole of $l_1(\omega)$ occurs at $\omega = 3$. The remaining two functions $l_2(\omega)$ and $l_3(\omega)$ have only one pole each ($I_2 = I_3 = 1$). $l_1(\omega)$ is monotonically decreasing in each of the intervals $(-\infty, -3)$, $(-3, 3)$ and $(3, \infty)$, $l_2(\omega)$ in the intervals $(-\infty, -1)$ and

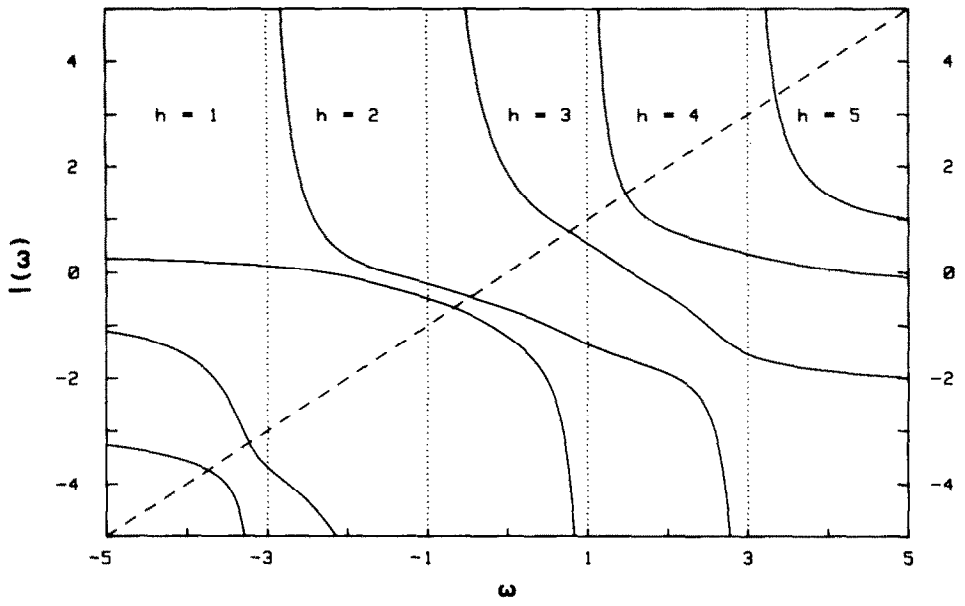

Fig. 5. Graphical determination of the eigenvalues of an arrow matrix **Y** for the multi-dimensional case $N = 3$ ($M = 4$). The full lines represent the three functions $l_1(\omega)$, $l_2(\omega)$ and $l_3(\omega)$; the poles of $\mathbf{L}(\omega)$ are indicated by vertical dotted lines. At each pole of $\mathbf{L}(\omega)$ exactly one $l_i(\omega)$ has a simple pole. There are three intersection points of the $l_i(\omega)$ with the dashed line $y = \omega$ in the interval $h = 3$, two in the interval $h = 1$, but none in the interval $h = 2$. The slope of $l_i(\omega)$ at an intersection determines the residues of the Green's function and the eigenvectors of **Y**.

$(-1, \infty)$ and $l_3(\omega)$ in $(-\infty, 1)$ and $(1, \infty)$. Similarly to the one-dimensional case, the 7 $(= N + M)$ eigenvalues of **Y** are obtained as the values of ω at the intersections of the dashed line $y = \omega$ with the curves $l_i(\omega)$. However, the separation theorem of the one-dimensional case no longer holds here. As can be seen from fig. 5 there are three eigenvalues of **Y** in the interval $h = 3$ and two in the interval $h = 1$, but none in the internal $h = 2$. Obviously, in contrast to the one-dimensional case, the number of possible eigenvalues in each of the intervals h varies. Since there are N functions $l_i(\omega)$, the upper limit for the number of intersection points in each interval h is N. The lower limit for these numbers is 1 in the first ($h = 1$) and last ($h = M + 1$) intervals and 0 otherwise.

Although there is no separation theorem for the multi-dimensional case, the number of eigenvalues in each of the intervals h can easily be determined. Suppose we want to know how many roots of **Y** are in a particular interval (c_k, c_{k+1}). As a first step we calculate the values $l_i(c_k)$ of the $(N - 1)$ functions $l_i(\omega)$ which are continuous at c_k as well as the values $l_i(c_{k+1})$ of the $(N - 1)$ functions which are continuous at c_{k+1}. According to eq. (4.24) this is done by diagonalizing the matrix $\mathbf{D}(\omega)$ of eq. (4.22) for $\omega = c_k$ and $\omega = c_{k+1}$, respectively. Since all $l_i(\omega)$ are monotonically decreasing in the interval (c_k, c_{k+1}), we can immediately tell which and how many $l_i(\omega)$ intersect the straight line $y = \omega$. Similarly, the rim intervals $(-\infty, c_1)$ and (c_M, ∞) can be investigated by taking into account the asymptotic behavior of the $l_i(\omega)$ (see property (b) below eq. (4.24)).

We now drop the condition that all c_m must be different. Suppose K elements of **C** are equal, say $c_k = c_{k+1} = \ldots = c_{k+K-1}$. The corresponding coupling matrix elements form K vectors $\mathbf{B}_k$,

$\mathbf{B}_{k+1},\ldots,\mathbf{B}_{k+K-1}$. Suppose further that J of this set of vectors are linearly independent. Since each of these vectors is of length N, $J \leq N$ and K. Although c_k is now a K-fold degenerate pole of $\mathbf{L}(\omega)$, the asymptotic behavior as well as the monotonicity of the set of $l_i(\omega)$ is not altered. However, instead of one, exactly J functions now have a simple pole at $\omega = c_k$. The remaining $(N-J)$ functions are continuous at this point. In order to compute the values of these functions at $\omega = c_k$ we return to eqs. (4.18) and (4.19) and replace the matrix $\mathbf{B}_k\mathbf{B}_k^\dagger$ by

$$\sum_{i=0}^{K-1} \mathbf{B}_{k+i}\mathbf{B}_{k+i}^\dagger.$$

This matrix is of rank J and, therefore, has J eigenvalues different from zero:

$$\beta_1^{(k)}, \beta_2^{(k)},\ldots,\beta_J^{(k)} \neq 0, \quad \beta_{J+1}^{(k)} = \ldots = \beta_N^{(k)} = 0. \tag{4.26}$$

Similarly to eq. (4.22) the diverging $l_i(\omega)$ decouple from the continuous ones and we arrive at the following relation

$$\mathbf{S}^\dagger\mathbf{L}(\omega)\mathbf{S} = \mathbf{H}(\omega) + \begin{pmatrix} \beta_1^{(k)} & & & & & \\ & \beta_2^{(k)} & & & 0 & \\ & & \ddots & & & \\ & & & \beta_J^{(k)} & & \\ & 0 & & & 0 & \\ & & & & & \ddots \\ & & & & & & 0 \end{pmatrix} \frac{1}{\omega - c_k}. \tag{4.27}$$

where

$$D_{ij}(\omega) = H_{ij}(\omega), \quad i,j = J+1, J+2,\ldots,N,$$

and $\mathbf{H}(\omega)$ has been defined in eq. (4.23). The values of the $(N-J)$ continuous functions $l_i(\omega)$ at $\omega = c_k$ are obtained as before as the eigenvalues of the submatrix $\mathbf{D}(c_k)$ which is now of the order $N-J$.

A few additional interesting points are worth mentioning if c_k is a K-fold degenerate pole of $\mathbf{L}(\omega)$. If the degenerate pole happens to be c_1 or c_M than there are at least J eigenvalues of $\mathbf{Y}$, i.e. poles of the Green's function, in the intervals $(-\infty, c_1)$ and (c_M, ∞), respectively. If $J = N$ for a particular c_k then there is at least one eigenvalue of $\mathbf{Y}$ in each of the two adjacent intervals (c_{k-1}, c_k) and (c_k, c_{k+1}). *Most importantly*: c_k itself is a $(K-J)$-fold degenerate root of $\mathbf{Y}$. These roots do not appear as poles of the Green's function, since the corresponding residues vanish.

To illustrate the effect of a degenerate pole of $\mathbf{L}(\omega)$ we have plotted in fig. 6 the three functions $l_1(\omega)$, $l_2(\omega)$ and $l_3(\omega)$ for the same set of parameters as used in fig. 5 with one additional pole at $\omega = -1$ which is now twofold degenerate. The coupling matrix elements are

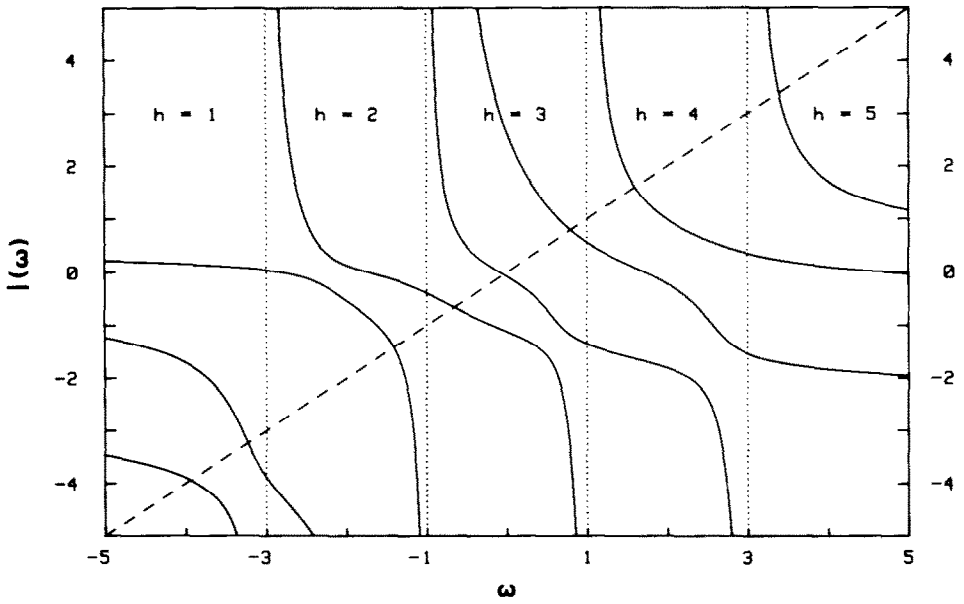

Fig. 6. Graphical determination of the eigenvalues of an arrow matrix **Y** for the multi-dimensional case $N = 3$ ($M = 5$). For the explanation of the symbols see fig. 5. The matrix $\mathbf{L}(\omega)$ is the same as in fig. 5 except that an additional pole has been added at $\omega = -1$. Therefore, two functions $l_i(\omega)$ have a pole at this point. The additional eigenvalue of **Y** lies in interval $h = 2$.

chosen such that the two vectors $\mathbf{B}_2$ and $\mathbf{B}_3$ are linearly independent, i.e. $J = 2$. Fig. 6 shows that at $\omega = -1$ both $l_2(\omega)$ and $l_3(\omega)$ have a pole in contrast to fig. 5 where $l_3(\omega)$ has been continuous at this point. Since the additional pole of $\mathbf{L}(\omega)$ increases the dimension of **Y** by 1, there must be one additional eigenvalue. From fig. 6 it follows that this solution lies in the interval $h = 2$. It should be noted that the number of eigenvalues in a given interval h can still be easily calculated by the procedure described above for the non-degenerate case.

Finally, we turn to the computation of the eigenvectors of **Y**. The relation between the eigenvector matrix **X** and the residues of the Green's function is given in eq. (4.7). The first N components of any eigenvector of **Y** are obtained from the derivative of $l_i(\omega)$ with respect to ω at its intersection point $\omega = e_n$ with the straight line $y = \omega$:

$$x_{pn} = F_{pi}(e_n)\left[1 - \partial l_i(e_n)/\partial\omega\right]^{-1/2}, \quad 1 \le p \le N. \tag{4.28}$$

$F_{pi}(\omega)$ are the elements of the eigenvector matrix $\mathbf{F}(\omega)$ which diagonalizes $\mathbf{L}(\omega)$, see eq. (4.16). The derivatives of $l_i(\omega)$ with respect to ω can be given explicitly

$$\frac{\partial l_i(\omega)}{\partial\omega} = -\sum_{m=1}^{M} \frac{|\alpha_{im}|^2}{(\omega - c_m)^2}, \tag{4.29a}$$

where

$$\alpha_{im} = \sum_{n=1}^{N} F_{ni}(\omega) b_{nm}. \tag{4.29b}$$

These relations complete the evaluation of the Green's function. It might, however, be of interest to determine also the remaining M components (corresponding to the submatrix **C**) of the eigenvectors of **Y**. These components – which do not enter the Green's function expression (4.7) – may serve as a tool to idenfity the contributions of higher excited configurations. They are determined by the relation

$$x_{N+p,n} = \sum_{j=1}^{N} b_{pj}^{*} x_{jn}/(e_n - c_p), \quad 1 \leq p \leq M \tag{4.30}$$

for $e_n \neq c_p$. The less interesting case $e_n = c_p$ (the corresponding residue of the Green's function usually vanishes in this case) is treated in ref. [37].

4.3. A pole search algorithm for solving the eigenvalue problem of Hermitian arrow matrices

The preceding analysis has shown that there is an equivalence between the eigenvalues of Hermitian arrow matrices having non-vanishing eigenvector components with respect to the submatrix **A** on one hand and the poles of the Green's function for **Y** on the other hand. Numerically, this equivalence can be utilized to compute the Green's function $\mathbf{G}(\omega)$. For this purpose, the results of the last section for the multi-dimensional case $N > 1$ can be converted into a general algorithm for obtaining all poles of the Green's function. In the following we present the essential features of such a pole search algorithm:

1) The M known poles of $\mathbf{L}(\omega)$ give a straightforward way of dividing the range of ω and hence the spectrum of the eigenvalues of **Y** into the $M + 1$ intervals $(-\infty, c_1), (c_1, c_2), \ldots (c_M, \infty)$. Since each of these intervals can be investigated separately, one may restrict the eigenvalue analysis to *any* interval (a, b) without having to solve the whole problem.
2) For a particular interval $h = (c_k, c_{k+1})$ the number of eigenvalues e_n of **Y** in h is determined in the following way: The values of the continuous functions $l_i(\omega)$ at $\omega = c_k$ and $\omega = c_{k+1}$ are calculated by diagonalizing the matrices $\mathbf{D}(c_k)$ and $\mathbf{D}(c_{k+1})$ as described in section 4.2. Since each $l_i(\omega)$ is monotonically decreasing in h, there is at most one intersection point of a particular $l_i(\omega)$ with the straight line $y = \omega$. Knowing the numerical values of $l_i(c_k)$ and $l_i(c_{k+1})$ makes it possible to determine which functions $l_i(\omega)$ are intersected and, consequently, how many eigenvalues of **Y** lie in h. If $h = (-\infty, c_1)$ or (c_M, ∞) one must also take into account the asymptotic behaviour of the set of functions $l_i(\omega)$. Scanning all $M + 1$ intervals in this way guarantees that no eigenvalue of **Y** is omitted.
3) A particular eigenvalue e_n is determined by solving the equation $\omega - l_i(\omega) = 0$. This has to be done iteratively, e.g. using a Newton–Raphson procedure. The iteration involves the evaluation of $l_i(\omega)$ at iteration points ω_ν where $c_k < \omega_\nu < c_{k+1}$. To calculate $l_i(\omega_\nu)$ the matrix

elements $L_{ij}(\omega_\nu)$ are constructed via eq. (4.4) and the resulting matrix $\mathbf{L}(\omega_\nu)$ is diagonalized. The ith (ordered) eigenvalue of $\mathbf{L}(\omega_\nu)$ then corresponds to $l_i(\omega_\nu)$. In the iterative cycle only matrices of order N need to be manipulated which means that for fixed N the computational time for a particular e_n is proportional to M.

4) For a particular eigenvalue e_n the corresponding eigenvector is obtained via the derivative of $l_i(\omega)$ with respect to ω at $\omega = e_n$. The derivative is given analytically and hence the corresponding eigenvector components can directly be evaluated via eqs. (4.28)–(4.30). For fixed N the computational time for a particular eigenvector is linear in M, i.e. the time for calculating the hole eigenvector matrix is proportional to M^2.
5) To complete the eigenvalue analysis one must determine the eigenvalues of **Y** having vanishing eigenvector components with respect to the submatrix **A**, which due to vanishing residues cannot show up as poles of $\mathbf{G}(\omega)$. Such special eigenvalues can only occur if a pole c_k is degenerate. In this case one analyzes the structure of the coupling matrix elements $\mathbf{B}_k$. If c_k is K-fold degenerate and the number J of linearly independent vectors of the set $\mathbf{B}_k, \ldots, \mathbf{B}_{k+K-1}$ is less than K, it follows that c_k is a $(K-J)$-fold degenerate eigenvalue of **Y**.

The features of the pole search algorithm as outlined above suggest that it will be particularly efficient for two practical applications one is often faced with: either only a certain range of the eigenvalue spectrum is needed or many (or even all) eigenvalues together with the corresponding eigenvectors have to be evaluated. In both cases the efficiency of the above algorithm increases the larger the "tail" M of the arrow is compared to the dimension N of the submatrix **A**. If all eigenvectors are to be calculated even for medium sized matrices ($M = 300$) we have found that, compared to standard diagonalization routines for $N = 3$, a factor of 7 in CPU time is gained. For $N = 6$ this saving is reduced to a factor of 3. The drastic reduction of computing time is, of course, due to the fact that the time for evaluating all eigenvectors is proportional to M^2 whereas standard routines exhibit an M^3 dependence. A further saving is accomplished if not all eigenvalues are needed. The latter is particularly important for very large matrices. In this case one often encounters the problem of determining all eigenvalues within a given range. The pole search algorithm is ideally suited for this sort of problem because all intervals (a, b) are treated with the same accuracy. For such large matrices a comparison with the Lanczos [87] algorithm shows that as long as only eigenvalues are computed the CPU times for the two methods are roughly the same. However, the great numerical stability of the pole search algorithm is a quality which cannot be matched by the Lanczos algorithm. With the latter considerable numerical effort is required to eliminate spurious eigenvalues or to calculate eigenvectors. We also would like to emphasize that very close or degenerate eigenvalues of **Y** do not pose any additional difficulties within the framework of the above algorithm because this problem is reduced to the problem of coping with degeneracies of the very small $N \times N$ matrix $\mathbf{L}(\omega)$.

5. Applications

The one-particular Green's function method has been applied to a large number of atoms and molecules ranging from He to SF_6 and transition metal compounds. Most of the calculations have

been carried out with the objective of explaining ionization spectra like photoelectron and (e, 2e) spectra. Some applications are available to the electron affinities and electron–vibration (vibronic) coupling constants in molecules. The latter quantities are of interest when calculating the vibronic structure in molecular ionization spectra and the nuclear geometry of the molecular ions. Only little is known about the usefulness of computing electronic correlation energies via Green's functions. Applications of Green's functions to electronic correlation energies have been reported [23,47–49] on a few small systems: He, Be, LiH, N_2, CO and H_2O. The self-energy part can also be used to calculate the cross section for collisions of electrons with atoms and molecules (see section 2.1). The concept has been applied to electron scattering off He, H_2 and N_2 [50–52].

In table 1 we have collected the atoms and molecules on which ab initio Green's function and EOM calculations have been carried out. It should be mentioned that many semiempirical applications of Green's functions are also available in the literature. Of these the OVGF calculations on several metal–organic compounds using a newly parameterized INDO Hamiltonian deserve special attention [53,54]. All calculations in table 1 are based on finite basis set methods. In the molecular calculations Gaussian atomic orbitals have predominantly been used (see section 3.1). In the case of atoms use has been made [18] of the spherical symmetry to reduce the extended 2ph-TDA equations to radial equations. In this version the equations have been solved using Slater type orbitals. As mentioned in preceding sections, the OVGF equations can be solved for extended basis sets without truncation. Indeed, the basis sets have been exhausted in most OVGF calculations included in table 1. Since the 2ph-TDA method is based on matrix diagonalization, it is much more cumbersome to exhaust the basis sets. In many of the 2ph-TDA computations reported in table 1 diagonalization procedures have been used which are less sophisticated than those described in this work and the basis sets were truncated. For the larger molecules and older calculations truncation errors might be significant, but nevertheless the results are useful for the interpretation of the experimental findings. In what follows we discuss a few applications of the OVGF and extended 2ph-TDA methods to the calculation of valence ionization potentials and electron affinities. The results are used to briefly interprete ionization spectra and some attention is paid to the ionization of inner-valence electrons. The complex inner-valence-shell ionization spectra of molecules are the subject of current experimental and theoretical investigations. As an example one may consider the model molecules N_2 and CO. Recently new experimental data [55] have been obtained by synchrotron radiation at various photon energies. These experimental spectra corroborating previously experimental work [56–62] show an extended structure comprising numerous peaks in the region of 25–45 eV binding energy which cannot be explained by the single-particle picture of ionization. Due to strong configuration mixing between the inner-valence hole configuration and higher excited configurations, e.g., two-hole–one-particle (2ph–1p) excitations, there may occur a multitude of final ionic states which share the partial ionization cross section for the respective inner-valence orbital. This breakdown of the single-particle picture for the ionization of inner-valence electrons is a common phenomenon, as has been demonstrated by theoretical studies in N_2 [39,24] and CO [39,24,63] and in many other molecules [64]. General aspects of the phenomenon are discussed in refs. [65,66].

As examples we choose N_2, $C_2N_4H_2$ (s-tetrazine) and $ZnCl_2$ for the discussion of the ionization spectra and C_2, P_2, SO_2 and O_3 for a short presentation of the electron affinities. The model molecule N_2 is discussed in some detail as an introduction to the use of the method and

Table 1
Compilation of calculations on atoms and molecules performed with Green's functions or related methods

Molecule [a]	Method [c]	Refs. [b]	Remarks [c]
He	GF	(1–5)	IP, e–S, E_c
Li	GF	(6,7)	IP, EA
Be	GF, 2ph-TDA	(1,8,9)	IP, E_c
F	EOM	(10)	EA
Ne	OVGF, GF, EOM, 2ph-TDA	(10–17,122)	IP
Na	GF	(7)	IP, EA
Mg	GF, 2ph-TDA	(8,14)	IP
Ca	2ph-TDA	(8)	IP
H_2	GF	(18–20)	IP, e–S
Li_2	GF, 2ph-TDA	(15,16,122)	IP,EA
Be_2	EOM	(21)	EA
C_2	OVGF	(22)	EA
N_2	OVGF, GF, EOM, 2ph-TDA	(2,13,23–28, 29,30–36,9,122)	IP, e–S, E_c
O_2	GF	(37)	IP
F_2	OVGF, 2ph-TDA	(13,38,39)	IP
P_2	OVGF, 2ph-TDA	(13,22,40)	IP,EA
Cl_2	OVGF, GF, 2ph-TDA	(41,42)	IP, EA
Br_2	OVGF, 2ph-TDA	(42)	IP
LiH	EOM, GF	(15,16,43–46)	IP, EA, E_c
BeH	EOM, GF	(7,47)	IP, EA
BH	EOM	(10,48)	IP, EA
OH	EOM	(10)	EA
FH	OVGF, 2ph-RDA, EOM	(10,39,43,49, 50)	IP, EA
NaH	EOM	(43)	EA
ClH	OVGF, 2ph-TDA	(50,51)	IP
BrH	OVGF, 2ph-TDA	(50,51)	IP
IH	OVGF, 2ph-TDA	(50,51)	IP
BO	EOM	(52)	EA
CO	OVGF, 2ph-TDA	(31,53,9)	IP, E_c
CN	EOM, GF, 2ph-TDA	(35,41,52,54)	EA
CS	OVGF, 2ph-TDA	(40,55)	IP
PN	OVGF, 2ph-TDA	(40,56)	IP
SiO	OVGF, 2ph-TDA	(53)	IP
SiS	OVGF, 2ph-RDA	(53)	IP
HCN	OVGF, 2ph-TDA	(53,57–60)	IP, ve
HNC	OVGF, 2ph-TDA	(53,57)	IP
CO_2	OVGF, 2ph-TDA	(13,61)	IP
COS	OVGF, 2ph-TDA	(53,62)	IP
CS_2	OVGF, 2ph-TDA	(63)	IP
N_2O	OVGF, 2ph-TDA	(53,61,64)	IP, ve
FCN	OVGF, 2ph-TDA	(59,65)	IP
$ZnCl_2$	OVGF, 2ph-TDA	(66)	IP
$CdCl_2$	OVGF, 2ph-TDA	(66)	IP
$NiCl_2$	OVGF, 2ph-TDA	(66)	IP

Table 1 (continued)

Molecule [a]	Method [c]	Refs. [b]	Remarks [c]
H_2O	OVGF, GF, 2ph-TDA	(13–17,25,35, 38,43–45,53,9,122)	IP, E_c
NH_2	EOM, GF	(54,67)	EA
PH_2	GF	(54)	EA
H_2S	OVGF, 2ph-TDA	(13,42,68,69)	IP
HNO	OVGF, 2ph-TDA	(53)	IP
Be_3	EOM	(21)	EA
NO_2	EOM	(70)	EA
O_3	OVGF	(71,72)	IP, EA
SO_2	OVGF, 2ph-TDA	(53,71,72)	IP, EA
OF_2	OVGF, 2ph-TDA	(73)	IP
SF_2	OVGF, 2ph-TDA	(73)	IP
C_2H_2	OVGF, 2ph-TD	(38,53,74–76)	IP
H–C≡C–F	OVGF, 2ph-TDA	(39,75)	IP
F–C≡C–F	OVGF, 2ph-TDA	(39,75,77)	IP
N≡C–C≡N	OVGF, 2ph-TDA	(53,69,78–80)	IP, vs, ve, ig
N≡C–N≡C	OVGF, 2ph-TDA	(53)	IP
NH_3	OVGF, 2ph-TDA, GF	(25,42,81–83,122)	IP, vs, ve, ig
PH_3	2ph-TDA	(69)	IP
N_2H_2 (trans-, cis-, 1, 1-)	OVGF	(84)	IP, vs
H_2CO	OVGF, 2ph-TDA	(38,53,85–88)	IP, vs
H_2CS	OVGF, 2ph-TDA	(53,68)	IP, vs
HNCS	OVGF, 2ph-TDA	(53)	IP
Be_4	EOM	(21)	EA
BF_3	OVGF, 2ph-TDA	(65,89,90)	IP, vs, ve, ig
N_2F_2 (trans-, cis-)	OVGF	(91)	IP
SO_3	OVGF	(92)	IP, EA
S_2N_2	OVGF, 2ph-TDA	(93)	IP
H–C≡C–CN	OVGF, 2ph-TDA	(53,59,79)	IP
H–C≡C–NC	OVGF, 2ph-TDA	(53)	IP
F–C≡C–CN	OVGF, 2ph-TDA	(59)	IP
CH_4	OVGF, 2ph-TDA, GF	(25,74,76,94,122)	IP
CH_3F	OVGF, 2ph-TDA, GF	(39,94,122)	IP
CH_3Cl	OVGF, 2ph-TDA	(51)	IP
CH_3Br	OVGF, 2ph-TDA	(51)	IP
CH_3I	OVGF, 2ph-TDA	(51)	IP
CH_2F_2	OVGF, 2ph-TDA	(94)	IP
CH_2Cl_2	OVGF, 2ph-TDA	(91)	IP
CHF_3	OVGF, 2ph-TDA	(95)	IP
CF_4	OVGF, 2ph-TDA	(95)	IP
H_2NCN	OVGF, 2ph-TDA	(53)	IP
H_2CNH	OVGF, 2ph-TDA	(53)	IP
HCOOH	OVGF, 2ph-TDA	(58,88)	IP
CH_2N_2 (diazirine)	OVGF, 2ph-TDA	(96)	IP
CH_2O_2 (dioxirane)	OVGF, 2ph-TDA	(96)	IP
H–C≡C–C≡C–H	OVGF, 2ph-TDA	(53,75,76)	IP
H–C≡C–C≡C–F	OVGF, 2ph-TDA	(75)	IP
F–C≡C–C≡C–F	OVGF, 2ph-TDA	(39,77)	IP

Table 1 (continued)

Molecule [a]	Method [c]	Refs. [b]	Remarks [c]
NC–C≡C–CN	OVGF, 2ph-TDA	(53,59,79)	IP
NC–C≡C–NC	OVGF, 2ph-TDA	(53)	IP
CH_3OH	OVGF, 2ph-TDA	(88)	IP
CH_3SH	OVGF, 2ph-TDA	(53)	IP
$HCONH_2$	OVGF, 2ph-TDA	(65,97)	IP
CH_3CN	OVGF, 2ph-TDA	(59,79)	IP
CH_3NC	OVGF, 2ph-TDA	(79)	IP
CF_3CN	OVGF, 2ph-TDA	(59,65)	IP
C_2H_4	OVGF, 2ph-TDA	(74,76,98–100,123)	IP, ve, ig
C_2H_3F	OVGF, 2ph-TDA	(39,101,102)	IP
C_2H_3Cl	OVGF, 2ph-TDA	(51)	IP
$C_2H_2F_2$ (trans-, cis-, 1, 1-)	OVGF, 2ph-TDA	(39,101)	IP
$C_2H_2Cl_2$ (trans-, cis-, 1, 1-)	OVGF, 2ph-TDA	(51)	IP
C_2HF_3	OVGF, 2ph-TDA	(39,101)	IP
C_2HCl_3	OVGF, 2ph-TDA	(51)	IP
C_2F_4	OVGF, 2ph-TDA	(39,101)	IP
C_2Cl_4	OVGF, 2ph-TDA	(51)	IP
$C_2H_2O_2$ (trans-, cis-glyoxal)	OVGF, 2ph-TDA	(88,103)	IP
$C_2F_2O_2$ (trans-)	OVGF	(104)	IP
H–C≡C–CHO	OVGF, 2ph-TDA	(88,105)	IP
N_2O_4	OVGF, 2ph-TDA	(106)	IP
CH_3NH_2	OVGF, 2ph-TDA	(42)	IP
CH_3NO_2	OVGF, 2ph-TDA	(65)	IP
C_2H_4O (ethylene oxide)	OVGF, 2ph-TDA	(42,107)	IP
CH_3CHO	OVGF, 2ph-TDA	(42)	IP
C_2H_4S (thiirane)	OVGF, 2ph-TDA	(96)	IP
C_3H_4 (allene)	OVGF, 2ph-TDA	(74,98)	IP
C_3H_4 (cyclopropene)	OVGF, 2ph-TDA	(96)	IP
CH_3–C≡C–H	OVGF, 2ph-TDA	(53)	IP
C_2H_3CN	OVGF, 2ph-TDA	(42)	IP
trans-C_2H_2FCN	OVGF, 2ph-TDA	(42)	IP
H–C≡C–COOH	OVGF, 2ph-TDA	(88,105)	IP
H–C≡C–C≡C–CN	OVGF, 2ph-TDA	(53)	IP
SF_6	OVGF	(42,108,109)	IP
C_2H_6	OVGF, 2ph-TDA, GF	(74,76,110)	IP
C_2H_5N (ethyleneimine)	OVGF, 2ph-TDA	(42,107)	IP
$C_2H_2N_4$ (s-tetrazine)	OVGF, 2ph-TDA	(111)	IP
$C_2H_2(CN)_2$ (trans-, cis-, 1, 1-)	OVGF, 2ph-TDA	(42)	IP
$HCOOCH_3$	OVGF, 2ph-TDA	(53)	IP
H–C≡C–CH_2OH	OVGF, 2ph-TDA	(88,105)	IP
H_2C=CHCHO (acrolein)	OVGF, 2ph-TDA	(88)	IP
C_4H_4 (butatriene)	OVGF, 2ph-TDA	(74,98,112)	IP, ve, ig
CH_3–C≡C–CN	OVGF, 2ph-TDA	(53,59,79)	IP
H–C≡C–C≡C–C≡C–H	OVGF, 2ph-TDA	(53,76)	IP
NC–C≡C–C≡C–CN	OVGF, 2ph-TDA	(53)	IP
B_2H_6	OVGF, 2ph-TDA	(65)	IP
CH_3OCH_3	OVGF, 2ph-TDA	(42)	IP
CH_3CH_2OH	OVGF, 2ph-TDA	(53)	IP
C_3H_6 (cyclopropane)	OVGF, 2ph-TDA	(42,74,107)	IP

Table 1 (continued)

Molecule [a]	Method [c]	Refs. [b]	Remarks [c]
CH_3CH_2CN	OVGF, 2ph-TDA	(53)	IP
$C_3H_3N_3$ (s-triazine)	OVGF, 2ph-TDA	(111)	IP
C_4H_4O (furan)	OVGF, 2ph-TDA	(42,113)	IP
C_4H_4S (thiophene)	OVGF, 2ph-TDA	(42,113)	IP
H-C≡C-C≡C-C≡C-CN	OVGF, 2ph-TDA	(53)	IP
CH_3COCH_3	OVGF, 2ph-TDA	(42)	IP
C_4H_6 (1,3-butadiene)	OVGF, 2ph-TDA	(74,76)	IP
C_4H_5N (pyrrole)	OVGF, 2ph-TDA	(42,114)	IP
C_4H_5P (phosphole)	OVGF	(114)	IP
$C_4H_4N_2$ (pyrazine, pyrimidine, pyridazine)	OVGF, 2ph-TDA	(111)	IP
$C_2(CN)_4$	OVGF, 2ph-TDA	(42)	IP
C_5H_6(cyclopentadiene)	OVGF, 2ph-TDA	(42,115)	IP
C_4H_6Si (silacyclopentadiene)	OVGF	(115)	IP
C_5H_5N (pyridine)	OVGF, 2ph-TDA	(111,116)	IP
C_5H_5P (phosphoridine)	OVGF	(116)	IP
C_6H_6 (benzene)	OVGF, 2ph-TDA	(74,76,117)	IP, vs
p-$C_6H_4F_2$ (para-difluorobenzene)	OVGF, 2ph-TDA	(39,118)	IP
C_7H_8 (norbornadiene)	OVGF, 2ph-TDA	(42,119)	IP
p-$C_6H_4(NO_2)(NH_2)$ para-nitroaniline)	2ph-TDA	(120,121)	IP

[a] The ordering of the atoms and molecules is with respect to the nuclear charge and the number of atoms in the molecule. Within each group of n-atomic molecules the ordering is somewhat arbitrary. For the larger molecules organic ones are listed first and they are ordered with respect to the number of carbon atoms in the molecule.

[b] The references to the table are compiled below as supplementary references.

[c] The following abbreviations have been used:

OVGF	present outer valence Green's function method or closely related version;
2ph-TDA	2ph-TDA, extended 2ph-TDA or closely related method;
EOM	equation of motion method;
GF	some other type of Green's function method;
IP	ionization potential. Relative intensities are often also given and available ionization spectra (photoelectron and (e, 2e) spectra) are discussed;
EA	electron affinity;
e–S	electron–atom or electron–molecule scattering cross sections;
E_c	electron correlation energy;
ve	vibronic coupling effects in the ionization spectrum, e.g. Jahn–Teller effect;
vs	vibrational structure in the ionization spectrum;
ig	geometry of the molecular ion.

List of supplementary references to table 1

(1) J.D. Doll and W.P. Reinhardt, J. Chem. Phys. 57 (1972) 1169.
(2) G.D. Purvis and Y. Öhrn, J. Chem. Phys. 60 (1974) 4063.
(3) M. Berman and U. Kaldor, Chem. Phys. Lett. 79 (1981) 489.

(4) M. Berman and U. Kaldor, J. Phys. B 14 (1981) 3993.
(5) P.W. Langhoff and A.J. Hernandez, Chem. Phys. Lett. 49 (1977) 361.
(6) W.P. Reinhardt and J.B. Smith, J. Chem. Phys. 58 (1973) 2148.
(7) P. Albertsen and P. Jörgensen, J. Chem. Phys. 70 (1979) 3254.
(8) O. Walter and J. Schirmer, J. Phys. B 14 (1981) 3805.
(9) O. Walter, W. von Niessen, J. Schirmer and L.S. Cederbaum, unpublished results.
O. Walter, Thesis, Heidelberg (1983).
(10) M.F. Herman, K.F. Freed, D.L. Yeager and B. Liu, J. Chem. Phys. 72 (1980) 611.
(11) L.S. Cederbaum and W. von Niessen, Chem. Phys. Lett. 24 (1974) 263.
(12) G.D. Purvis and Y. Öhrn, J. Chem. Phys. 65 (1976) 917.
(13) W. von Niessen, L.S. Cederbaum and G.H.F. Diercksen, J. Chem. Phys. 67 (1977) 4124.
(14) H. Yamakawa, T. Aoyama and H. Ichikawa, Chem. Phys. Lett. 47 (1977) 269.
(15) H.A. Kurtz and Y. Öhrn, J. Chem. Phys. 69 (1978) 1162.
(16) M.F. Herman, K.F. Freed and D.L. Yeager, Advan. Chem. Phys. 48 (1981) 1.
(17) H. Reitz and W. Kutzelnigg, Chem. Phys. Lett. 37 (1979) 111.
(18) R. Moccia, R. Resta and M. Zandomeneghi, Chem. Phys. Lett. 37 (1976) 556.
(19) A. Klonover and U. Kaldor, Chem. Phys. Lett. 51 (1977) 321.
(20) A. Klonover and U. Kaldor, J. Phys. B 12 (1979) 3797.
(21) K.D. Jordan and J. Simons, J. Chem. Phys. 67 (1977) 4027.
(22) L.S. Cederbaum, W. Domcke and W. von Niessen, J. Phys. B 10 (1977) 2963.
(23) L.S. Cederbaum, G. Hohlneicher and W. von Niessen, Chem. Phys. Lett. 18 (1973) 503.
(24) L.S. Cederbaum and W. von Niessen, J. Chem. Phys. 62 (1975) 3824.
(25) P.-O. Nerbrant, Intern. J. Quantum Chem. 9 (1975) 901.
(26) G.B. Bacskay and N.S. Hush, Chem. Phys. 16 (1976) 219.
(27) H. Kurtz, G.D. Purvis and Y. Öhrn, Intern. J. Quantum Chem. S10 (1976) 331.
(28) M.F. Herman, D.L. Yeager, K.F. Freed and V. McKoy, Chem. Phys. Lett. 46 (1977) 1.
(29) T.-T. Chen, W.D. Smith and J. Simons, Chem. Phys. 62 (1974) 296.
(30) G.D. Purvis and Y. Öhrn, Intern. J. Quantum Chem. S11 (1977) 359.
(31) J. Schirmer, L.S. Cederbaum, W. Domcke and W. von Niessen, Chem. Phys. 26 (1977) 149.
(32) M.F. Herman, D.L. Yeager and K.F. Freed, Chem. Phys. 29 (1978) 77.
(33) M.F. Herman, K.F. Freed and D.L. Yeager, Chem. Phys. 32 (1978) 437.
(34) J. Baker and B.T. Pickup, Chem. Phys. Lett. 76 (1980) 537.
(35) M. Mishra and Y. Öhrn, Chem. Phys. Lett. 71 (1980) 549.
(36) M. Berman, O. Walter and L.S. Cederbaum, Phys. Rev. Lett. 50 (1983) 1979.
(37) G.D. Purvis and Y. Öhrn, J. Chem. Phys. 62 (1975) 2045.
(38) L.S. Cederbaum, G. Hohlneicher and W. von Niessen, Mol. Phys. 26 (1973) 1405.
(39) G. Bieri, L. Åsbrink and W. von Niessen, J. Electron Spectr. 23 (1981) 281.
(40) J. Schirmer, W. Domcke, L.S. Cederbaum and W. von Niessen, J. Phys. B 11 (1978) 1901.
(41) J.V. Ortiz B. and Y. Öhrn, J. Chem. Phys. 72 (1980) 5744.
(42) G. Bieri, L. Åsbrink and W. von Niessen, J. Electron Spectr. 27 (1982) 129.
(43) K.M. Griffing, J. Kenney, J. Simons and K.D. Jordan, J. Chem. Phys. 63 (1975) 4073.
(44) V. Carravetta and R. Moccia, Mol. Phys. 35 (1978) 129.
(45) I. Cacelli, R. Moccia and V. Carravetta, Chem. Phys. Lett. 70 (1980) 569.
(46) M. Jascunski, B.T. Pickup and R. McWeeny, Chem. Phys. Lett. 90 (1982) 167.
(47) J. Kenney and J. Simons, J. Chem. Phys. 62 (1975) 592.
(48) K.M. Griffing and J. Simons, J. Chem. Phys. 62 (1975) 535.
(49) W.D. Smith, T.-T. Chen and J. Simons, J. Chem. Phys. 61 (1974) 2670.
(50) W. von Niessen, L.S. Cederbaum, W. Domcke and G.H.F. Diercksen, Chem. Phys. 56 (1981) 43.
(51) W. von Niessen, L. Åsbrink, G. Bieri and A. Svensson, J. Electron Spectr. 26 (1982) 173.
(52) K.M. Griffing and J. Simons, J. Chem. Phys. 64 (1976) 3610.
(53) W. von Niessen, L.S. Cederbaum, J. Schirmer, G.H.F. Diercksen and W.P. Kraemer, J. Electron Spectr. 28 (1982) 45.

(54) J.V. Ortiz B. and Y. Öhrn, Chem. Phys. Lett. 77 (1981) 548.
(55) W. Domcke, L.S. Cederbaum, W. von Niessen and W.P. Kraemer, Chem. Phys. Lett. 43 (1976) 258.
(56) W. Domcke, L.S. Cederbaum, W. von Niessen and G.H.F. Diercksen, J. Electron Spectr. 11 (1979) 239.
(57) W. von Niessen, L.S. Cederbaum, W. Domcke and G.H.F. Diercksen, Mol. Phys. 32 (1976) 1057.
(58) J. Schirmer, L.S. Cederbaum, W. Domcke and W. von Niessen, Chem. Phys. Lett. 57 (1978) 582.
(59) G. Bieri, E. Heilbronner, V. Hornung, E. Kloster-Jensen, J.P. Maier, F. Thommen and W. von Niessen, Chem. Phys. 36 (1979) 1.
(60) H. Köppel, L.S. Cederbaum, W. Domcke and W. von Niessen, Chem. Phys. 37 (1979) 303.
(61) W. Domcke, L.S. Cederbaum, J. Schirmer, W. von Niessen, C.E. Brion and K.H. Tan, Chem. Phys. 40 (1979) 171.
(62) J.P.D. Cook, M.J. White, C.E. Brion, W. Domcke, L.S. Cederbaum and W. von Niessen, J. Electron Spectr. 22 (1981) 261.
(63) J. Schirmer, W. Domcke, L.S. Cederbaum, W. von Niessen and L. Åsbrink, Chem. Phys. Lett. 61 (1979) 30.
(64) H. Köppel, L.S. Cederbaum and W. Domcke, Chem. Phys. 69 (1982) 175.
(65) L. Åsbrink, A. Svensson, W. von Niessen and G. Bieri, J. Electron Spectr. 24 (1981) 293.
(66) W. von Niessen and L.S. Cederbaum, Mol. Phys. 43 (1981) 897.
(67) E. Andersen and J. Simons, J. Chem. Phys. 65 (1976) 5393.
(68) W. von Niessen, L.S. Cederbaum, W. Domcke and G.H.F. Diercksen, J. Chem. Phys. 66 (1977) 4893.
(69) W. Domcke, L.S. Cederbaum, J. Schirmer, W. von Niessen and J.P. Maier, J. Electron Spectr. 14 (1978) 59.
(70) E. Andersen and J. Simons, Chem. Phys. 66 (1977) 2427.
(71) L.S. Cederbaum, W. Domcke and W. von Niessen, Mol. Phys. 33 (1977) 1399.
(72) L.S. Cederbaum, W. Domcke, W. von Niessen and W.P. Kraemer, Mol. Phys. 34 (1977) 381.
(73) W. von Niessen, J. Electron Spectr. 17 (1979) 197.
(74) L.S. Cederbaum, W. Domcke, J. Schirmer, W. von Niessen, G.H.F. Diercksen and W.P. Kraemer, J. Chem. Phys. 69 (1978) 1591.
(75) G. Bieri, A. Schmelzer, L. Åsbrink and M. Jonsson, Chem. Phys. 49 (1980) 213.
(76) G. Bieri and L. Åsbrink, J. Electron Spectr. 20 (1980) 149.
(77) G. Bieri, E. Heilbronner, J.-P. Stadelmann, J. Vogt and W. von Niessen, J. Am. Chem. Soc. 99 (1977) 6832.
(78) L.S. Cederbaum, W. Domcke and W. von Niessen, Chem. Phys. 10 (1975) 459.
(79) L. Åsbrink, W. von Niessen and G. Bieri, J. Electron Spectr. 21 (1980) 93.
(80) L.S. Cederbaum, W. Domcke, J. Schirmer and H. Köppel, J. Chem. Phys. 72 (1980) 1348.
(81) W. Domcke, L.S. Cederbaum, H. Köppel and W. von Niessen, Mol. Phys. 34 (1977) 1759.
(82) H. Köppel, L.S. Cederbaum, W. Domcke and W. von Niessen, Mol. Phys. 35 (1978) 1283.
(83) E. Haller, L.S. Cederbaum, W. Domcke and H. Köppel, Chem. Phys. Lett. 72 (1980) 427.
(84) W. von Niessen, W. Domcke, L.S. Cederbaum and W.P. Kraemer, J. Chem. Phys. 67 (1977) 44.
(85) L.S. Cederbaum, G. Hohlneicher and S. Peyerimhoff, Chem. Phys. Lett. 11 (1971) 421.
(86) L.S. Cederbaum, W. Domcke and W. von Niessen, Chem. Phys. Lett 34 (1975) 60.
(87) W. Domcke and L.S. Cederbaum, J. Chem. Phys. 64 (1976) 612.
(88) W. von Niessen, C. Bieri and L. Åsbrink, E. Electron Spectr. 21 (1980) 175.
(89) E. Haller, H. Köppel, L.S. Cederbaum, G. Bieri and W. von Niessen, Chem. Phys. Lett. 85 (1982) 12.
(90) E. Haller, H. Köppel, L.S. Cederbaum, W. von Niessen and G. Bieri, J. Chem. Phys. 78 (1983) 1359.
(91) W. von Niessen, W.P. Kraemer and L.S. Cederbaum, Chem. Phys. 24 (1977) 245.
(92) W. von Niessen, L.S. Cederbaum and W.P. Kraemer, Mol. Phys. 33 (1977) 1415.
(93) W. von Niessen and G.H.F. Diercksen, J. Electron Spectr. 20 (1980) 95.
(94) R. Cambi, G. Ciullo, A. Sgamellotti, F. Tarantelli, R. Fantoni, A. Giardini-Guidoni and A. Sergio, Chem. Phys. Lett. 80 (1981) 295.
(95) R. Fantoni, A. Giardini-Guidoni, M. Rosi, R. Tiribelli, R. Cambi, G. Ciullo, A. Sgamellotti and F. Tarantelli, Chem. Phys. Lett. 90 (1982) 445.
(96) W. von Niessen, W.P. Kraemer and J. Schirmer, Faraday Trans. II 77 (1981) 1461.
(97) W. von Niessen, Chem. Phys. 45 (1980) 47.
(98) W. von Niessen, G.H.F. Diercksen, L.S. Cederbaum and W. Domcke, Chem. Phys. 18 (1976) 469.
(99) H. Köppel, W. Domcke, L.S. Cederbaum and W. von Niessen, J. Chem. Phys. 69 (1978) 4252.

(100) H. Köppel, L.S. Cederbaum and W. Domcke, J. Chem. Phys. 77 (1982) 2014.
(101) G. Bieri, W. von Niessen, L. Åsbrink and A. Svensson, Chem. Phys. 60 (1981) 61.
(102) R. Fantoni, A. Giardini-Guidoni, R. Tiribelli, R. Cambi, G. Ciullo, A. Sgamellotti and F. Tarantelli, Mol. Phys. 45 (1982) 839.
(103) W. von Niessen, J. Am. Chem. Soc. 99 (1977) 7151.
(104) W. von Niessen, G.H.F. Diercksen and L.S. Cederbaum, J. Am. Chem. Soc. 100 (1978) 6347.
(105) W. von Niessen, G. Bieri, J. Schirmer and L.S. Cederbaum, Chem. Phys. 65 (1982) 157.
(106) W. von Niessen, W. Domcke, L.S. Cederbaum and J. Schirmer, Faraday Trans. II 74 (1978) 1550.
(107) W. von Niessen, L.S. Cederbaum and W.P. Kraemer, Theoret. Chim. Acta 44 (1977) 85.
(108) W. von Niessen, L.S. Cederbaum and G.H.F. Diercksen, Chem. Phys. 11 (1976) 399.
(109) W. von Niessen, W.P. Kraemer and G.H.F. Diercksen, Chem. Phys. Lett. 63 (1979) 65.
(110) I. Cacelli, R. Moccia and V. Carravetta, Theoret. Chim. Acta 59 (1981) 461.
(111) W. von Niessen, W.P. Kraemer and G.H.F. Diercksen, Chem. Phys. 41 (1979) 113.
(112) L.S. Cederbaum, W. Domcke, H. Köppel and W. von Niessen, Chem. Phys. 26 (1977) 169.
(113) W. von Niessen, W.P. Kraemer and L.S. Cederbaum, J. Electron Spectr. 8 (1976) 179.
(114) W. von Niessen, L.S. Cederbaum and G.H.F. Diercksen, J. Am. Chem. Soc. 98 (1976) 2066.
(115) W. von Niessen, W.P. Kraemer and L.S. Cederbaum, Chem. Phys. 11 (1976) 385.
(116) W. von Niessen, G.H.F. Diercksen and L.S. Cederbaum, Chem. Phys. 10 (1976) 349.
(117) W. von Niessen, L.S. Cederbaum and W.P. Kraemer, J. Chem. Phys. 65 (1976) 1378.
(118) W. von Niessen, G.H.F. Diercksen and L.S. Cederbaum, Chem. Phys. Lett. 45 (1977) 295.
(119) W. von Niessen and G.H.F. Diercksen, J. Electron Spectr. 16 (1979) 351.
(120) W. Domcke, L.S. Cederbaum, J. Schirmer and W. von Niessen, Phys. Rev. Lett. 42 (1979) 1237.
(121) W. Domcke, L.S. Cederbaum, J. Schirmer and W. von Niessen, Chem. Phys. 39 (1979) 149.
(122) J. Baker and B.T. Pickup, Mol. Phys. 49 (1983) 651.
(123) J. Baker, Chem. Phys. Lett. 101 (1983) 136.

the other molecules are only briefly addressed. S-tetrazine represents an organic molecule of chemical interest and $ZnCl_2$ is a simple representative of inorganic compounds with transition metal atoms which have received much attention lately.

5.1. N_2

The objective of this section is to provide model applications demonstrating the capabilities of the extended 2ph-TDA. This approximation is identical to the full third-order ADC approximation, i.e. to ADC(3), and closely related to the third-order approximation derived within the EOM approach. The capabilities of the OVGF method, which is also correct to third order, have been discussed in detail elsewhere [28,67] and will receive only minor attention here. We follow here very closely the recent work of Schirmer and Walter [68] on N_2 and CO.

The HF one-particle data for N_2 have been obtained from LCAO – SCF calculations for the neutral molecule ground states using the experimental equilibrium position $R = 2.0693$ au. The basis set is built up of Cartesian Gaussian functions.

It consists of eleven functions of s-type and seven function of p-type contracted to five functions of s-type and four functions of p-type. The exponential parameters and contraction coefficients are taken from the work of Salez and Veillard [69]. (We choose the following contractions: no. 14 for s, no. 8 for p.) In addition, one function of d-type is added to the basis set ($\alpha_d = 0.75$).

The 2ph-TDA calculation is performed by the two-step diagonalization procedure outlined in section 3 using the spin-free formulation of these equations (appendix A). The spatial symmetry has been exploited by selecting the configurations with respect to the subgroup D_{2h}. The orbital space has almost completely been exhausted. Out of 46 HF-orbitals 42 orbitals are maintained. Those omitted are the two 1s core orbitals and the highest two virtual orbitals which are counterparts to the core orbitals. The largest dimension of the configuration space II (2h–1p) is 146 and a full diagonalization was possible. This was no longer possible for the 2p–1h block I where the maximum dimension is 1028. Here, a matrix of 400 selected configurations was diagonalized. The remaining configurations (j, k, l) were included in the arrow-type matrix **A** by taking the first-order approximations (see section 3.2).

$$\omega_{jkl} = -\epsilon_j + \epsilon_k + \epsilon_l + C^{\mathrm{I}}_{jkl,jkl}$$

for the eigenvalues and

$$m_p^{(j,k,l)} = U_{p,jkl}$$

for the coupling amplitudes. As selection criterion the coupling strength of eq. (3.12) was used. Certainly, this technical approximation in the diagonalization of block I will only affect the results for the $N-1$ particle states very little, since they are energetically well separated from the 2p–1h configurations, which we treat approximately. The diagonalization of **A** (Dyson equation) was done for the full space of 2h–1p (II) and 2p–1h (I) configurations. The diagonalization procedure used to diagonalize **A** is discussed in section 4. The static self-energy part has been determined iteratively by inserting repeatedly the result of eq. (2.26) in eq. (2.31). The final results are obtained after three iterations.

The results of both the 2ph-TDA and extended 2ph-TDA calculations for N_2 is shown in table 2. Also some experimental ionization potentials are presented. The vertical ionization potentials which are considered here are taken as the centroids of the bands in the photoelectron spectrum. A correction, which in general is small, arises from a different (harmonic) curvature of the ground and the ionic potential curves at the ground-state geometry and from anharmonicities in the potential curves [6]. The vertical experimental values derived for N_2 should be correct to ± 0.1 eV.

The ionic main states $X^2\Sigma_g^+$, $A^2\Pi_u$ and $B^2\Sigma_u^+$ of N_2^+ corresponding to the outer valence orbitals $3\sigma_g$, $1\pi_u$ and $2\sigma_u$ are well described by the present extended 2ph-TDA calculations. The discrepancy between the calculated ionization potentials (IP's) and the experimental values is smaller than 0.2 eV, which at present is considered as the bench mark of accuracy for good "state of the art" calculations [28,70–73]. For comparison we present and discuss some representative results of other approaches (see table 3). In table 3 we also present the results of the complete OVGF calculation for the present basis set. These results are in close agreement with those obtained previously for larger basis sets (which invoke more than one polarization function) and are reported in ref. [28]. The most extensive configuration interaction (CI) calculations on the N_2 ionization potentials have been performed by Ermler and McLean [73]. The results in table 3 are obtained for a large basis of Slater type functions (6s4p3d2f). The CI procedure takes into account all single and double excitations with respect to the neutral and ionic Hartree–Fock

Table 2
Vertical ionization energies I_n (eV) and intensity coefficients $x_p^{(n)^2}$ in N_2 obtained from 2ph-TDA and extended 2ph-TDA (ADC(3)) calculations. States with $x_p^{(n)^2} < 0.01$ are omitted except for the first satellite states in each symmetry

Orbital p	HF $-\epsilon_p$	2ph-TDA		Ext. 2ph-TDA		Experiment I_n	Leading configurations
		I_n	$x_p^{(n)^2}$	I_n	$x_p^{(n)^2}$		
$1\pi_u$	16.80	16.38	0.91	16.85	0.92	17.0 [a]	$1\pi_u^{-1}$
		28.63	< 0.01	28.63	< 0.01		$2\sigma_u^{-1}3\sigma_g^{-1}1\pi_g$
		35.53	< 0.01	35.57	< 0.01		$2\sigma_u^{-1}3\sigma_g^{-1}1\pi_g$
$3\sigma_g$	17.28	14.21	0.88	15.70	0.91	15.6 [a]	$3\sigma_g^{-1}$
$2\sigma_u$	21.17	17.22	0.81	18.96	0.82	18.8 [a]	$2\sigma_u^{-1}$
		24.98	0.04	25.13	0.07	25.2 [b]	$3\sigma_g^{-1}1\pi_u^{-1}1\pi_g$
		35.90	0.04	35.34	0.02		$3\sigma_g^{-1}1\pi_u^{-1}1\pi_g$
$2\sigma_g$	40.27						
		28.87	0.14	29.20	0.10	29.4 [c]	$2\sigma_u^{-1}1\pi_u^{-1}1\pi_g$
		36.41	0.49	37.43	0.30		$2\sigma_u^{-1}1\pi_u^{-1}1\pi_g$
		37.53	0.01	37.56	0.10		$3\sigma_g^{-2}4\sigma_g$
		39.18	0.01	38.97	0.14		$3\sigma_g^{-1}1\pi_u^{-1}2\pi_u$
		39.25	0.04	39.25	0.04		$3\sigma_g^{-1}2\sigma_u^{-1}3\sigma_u$
		40.02	0.09	39.94	0.15		$2\sigma_u^{-2}4\sigma_g$
		40.76	0.09	40.62	0.06		$1\pi_u^{-2}5\sigma_g$
							$2\sigma_g^{-1}$
$1\pi_g$ [d]	−3.66						
		24.36	< 0.01	24.38	< 0.01		$1\pi_u^{-2}1\pi_g$
		24.56	< 0.01	24.56	< 0.01		$3\sigma_g^{-2}1\pi_g$
$1\delta_u$ [d]	−58.55						
		25.47	< 0.01	25.48	< 0.01		$3\sigma_g^{-1}1\pi_u^{-1}1\pi_g$
		26.26	< 0.01	26.26	< 0.01		$3\sigma_g^{-1}1\pi_u^{-1}1\pi_g$
$1\delta_g$ [d]	−43.78						
		29.33	< 0.01	29.33	< 0.01		$2\sigma_u^{-1}1\pi_u^{-1}1\pi_g$
		31.55	< 0.01	31.56	< 0.01		$2\sigma_u^{-1}1\pi_u^{-1}1\pi_g$

[a] Turner et al. [85].
[b] Åsbrink and Fridh [61].
[c] Krummacher et al. [55].
[d] These orbitals are not occupied in the Hartree–Fock ground state. Non-vanishing intensity coefficients $x_p^{(n)^2}$ for the satellite states n arise from ground state correlation.

configurations. The contribution of quadruple excitations is estimated by the Davidson correction [88–91]. Chong and Langhoff [74] have calculated the ionization potentials of N_2 using third-order Rayleigh–Schrödinger perturbation theory plus a geometrical approximation. The results shown in table 3 are obtained with the same basis as the present one except for a different 11s to 5s contraction.

Within the EOM approach several calculations on the N_2 ionization potentials have been reported [70,74,75]. In table 3 the results of Herman et al. [70] are shown. These data are

Table 3
Comparison of outer-valence vertical ionization energies (eV) in N_2

	ADC(3) [a]	OVGF [b]	EOM [c]	RSPT [d]	CI [e]	Exp. [f]
$X^2\Sigma_g^+$	15.70	15.44	15.94	15.45	15.65	15.6
$A^2\Pi_u$	16.85	16.74	17.20	16.48	16.79	17.0
$B^2\Sigma_u^+$	18.96	18.89	19.01	19.04	19.00	18.8

[a] Present results.
[b] Von Niessen [84].
[c] Herman et al. [70].
[d] Chong and Langhoff [72].
[e] Ermler and McLean [73].
[f] Turner et al. [85].

obtained from a double-zeta plus polarization basis of Slater functions (4s2p1d) being qualitatively comparable to our basis. As in our calculation and in the OVGF calculation, the virtual orbital space has been essentially exhausted. The EOM-equations employed by Herman et al. differ from the extended 2ph-TDA equations by the expression for the static self-energy part $\boldsymbol{\Sigma}(\infty)$ in the one-particle block of eq. (2.31). In order to obtain a treatment that is consistent through third order one has to employ at least the complete third order contribution $\boldsymbol{\Sigma}^{(3)}(\infty)$ for the static self-energy part. The EOM calculations discussed here, however, use only a part of $\boldsymbol{\Sigma}^{(3)}(\infty)$ according to the original derivation of the EOM-equations by Simons and Smith [76], namely the parts A1 and A2 (adopting here the terminology of ref. [17]). In the extended 2ph-TDA, on the other hand, the static self-energy part is obtained self-consistently according to eqs. (2.26), (2.17) and (2.28). This leads to an approximation for $\boldsymbol{\Sigma}(\infty)$ that is complete through fourth-order in perturbation theory and moreover contains contributions through infinite order. A good approximation for $\boldsymbol{\Sigma}(\infty)$ is essential to obtain accurate results, since, in general, the contributions introduced by these terms are often of the order 0.5 eV. A shift $\Delta\Sigma_{pp}(\infty)$ in the diagonal element corresponding to the orbital p introduces approximately the shift

$$\Delta I_p = -x_p^2 \Delta\Sigma_{pp}(\infty)$$

for the ionization potential I_p. Here, x_p denotes the transition amplitude obtained for $\Delta\Sigma_{pp}(\infty) = 0$. In table 4 the diagonal elements $\Sigma_{pp}(\infty)$ are shown for the valence orbitals of N_2 in the

Table 4
Diagonal static self-energy contributions $\Sigma_{pp}(\infty)$ (eV) for the valence orbitals in N_2 [a]

Orbital	Third order	$A1 + A2$	ADC(3)
$3\sigma_g$	0.80	0.33	0.58
$1\pi_u$	0.69	0.42	0.46
$2\sigma_u$	0.68	0.30	0.50
$2\sigma_g$	0.70	0.25	0.43

[a] The employed basis set and orbital space are specified in section 5.1.

three approximations discussed above. The difference between the partial and the full third-order contribution is considerable (up to 0.5 eV). The self-consistent fourth- (and higher-)order approximation and probably the exact values mediate between the other two versions. We mention that the incomplete consideration of $\mathbf{\Sigma}^{(3)}(\infty)$ in otherwise consistent third-order equations leads to a severe dependence of the results on the truncation of the virtual space. This effect certainly limits the value of the results in the work of Bacskay and Hush [77].

In the region of higher ionization energy (> 20 eV) secondary (satellite) peaks appear in the spectrum which correspond to 2h–1p configurations (single hole plus single excitations). These states obtain spectral intensity via the admixture of single hole (or particle) configurations, measured by the transition amplitudes $x_p^{(n)}$ of eq. (2.12). A prominent example is the $C^2\Sigma_u^+$ state appearing in the experimental spectra [61] at 25.2 eV (estimated centroid). This satellite being associated with the $3\sigma_g^{-1}1\pi_u^{-1}1\pi_g$ configuration has 7% of the total intensity available for the $2\sigma_u$ orbital according to the extended 2ph-TDA results. A second $^2\Sigma_u$ satellite corresponding to this configuration bearing 2% of the $2\sigma_u$ partial cross section is found 10 eV above the C state. The ionization energies of the 2h–1p excited states are treated consistently through first-order both in the previous 2ph-TDA and in the present extended version. Accordingly, one finds only small changes when comparing the resulting energies in the two methods. On the other hand, the transition amplitudes are given exactly up to second order in the extended 2ph-TDA. This introduces a considerable modification of the intensities with respect to the previous results as can be seen by inspecting the relative intensities of the $^2\Sigma_u$ satellites. The good agreement for the ionization energy of the C state is probably fortuitous since, in general, the first order-treatment is not sufficient to provide accurate results.

It should be noted that these satellite states have been studied in previous theoretical work. A qualitative description has been given by full CI calculations which include only a few occupied and virtual orbitals [78–82]. A more extensive CI treatment has been presented by Kosugi et al. [83] and by Langhoff et al. [24]. A third-order EOM calculation employing the full third-order static self-energy part $\mathbf{\Sigma}^{(3)}(\infty)$ and a double zeta plus polarization basis of Slater functions has been presented by Herman et al. [75]. Although there are differences with respect to basis sets and the methods employed, all calculations give very similar results for the ionization energies of the energetically lowest (2h–1p) satellite states.

A different situation is found for the ionization out of the inner valence $2\sigma_g$ orbital of N_2. The $2\sigma_g$ hole-configuration lying energetically above the first 2h–1p configurations couples strongly to several of the latter (and higher excited) configurations. As a consequence one no longer finds an ionic $2\sigma_g$ main state but a multitude of final $^2\Sigma_g$ states sharing the partial $2\sigma_g$ intensity. For the $2\sigma_g$ ionization of N_2 this effect is demonstrated by the present results in table 2 and by the previous results [24,39,75]. Our calculation finds seven major ($x_p > 0.01$) $^2\Sigma_g$ components extending from 29.2–40.6 eV. The first state characterized as the $\pi\pi^*$ excitation $1\pi_u^{-1}1\pi_g$ on the $2\sigma_u$ hole configuration can be assigned to the peak at 29.4 eV (peak maximum) in the experimental spectrum. Whereas this state is similarly reproduced by all previous calculations [24,39,75,83], the theoretical $^2\Sigma_g$ spectrum at higher binding energy is extremely sensitive to details of the calculation, such as basis sets, truncation of the virtual space and the methods employed. This can be seen by comparing the results of the two 2ph-TDA versions as well as the results of previous 2ph-TDA [24,39], CI [24] and EOM [75] calculations. Without going into detail one may state that only the breakdown effect as such is reproduced by the calculations,

whereas the detailed structure of the theoretical spectrum is still beyond an even qualitative agreement with experiment.

There are several reasons for this situation. The first deficiency arises from the use of a finite discrete basis of one-particle (HF) states. The energy region considered here is already close to the first double ionization threshold of N_2 (≈ 43 eV) to which several Rydberg series of N_2^+ excited states converge. Using a finite discrete basis only the very first members of such (2h–1p) excited Rydberg states are described properly. One obtains artificial states and thus an artificial spectral structure at higher excitation energy which can be viewed as an inadequate simulation of higher Rydberg and continuum states. The calculation still provides valuable information, since it specifies the various series that couple to the $2\sigma_g$ state (see table 2). However, the specific discrete structure may not be reliable. This explains the strong basis set dependence of the results which is experienced in the present calculations.

Besides this general deficiency there are shortcomings that are specific to the present extended 2ph-TDA and the third-order EOM approach. As has been mentioned, the ionization energies of the 2ph–1p excited states are treated consistently only to first-order, which certainly is not satisfactory, since both of the two (partially compensating) effects, i.e. ground-state correlation and coupling to the 3h–2p and 4h–3p excited configurations, are neglected. Moreover, some of the lowest 3h–2p excitations explicitly appear in the inner valence ionization spectrum. Both the CI calculations of Kosugi et al. [83] and of Langhoff et al. [24] predict states characterized as mainly $3\sigma_g^{-1}1\pi_u^{-2}1\pi_g^2$ at about 35 eV binding energy. Configurations of this type are also expected to mix with the 2h–1p configurations leading to a considerable modification of the present extended 2ph-TDA results. These types of deficiencies of the extended 2ph-TDA (ADC(3)) can be removed [19] by employing the ADC(4) which is the natural extension of ADC(3). The numerical effort required in solving the ADC(4) is, however, considerable.

5.2. s-tetrazine

The solution of the extended 2ph-TDA for larger molecules like s-tetrazine requires a considerable numerical effort when a good quality basis set is used. For such molecules the computation is rewarding because of the existing rich satellite structure and the failure of the Hartree–Fock calculation to assign even the main bands in the ionization spectrum. Extended basis sets can be used in the OVGF calculation, but only a small portion of the spectrum can be evaluated owing to the rich satellite structure which restricts the applicability of the method. To save computer time we have performed an extended 2ph-TDA calculation on s-tetrazine using a double-zeta basis without augmenting it by polarization functions. We use the results to qualitatively interprete the experimental observations [94,95]. A theoretical discussion of the ionization spectra of the azabenzenes including s-tetrazine has been given before [96,97].

The basis set used in the calculation on s-tetrazine is of double-zeta quality: [9s5p/4s]/(4s2p/2s) and consists of the basis sets of Huzinaga for the C, N and H atoms [93]. The Huzinaga contraction has been used. The core orbitals and their virtual counterparts have been omitted from the orbital basis in the extended 2ph-TDA calculation. In addition the energetically highest 8 virtual orbitals were left out. This leads to an orbital basis of 15 occupied and 29 virtual orbitals. For the different symmetry species the dimension of the matrices of block I range from 1400 to 1700 and of the matrices of block II from 700 to 900. In all cases 500 configurations were

selected and the resulting matrices were diagonalized completely. The remaining configurations were taken into account in a diagonal approximation in the Dyson equation. In the case of block I the selection was done according to the selection criterion of eq. (3.12), in the case of block II, on the other hand, the selection was done using eq. (3.10).

The extended 2ph-TDA predicts a large number of ionic states which acquire intensity in the photoelectron spectrum. For simplicity we have drawn in fig. 7 the calculated spectrum together with the experimental spectrum [94] recorded using He II radiation. The calculated ionization peaks are drawn as vertical bars at the computed ionization energies I_n. The height of a bar n is given by the sum over the pole strengths $|x_p^{(n)}|^2$. Since the Green's function matrix is nearly diagonal for s-tetrazine, a specific $|x_p^{(n)}|^2$ dominates in this sum and every bar can be assigned to originate from a given orbital. For the relation between the intensity of a line in the spectrum and the spectroscopic amplitude $x_p^{(n)}$ see section 2.1.

Let us briefly discuss the photoelectron spectrum. The observed and computed spectra exhibit

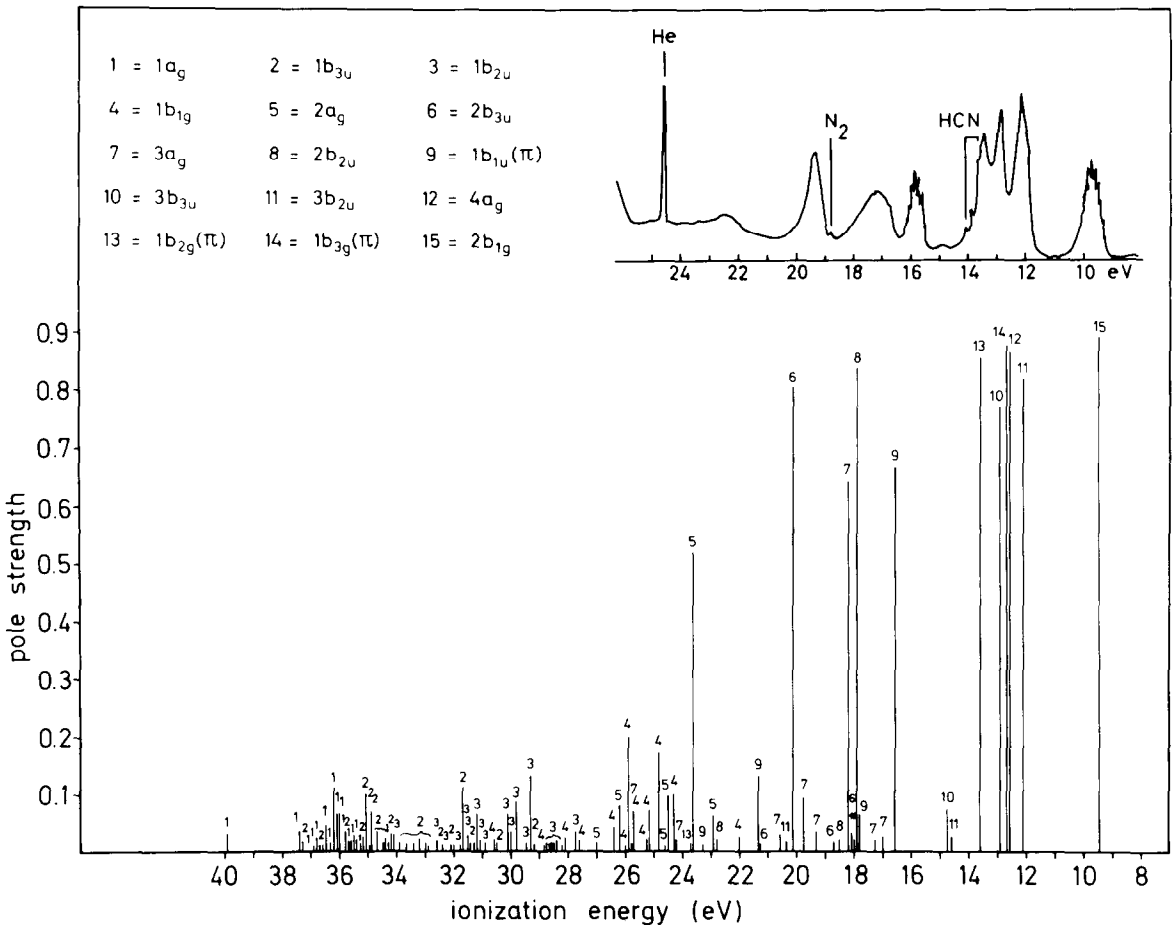

Fig. 7. Experimental and calculated photoelectron spectrum of s-tetrazine. The experimental spectrum [94] has been recorded using HeII radiation. The theoretical bar spectrum is calculated via the extended 2ph-TDA (for more details see text). Only lines with pole strengths greater or equal to 0.01 are shown. The numbering of the orbitals is according to the Hartree–Fock sequence.

a first main band just below 10 eV. The band arises from the ionization out of the outermost orbital $2b_{1g}$. The second band in the spectrum lies between 12 and 14 eV and is seen to include several main ionization peaks, the number of which is difficult to determine on experimental grounds alone. The calculation predicts this band to consist of five main ionization peaks. The ordering of the corresponding orbitals does not follow the ordering predicted by the Hartree–Fock calculation. The first peak, for example, is attributed to the $3b_{2u}$ orbital which is the fifth outermost orbital instead to the second outermost orbital $1b_{3g}$ (see fig. 7). The relative position of the closely lying main ionization potentials corresponding to the $4a_g$ and $1b_{3g}$ orbitals cannot be reliably determined. Probably a more adequate basis set could resolve the problem in case it leads to a larger separation of the energies. The third, fourth, fifth and sixth main band in the observed spectrum are predicted to correspond to the $1b_{1u}$, $2b_{2u} + 3a_g$, $2b_{3u}$ and $2a_g$ orbitals, respectively.

The calculated spectrum in fig. 7 exhibits numerous satellite lines above 14 eV. The breakdown of the one-particle picture of ionization is evident for the $1a_g$, $1b_{3u}$, $1b_{2u}$ and $1b_{1g}$ orbitals. Several of the remaining valence orbitals, e.g. $2a_g$ and $3a_g$, have lost considerable strength to satellite states. The experimental spectrum [94], which unfortunately extends only up to 25 eV, possesses a continuously growing underground which might be an indication for the rich satellite structure. Since there is an energy gap in the spectrum between the second and third main bands, it is possible to experimentally substantiate the theoretical prediction made by the extended 2ph-TDA that satellite peaks fall into this gap (see fig. 7).

5.3. Zinc dichloride

The field of high-temperature photoelectron spectroscopy of vapours has become very popular and with it the study of the ionic states of transition metal compounds. The interesting experimental spectra have stimulated theoretical work on the subject and a vast number of computations have been carried out (see, e.g., ref. [98–100] and references therein). In the following we briefly discuss our OVGF and extended 2ph-TDA computations on $ZnCl_2$ [100] which is a prototype of the many transition-metal dihalides studied in the literature. This molecule has been investigated several times experimentally [101–105], thereby serving as a model for testing new instrumental resolution techniques.

$ZnCl_2$ has been studied before [100] by the OVGF and 2ph-TDA methods and compared with $CdCl_2$ and $NiCl_2$. Let us briefly discuss the results qualitatively. The calculated ionization spectrum of $ZnCl_2$ exhibits three groups of lines. The first group at lowest binding energy corresponds to the outer valence orbitals $2\pi_g$, $1\pi_u$, $2\sigma_u$ and $3\sigma_g$ which are responsible for the bonding of the molecule. The second group of lines consists of three closely spaced lines. These correspond to the orbitals $1\delta_g$, $2\pi_g$ and $2\sigma_g$ which derive from the metal core d levels in a cylindrical ligand field. It is not useful to assign the observed peaks to the computed lines, since the observed peak separations are of a similar magnitude as the spin–orbit coupling constant for the zinc d subshell [104]. The third group of lines results upon ionization out of the $1\sigma_u$ and $1\sigma_g$ orbitals which have mainly chlorine 3s character. For these orbitals a breakdown of the molecular orbital picture of ionization is predicted.

We have recalculated the ionization spectrum of $ZnCl_2$ with the OVGF and extended 2ph-TDA methods using a slightly larger basis set than in the previous calculations. The basis set is [14s11p6d/12s9p]/(9s6p3d/6s4p). It consists of the basis set of Veillard for the Cl atoms [92]

Table 5
Vertical ionization energies of $ZnCl_2$ obtained from OVGF and extended 2ph-TDA calculations (all energies in eV)

Orbital	Orbital energy	OVGF	Extended 2ph-TDA	Experiment [105]
$2\pi_g$	12.60	11.82	11.69	11.87
$1\pi_u$	13.02	12.29	12.20	12.42
$2\sigma_u$	13.68	13.04	12.88	13.12
$3\sigma_g$	14.58	14.11	13.85	14.15

and the [14s9p5d] basis set of Huzinaga for the Zn atom [106] which is a slightly modified version of the basis of Wachters [107]. The two most diffuse s-type functions have been replaced with two s-type functions with exponential parameters $\alpha_s(Zn) = 0.32$, 0.08 to account for the effect of orbital contraction in chemical bonding. Two diffuse p-type functions with $\alpha_p(Zn) = 0.3$, 0.07 have been added to describe the 4p orbital on Zn and a further d-type function with $\alpha_d(Zn) = 0.2$ has been added following the recommendation of Hay [108]. 13 occupied and 43 virtual orbitals have been included in the OVGF calculation which exhausts the valence virtual orbital space; in the extended 2ph-TDA calculation 36 virtual orbitals were included; virtual orbitals with an orbital energy exceeding 4 au were thus left out. For the different symmetry species the dimension of the matrices of block I range from 1400 to 2400 and of block II from 700 to 850. Out of these 500 configurations were selected and the resulting matrices were diagonalized. The remaining configurations were taken into account in a diagonal approximation in the Dyson equation. In the case of block I the selection was done according to the selection criterion of eq. (3.12), in the case of block II, the selection was done using eq. (3.10).

The results of the present computations lead to the same qualitative interpretation of the spectrum as discussed above. The main quantitative difference is found for the ionization potentials derived from metal core d levels. In the 2ph-TDA we have found these ionization potentials to be centered around 17 eV and in the extended version we now obtain the values 20.0, 20.3 and 20.4 eV for the ionization of the $2\sigma_g$, $1\delta_g$ and $1\pi_g$ orbitals, respectively. Experimentally, the corresponding peaks are located between 19.0 and 19.5 eV implying a substantial improvement of the extended 2ph-TDA over the original version. Furthermore, the calculations indicate that basis set effects play an important role for this type of localized levels.

In table 5 we have collected the ionization potentials of the four outermost valence orbitals $2\pi_g$, $1\pi_u$, $2\sigma_u$ and $3\sigma_g$ calculated in the OVGF and extended 2ph-TDA methods. The ordering of the ionization potentials remains the same at all levels of theory ranging from the Hartree–Fock to the extended 2ph-TDA. The values obtained with the OVGF method using the present basis set are in excellent agreement with the measured values and differ only slightly (≈ 0.1 eV) from those previously determined via the same method and the smaller basis set. The results obtained with the extended 2ph-TDA show a significant improvement over the results of the 2ph-TDA computation by approximately an overall shift of 0.7 eV to higher binding energies. The former values are much closer to those of the OVGF and in good accord with the experiments.

5.4. *Electron affinities of C_2, P_2, SO_2 and O_3*

The knowledge of electron affinities of atoms and molecules is important for the understanding of a variety of physical and chemical processes. Unfortunately, the experimental as well as the

Table 6
Electron affinities of C_2, P_2, O_3 and SO_2 calculated with different basis sets (in eV)

Basis [f]	Vertical (HF)	Vertical (OVGF)	Adiabatic (OVGF)	Adiabatic (Experiment)
C_2				
[11s7p1d]/(5s4p1d)	3.19	3.46	3.47	
[12s8p1d]/(6s5p1d)	3.24	3.54	3.55	3.54 [a]
[11s7p2d]/(5s4p2d)	3.20	3.59	3.60	
P_2				
[12s9p2d]/(7s5p2d)	−0.59	0.002	0.12	0.3 ± 0.5 [b]
[12s9p3d]/(7s5p3d)	−0.60	0.006	0.13	0.24 ± 0.23 [c]
[13s10p2d]/(7s5p2d)	−0.38	0.176	0.30	
O_3				
[11s7p1d]/(5s4p1d)	1.44	1.76	2.26	
[10s6p1d]/(5s3p1d)	1.60	1.67	2.17	2.1028 [d]
SO_2				
[12s9p1d/9s5p]/(6s4p1d/4s2p)	0.73	0.84	1.08	1.097 [e]
[13s10p1d/10s6p1d]/(7s5p1d/5s3p1d)	0.51	0.69	0.93	

[a] Ref. [118].
[b] Ref. [119].
[c] Ref. [120].
[d] Ref. [121].
[e] Ref. [122].
[f] Basis sets and results on C_2 and P_2 are taken from ref. [115] and on SO_2 and O_3 from ref. [123].

theoretical determination of accurate electron affinities is difficult (see e.g., refs. [109,110]). The most accurate experimental method is the photodetachment method [109,111] which, however, can only be applied to species of which the negative ions are available with sufficiently high concentration. The theoretical approaches which have been used to compute electron affinities include configuration-interaction (see, e.g., refs. [112,113]), equation-of-motion [114], Green's function [115,116] and variation–perturbation [117] methods or in appropriate cases the ab initio SCF method with very extended basis sets [124]. These calculations indicate that extended basis sets must be used for a proper description of the electron correlation in the negative ion. Clearly, a method as the OVGF method, which does not involve the diagonalization of matrices, is particularly efficient when extended basis sets are to be used. We have tested the OVGF method in several cases and present here briefly the results for a few molecules. The extended 2ph-TDA has not yet been systematically applied to compute electron affinities using extended basis sets.

Table 6 shows the vertical and adiabatic electron affinities of C_2, P_2, O_3 and SO_2 computed via the OVGF method for several basis sets. The experimental adiabatic electron affinities are shown as well. The vertical electron affinity of a molecule M is defined as the difference between the total electronic energies of the negative ion M^- and M taken at the equilibrium geometry of M. The adiabatic electron affinity is given as the difference between the ground state energies of M^- and M. The energy separation between the adiabatic and vertical electron affinities is a measure for the change of equilibrium geometry due to electron attachment to M. Except for C_2, the

equilibrium geometries of the molecules shown in table 6 differ noticeably from the equilibrium geometries of the corresponding negative ions.

C_2^-, SO_2^- and O_3^- are seen to be stable molecules already on the Hartree–Fock level. The corresponding states may thus be characterized by the index of a single Hartree–Fock orbital which are $3\sigma_g$, $3b_1(\pi)$,and $2b_1(\pi)$, respectively. In all cases the many-body effects act to stabilize the negative ion. This finding is of crucial importance for P_2^- which is predicted to be unstable on the Hartree–Fock level, but stable when many-body effects are included. Basis set effects are seen to be important for P_2, O_3 and SO_2 and less important for C_2 for which the basis set is probably nearly large enough to achieve convergence. As is best demonstrated in the case of ozone, changes in the basis set may have different impact on the calculated Hartree–Fock and final electron affinity. In all cases the inclusion of diffuse functions in the basis set is essential for obtaining a reliable prediction on the value of the electron affinity. The need to include diffuse functions is quite obvious, since the attached electron is not as localized at the molecular site as are the electrons of the neutral molecule. A more detailed discussion of the present calculations including the description of the basis sets and the investigation of the changes of geometry due to electron attachment can be found elsewhere [115,123].

6. Concluding remarks

The one-particle Green's function, which gives information on relevant physical properties of many-particle systems, has been investigated. This function is connected via the Dyson equation to the self-energy part which is an effective energy-dependent one-particle potential. For the self-energy part a systematic series of approximation schemes, termed ADC(n), exists. The application of the ADC(n) gives rise to a self-energy part which is exact up to (and including) nth order in the perturbation expansion in terms of the electron–electron interaction. A partial summation of certain perturbation terms up to infinite order is also included. In the present work we have thoroughly studied the applicability of the ADC(3) which is also named extended 2ph-TDA. The working equations of this third order scheme have been given explicitly and a numerical procedure for their evaluation discussed. The solution of the Dyson equation has been shown to reduce to the diagonalization of matrices of the arrow type. Emphasis has been put on the computational solution of the eigenvalue problem of arrow matrices. An efficient procedure which allows the determination of all eigenvalues in a preselected interval is developed.

In addition to the ADC(3) we have discussed the computational procedure of another third-order method, the OVGF method, which has been successfully used many times before. The OVGF method is restricted to low energies only, but is very efficient there, since its application does not involve the diagonalization of matrices. For illustrative purposes applications to a few molecules are presented using both the ADC(3) and the OVGF methods. It has been demonstrated that at energies for which the OVGF method is applicable, both methods give similar results and in good agreement with experiment. The extended 2ph-TDA can be used to calculate the complete valence ionization spectra of molecules. The systematic application of the 2ph-TDA to a vast number of molecules has lead to the manifestation of the breakdown of the single-particle picture of ionization as a common phenomenon. The main ionization energies are well described by the extended 2ph-TDA and the description of the energies of the satellite states is

less accurate. Substantial improvement on the latter energies is expected from the ADC(4) which, however, is computationally rather involved.

Acknowledgements

The authors would like to thank Dr. W. Domcke for useful discussions over many years and Dr. O. Walter for a close cooperation on the subject. The SCF calculations reported in this work have been performed with the program system MUNICH. The authors are indebted to Dr. G. Diercksen and Dr. W. Kraemer for the permission to use this SCF program system. Financial support of the Deutsche Forschungsgemeinschaft is gratefully acknowledged. Part of this work has also been supported by the Fonds der Deutschen Chemischen Industrie, for which the authors would like to thank.

Appendix A. Spin-free working equations of the extended 2ph-TDA

In this appendix the spin-free formulation of the extended 2ph-TDA (ADC(3)) equations is briefly summarized. Let us first consider the calculation of the dynamic self-energy parts $\mathbf{M}^{\mathrm{I,II}}(\omega)$ according to eqs. (2.35), (2.40) and (2.41). Since the treatment of the cases I and II is analogous, we restrict ourselves for the moment to case I and drop the superscript when unessential. The eigenvalue problem (2.40) and the expressions (2.44b) and (2.46) for $\mathbf{K}$ and $\mathbf{C}$, respectively, are defined with respect to the set (j, k, l) of spin-orbitals j, k and l. Now we further specify the one-particle quantum numbers according to

$$p \rightarrow p\gamma,$$

where the Roman letter denotes the spin-free orbital and the Greek letter denotes the magnetic spin quantum number ($\gamma = \pm \frac{1}{2}$). The eigenvector components of eq. (2.40) now read $Y^{(n)}_{j\gamma k\kappa l\lambda}$. Instead of these original components one may use components which result from a unitary transformation and which correspond to states which are eigenfunctions of $\boldsymbol{S}^2$ and S_z. For a given set of spin-free orbitals j, k, l, where $k < l$, there are eight spin components. These can be transformed into a quartet state ($S = 3/2$) and to two doublet states ($S = 1/2$). In the case $k = l$ there is only a doublet state. The spin-symmetry adapted eigenvector components in the case $S = 1/2$ read

$$\begin{aligned}
Y^{(n)}_{jkl(1)} &= \frac{1}{\sqrt{2}}\left(Y^{(n)}_{j\beta k\alpha l\beta} - Y^{(n)}_{j\beta k\beta l\alpha}\right), \quad k < l, \\
Y^{(n)}_{jkl(2)} &= \frac{1}{\sqrt{6}}\left(2Y^{(n)}_{j\alpha k\alpha l\alpha} + Y^{(n)}_{j\beta k\alpha l\beta} + Y^{(n)}_{j\beta k\beta l\alpha}\right), \quad k < l, \\
Y^{(n)}_{jkk(1)} &= Y^{(n)}_{j\beta k\alpha k\beta}, \quad k = l,
\end{aligned} \tag{A.1}$$

where α and β denote the special spin quantum numbers $m = +1/2$ and $m = -1/2$, respectively.

Here, the M quantum number is $M = 1/2$ ($M = -1/2$ in case II). The quartet component (with $M = 1/2$) is found to be

$$Y^{(3/2,n)}_{jkl} = \frac{1}{\sqrt{3}}\left(-Y^{(n)}_{j\alpha k\alpha l\alpha} + Y^{(n)}_{j\beta k\alpha l\beta} + Y^{(n)}_{j\beta k\beta l\alpha}\right), \quad k < l. \tag{A.2}$$

Obviously, eqs. (A.1) and (A.2) and the analogous equations for the other M quantum numbers induce a unitary transformation $\mathbf{W}$ between the original and the new eigenvector components. It is easy to check that the transformed eigenvalue problem,

$$\mathbf{W}(\mathbf{K} + \mathbf{C})\mathbf{W}^{\dagger}\mathbf{W}\mathbf{Y} = \mathbf{W}\mathbf{Y}\boldsymbol{\Omega}, \tag{A.3}$$

decouples with respect to the total spin S and the magnetic quantum numbers M. Moreover, for a given S the resulting equations do not depend on M. The eigenvalue for the doublet states in terms of the components of (A.1) can, finally, be written in the spin-free form

$$\left(\omega^{(n)} + \epsilon_j - \epsilon_k - \epsilon_l\right)Y^{(n)}_{jkl(a)} - \sum C^{(1/2)}_{jkl(a),j'k'l'(a')}Y^{(n)}_{j'k'l'(a')} = 0, \tag{A.4}$$

where the spin-free configurations (j, k, l) are restricted by $k \le l$. The components of the transformed matrix $C^{(1/2)}$ are as follows (case I):

$$C^{(1/2)}_{jkl(1),j'k'l'(1)} = \left\{\delta_{jj'}V_{klk'l'} + \delta_{kk'}\left(-V_{j'lj'l'} + \tfrac{1}{2}V_{j'll'j}\right) + \delta_{ll'}\left(-V_{j'kjk'} + \tfrac{1}{2}V_{j'kk'j}\right)\right\} + \{k' \leftrightarrow l'\}, \tag{A.5a}$$

$$C^{(1/2)}_{jkl(1),j'k'l'(2)} = \tfrac{1}{2}\sqrt{3}\left\{\left(\delta_{kk'}V_{j'll'j} - \delta_{ll'}V_{j'kk'j}\right) - (k' \leftrightarrow l')\right\}, \tag{A.5b}$$

$$C^{(1/2)}_{jkl(2),j'k'l'(1)} = \tfrac{1}{2}\sqrt{3}\left\{\left(\delta_{kk'}V_{j'll'j} - \delta_{ll'}V_{j'kk'j}\right) + (k' \leftrightarrow l')\right\}, \tag{A.5c}$$

$$C^{(1/2)}_{jkl(2),j'k'l'(2)} = \left\{\delta_{jj'}V_{klk'l'} + \delta_{kk'}\left(-V_{j'lj'l'} + \tfrac{3}{2}V_{j'll'j}\right) + \delta_{ll'}\left(-V_{j'kjk'} + \tfrac{3}{2}V_{j'kk'j}\right)\right\} - \{k' \leftrightarrow l'\}, \tag{A.5d}$$

$$C^{(1/2)}_{jkl(1),j'k'k'(1)} = \sqrt{2}\left\{\delta_{jj'}V_{klk'k'} + \delta_{kk'}\left(-V_{j'ljk'} + \tfrac{1}{2}V_{j'lk'j}\right) + \delta_{lk'}\left(-V_{j'kjk'} + \tfrac{1}{2}V_{j'kk'j}\right)\right\}, \tag{A.5e}$$

$$C^{(1/2)}_{jkl(2),j'k'k'(1)} = \sqrt{\tfrac{3}{2}}\left(\delta_{kk'}V_{j'lk'j} - \delta_{lk'}V_{j'kk'j}\right), \tag{A.5f}$$

$$C^{(1/2)}_{jkk(1),j'k'k'(1)} = \delta_{jj'}V_{kkk'k'} + \delta_{kk'}\left(-2V_{j'kjk'} + V_{j'kk'j}\right). \tag{A.5g}$$

In these expressions we suppose $k < l$ and $k' < l'$. The special case $k' = l'$ ($k = l$) is considered by eqs. (A.5e)–(A.5g).

In case I j denotes an unoccupied spatial orbital and k, l doubly occupied spatial orbitals.

The spin-free formulation of case II is formally identical except for a different overall sign of the matrix

$$\mathbf{C}^{(1/2)\mathrm{II}} = -\mathbf{C}^{(1/2)\mathrm{I}}. \tag{A.6}$$

The one-particle indices j, k, l have a different meaning: j is restricted to (doubly) occupied spatial orbitals and k, l denote unoccupied spatial orbitals.

For completeness we also give the interaction matrix for the quartet states ($S = 3/2$) in the case I

$$C^{(3/2)}_{jkl,j'k'l'} = \delta_{jj'}V_{kl[k'l']} - \left(\delta_{kk'}V_{j'ljl'} + \delta_{ll'}V_{j'kjk'}\right) + (k' \leftrightarrow l'). \tag{A.7}$$

Here, the configurations (j, k, l) are restricted by $k < l$.

As the next step one has to determine the Dyson amplitudes $m^{(n)}_p$ of eq. (2.41). Writing the spin-quantum numbers explicitly one obtains

$$m^{(n)}_{p\rho} = \sum U^{\dagger}_{p\rho,j\gamma k\kappa l\lambda} Y^{(n)}_{j\gamma k\kappa l\lambda}. \tag{A.8}$$

The effective coupling amplitudes $U^{\dagger}_{p\rho,j\gamma k\kappa l\lambda}$ in the extended 2ph-TDA are specified by eqs. (2.44a), (2.48) and (2.49). By employing the spin-symmetry adapted eigenvector components, (A.1), (A.2), it is easily checked that only the doublet components contribute to $m^{(n)}_{p\rho}$. The $M = -1/2$ and $M = 1/2$ components couple exclusively to $m^{(n)}_{p\alpha}$ and $m^{(n)}_{p\beta}$, respectively, and give equal contributions

$$m^{(n)}_p = \sum_{j,k\le l,s} U^{*}_{p,jkl(s)} Y^{(n)}_{jkl(s)}, \tag{A.9}$$

where (case I)

$$U^{\mathrm{I}}_{p,jkl(1)} = \frac{1}{\sqrt{2}}\left\{ V_{pj\{kl\}} - \tfrac{1}{2}\sum_{u,v}\frac{V_{kl\{uv\}}V^{*}_{pj\{uv\}}}{\epsilon_k + \epsilon_l - \epsilon_u - \epsilon_v} n_u n_v \right.$$
$$\left. + \left(\sum_{r,v} \frac{V_{kr\{vj\}}V^{*}_{pr\{vl\}} - 3V_{krjv}V^{*}_{prlv}}{\epsilon_k + \epsilon_r - \epsilon_v - \epsilon_j} \bar{n}_r n_v \right) + (k \leftrightarrow l) \right\},$$

$$U^{\mathrm{I}}_{p,jkl(2)} = \sqrt{\tfrac{3}{2}}\left\{ V_{pj[kl]} - \sum_{u<v}\frac{V_{kl[uv]}V^{*}_{pj[uv]}}{\epsilon_k + \epsilon_l - \epsilon_u - \epsilon_v} n_u n_v \right.$$
$$\left. + \left(\sum_{r,v} \frac{V_{kr\{vj\}}V^{*}_{pr\{vl\}} + V_{krjv}V^{*}_{prlv}}{\epsilon_k + \epsilon_r - \epsilon_v - \epsilon_j} \bar{n}_r n_v \right) - (k \leftrightarrow l) \right\}, \tag{A.10}$$

$$U^{\mathrm{I}}_{p,jkk(1)} = V_{pjkk} - \tfrac{1}{2}\sum_{u,v}\frac{V_{kkuv}V_{pj\{uv\}}}{2\epsilon_k - \epsilon_u - \epsilon_v} n_u n_v + \sum_{r,v}\frac{V_{kr\{vj\}}V^{*}_{pr\{vk\}} - 3V_{krjv}V^{*}_{prkv}}{\epsilon_k + \epsilon_r - \epsilon_v - \epsilon_j}\bar{n}_r n_v.$$

Here $V_{ij\{kl\}} = V_{ijkl} + V_{ijlk}$. The spin-free effective coupling amplitudes $U^{\mathrm{I}}_{p,jkl(s)}$ in eq. (A.10) are of the form

$$U^{\mathrm{I}}_{p,jkl(s)} = U^{(1)}_{p,jkl(s)} + U^{(2)}_{p,jkl(s)}, \tag{A.11}$$

where the superscripts (1) and (2) denote the first- and second-order contributions. A formally similar expression is obtained in the case II

$$U^{\mathrm{II}}_{p,jkl(s)} = U^{(1)}_{p,jkl(s)} - \bar{U}^{(2)}_{p,jkl(s)}. \tag{A.12}$$

Here $\bar{U}^{(2)}_{p,jkl(s)}$ results from the expression for $U^{(2)}_{p,jkl(s)}$ by exchanging the occupation numbers of the summation indices according to $n_i \leftrightarrow \bar{n}_i$:

$$\bar{U}^{(2)}_{p,jkl(s)} = U^{(2)}_{p,jkl}(n_i \leftrightarrow \bar{n}_i). \tag{A.13}$$

Finally, we consider the static self-energy part $\boldsymbol{\Sigma}(\infty)$ (eq. (2.26)). Obviously, $\boldsymbol{\Sigma}(\infty)$ exhibits the symmetry properties of the one-particle Green's function, that is

$$G_{p\alpha,q\alpha} = G_{p\beta,q\beta}, \quad G_{p\alpha,q\beta} = 0. \tag{A.14}$$

Using this property one arrives at the spin-free formulation of eq. (2.26) and (2.27)

$$\Sigma_{pq}(\infty) = \sum_{k,l} (2V_{pkql} - V_{pklq}) \Big(-\delta_{kl} + \sum_{n \in (N-1)} x^{(n)}_l x^{(n)}_k \Big). \tag{A.15}$$

Here, $x^{(n)}_l$ denotes the amplitudes of the spin-free Green's function. The summation over n in eq. (A.15) comprises all $N-1$ particle states. The HF expression (2.19) has been introduced in eq. (A.15).

Appendix B. A linear equation for the static self-energy part

For a given dynamic self-energy part

$$M_{lk}(\omega) = \sum_{n \in \mathrm{I}} \frac{m^{(n)}_l m^{(n)*}_k}{\omega - \omega_n + \mathrm{i}\eta} + \sum_{n \in \mathrm{II}} \frac{m^{(n)}_l m^{(n)*}_k}{\omega - \omega_n - \mathrm{i}\eta}, \tag{B.1}$$

the counter integration in eq. (2.30) can be readily performed yielding

$$\Sigma_{pq}(\infty) = \sum_{k,l} V_{pk\{ql\}} \left(\frac{\bar{n}_l n_k}{\epsilon_k - \epsilon_l} + \frac{n_l \bar{n}_k}{\epsilon_l - \epsilon_k} \right) \Sigma_{lk}(\infty) + B_{pq}, \tag{B.2a}$$

where the inhomogeneity B_{pq} is given by

$$B_{pq} = \sum_{k,l} V_{pk[ql]} \sum_{n\in \mathrm{I}} m_l^{(n)} m_k^{(n)*} \Bigg\{ - \frac{n_l n_k}{(\omega_n - \epsilon_k)(\omega_n - \epsilon_l)} + \frac{\bar{n}_l n_k}{(\epsilon_k - \epsilon_l)(\epsilon_k - \omega_n)} + \frac{n_l \bar{n}_k}{(\epsilon_l - \epsilon_k)(\epsilon_l - \omega_n)} \Bigg\} + \sum_{k,l} V_{pk[ql]} \sum_{n\in \mathrm{II}} m_l^{(n)} m_k^{(n)*} \Bigg\{ \frac{\bar{n}_l \bar{n}_k}{(\omega_n - \epsilon_k)(\omega_n - \epsilon_l)} - \frac{\bar{n}_l n_k}{(\epsilon_l - \epsilon_k)(\epsilon_l - \omega_n)} - \frac{n_l \bar{n}_k}{(\epsilon_k - \epsilon_l)(\epsilon_k - \omega_n)} \Bigg\}. \tag{B.2b}$$

For real one-particle states (which in general are used) $\Sigma(\infty)$ is symmetric and the set of linear equations (3.2) may be restricted to $p \le q$. Introducing in addition the spin-free formulation one obtains in matrix notation

$$\tilde{\boldsymbol{\Sigma}}(\infty) = \mathbf{B} + \mathbf{A}\tilde{\boldsymbol{\Sigma}}(\infty), \tag{B.3}$$

where $\tilde{\boldsymbol{\Sigma}}(\infty)$ denotes the vector with components $\Sigma_{p\alpha,q\alpha}(\infty)$ with $p \le q$. $\mathbf{B}$ denotes the vector with components $B_{p\alpha,q\alpha}(p \le q)$ and $\mathbf{A}$ is defined by

$$A_{pq,kl} = \left\{ 2\left(V_{pkql} + V_{plqk}\right) - \left(V_{pklq} + V_{plkq}\right) \right\} \frac{\bar{n}_l n_k}{\epsilon_k - \epsilon_l}, \quad p \le q, k \le l. \tag{B.4}$$

Obviously, the matrix $\mathbf{A}$ is of the form

$$\mathbf{A} = \begin{pmatrix} \mathbf{A}_{11} & \mathbf{0} \\ \mathbf{A}_{21} & \mathbf{0} \end{pmatrix}. \tag{B.5}$$

where 1 stands for p–h index pairs and 2 for pp- or hh-pairs.

The solution of eq. (B.3)

$$\tilde{\boldsymbol{\Sigma}}(\infty) = (\mathbf{1} - \mathbf{A})^{-1}\mathbf{B}, \tag{B.6}$$

thus can be expressed as

$$(\mathbf{1} - \mathbf{A})^{-1} = \begin{pmatrix} (\mathbf{1} - \mathbf{A}_{11})^{-1} & \mathbf{0} \\ \mathbf{A}_{21}(\mathbf{1} - \mathbf{A}_{11})^{-1} & \mathbf{1} \end{pmatrix} \tag{B.7}$$

by the inverse $(\mathbf{1} - \mathbf{A}_{11})^{-1}$ in the (small) ph-space.

Appendix C. Formulae for the OVGF method including terms up to third order

Notation: i, j, k, l denote occupied orbitals,
a, b, c, d denote virtual orbitals,
p, q, r, s denote orbitals with unspecified occupancy,

$$V_{pqrs} = \iint \varphi_p^*(1)\varphi_q^*(2)\frac{1}{r_{12}}\varphi_r(1)\varphi_s(2)\mathrm{d}\tau_1\mathrm{d}\tau_2,$$

$V_{pqrs} = [pr \mid qs]$ (charge density notation for integrals).

$$\Sigma_{pq}(\omega) = \Sigma_{pq}^{(2)}(\omega) + \Sigma_{pq}^{(3)}(\omega), \tag{C.1}$$

$$\Sigma_{pq}^{(2)}(\omega) = B1_{pq}(\omega) + B2_{pq}(\omega), \tag{C.2}$$

$$B1_{pq}(\omega) = \sum_a \sum_{i,j} \frac{(2V_{paij} - V_{paji})V_{qaij}}{\omega + \epsilon_a - \epsilon_i - \epsilon_j}, \tag{C.3}$$

$$B2_{pq}(\omega) = \sum_{a,b} \sum_i \frac{(2V_{piab} - V_{piba})V_{qiab}}{\omega + \epsilon_i - \epsilon_a - \epsilon_b}, \tag{C.4}$$

$$\Sigma_{pq}^{(3)}(\omega) = \sum_{I=1}^{6} \left(AI_{pq} + CI_{pq}(\omega) + DI_{pq}(\omega) \right), \tag{C.5}$$

$$A1_{pq} = -\sum_{a,b} \sum_{i,j,k} \frac{(2V_{pkqj} - V_{pkjq})(2V_{jiab} - V_{jiba})V_{abki}}{(\epsilon_j + \epsilon_i - \epsilon_a - \epsilon_b)(\epsilon_k + \epsilon_i - \epsilon_a - \epsilon_b)}, \tag{C.6}$$

$$A2_{pq} = \sum_{a,b,c} \sum_{i,j} \frac{(2V_{pcqb} - V_{pcbq})(2V_{jiab} - V_{jiba})V_{ijca}}{(\epsilon_j + \epsilon_i - \epsilon_a - \epsilon_b)(\epsilon_j + \epsilon_i - \epsilon_a - \epsilon_c)}, \tag{C.7}$$

$$A3_{pq} = \sum_{a,b,c} \sum_{i,j} \frac{(2V_{pcqj} - V_{pcjq})(2V_{jiab} - V_{jiba})V_{abci}}{(\epsilon_j + \epsilon_i - \epsilon_a - \epsilon_b)(\epsilon_j - \epsilon_c)}, \tag{C.8}$$

$$A4_{pq} = \sum_{a,b,c} \sum_{i,j} \frac{(2V_{pjqc} - V_{pjcq})(2V_{jiab} - V_{jiba})V_{abci}}{(\epsilon_j + \epsilon_i - \epsilon_a - \epsilon_b)(\epsilon_j - \epsilon_c)}, \tag{C.9}$$

$$A5_{pq} = -\sum_{a,b} \sum_{i,j,k} \frac{(2V_{pbqk} - V_{pbkq})(2V_{jiab} - V_{jiba})V_{ijka}}{(\epsilon_j + \epsilon_i - \epsilon_a - \epsilon_b)(\epsilon_k - \epsilon_b)}, \tag{C.10}$$

$$A6_{pq} = -\sum_{a,b} \sum_{i,j,k} \frac{(2V_{pkqb} - V_{pkbq})(2V_{jiab} - V_{jiba})V_{ijka}}{(\epsilon_j + \epsilon_i - \epsilon_a - \epsilon_b)(\epsilon_k - \epsilon_b)}, \tag{C.11}$$

$$C1_{pq}(\omega) = \sum_{a,b,c,d} \sum_{i} \frac{(2V_{piab} - V_{piba})V_{abcd}V_{qicd}}{(\omega + \epsilon_i - \epsilon_a - \epsilon_b)(\omega + \epsilon_i - \epsilon_c - \epsilon_d)}, \tag{C.12}$$

$$C2_{pq}(\omega) = \sum_{a,b} \sum_{i,j,k} \frac{(2V_{piab} - V_{piba})V_{abjk}V_{qijk}}{(\omega + \epsilon_i - \epsilon_a - \epsilon_b)(\epsilon_j + \epsilon_k - \epsilon_a - \epsilon_b)}, \tag{C.13}$$

$$C3_{pq}(\omega) = \sum_{a,b} \sum_{i,j,k} \frac{(2V_{pijk} - V_{pikj})V_{abjk}V_{qiab}}{(\omega + \epsilon_i - \epsilon_a - \epsilon_b)(\epsilon_j + \epsilon_k - \epsilon_a - \epsilon_b)}, \tag{C.14}$$

$$C4_{pq}(\omega) = \sum_{a,b,c} \sum_{i,j} \frac{(2V_{paij} - V_{paji})V_{ijbc}V_{qabc}}{(\omega + \epsilon_a - \epsilon_i - \epsilon_j)(\epsilon_i + \epsilon_j - \epsilon_b - \epsilon_c)}, \tag{C.15}$$

$$C5_{pq}(\omega) = \sum_{a,b,c} \sum_{i,j} \frac{(2V_{pabc} - V_{pacb})V_{ijbc}V_{qaij}}{(\omega + \epsilon_a - \epsilon_i - \epsilon_j)(\epsilon_i + \epsilon_j - \epsilon_b - \epsilon_c)}, \tag{C.16}$$

$$C6_{pq}(\omega) = \sum_{a} \sum_{i,j,k,l} \frac{(2V_{pakl} - V_{palk})V_{klij}V_{qaij}}{(\omega + \epsilon_a - \epsilon_i - \epsilon_j)(\omega + \epsilon_a - \epsilon_k - \epsilon_l)}, \tag{C.17}$$

$$D1_{pq}(\omega) = \sum_{a,b,c} \sum_{i,j} \left\{ \frac{V_{piab}\left[V_{ajic}(V_{qjcb} - 2V_{qjbc}) + V_{ajci}(V_{qjbc} - 2V_{qjcb})\right]}{(\omega + \epsilon_i - \epsilon_a - \epsilon_b)(\omega + \epsilon_j - \epsilon_b - \epsilon_c)} \right.$$
$$\left. + \frac{V_{piba}\left[V_{ajic}(4V_{qjbc} - 2V_{qjcb}) + V_{ajci}(V_{qjcb} - 2V_{qjbc})\right]}{(\omega + \epsilon_i - \epsilon_a - \epsilon_b)(\omega + \epsilon_j - \epsilon_b - \epsilon_c)} \right\}, \tag{C.18}$$

$$D2_{pq}(\omega) = \sum_{a,b,c} \sum_{i,j} \left\{ \frac{V_{pica}\left[V_{abij}(4V_{qbcj} - 2V_{qbjc}) + V_{abji}(V_{qbjc} - 2V_{qbcj})\right]}{(\omega + \epsilon_i - \epsilon_a - \epsilon_c)(\epsilon_i + \epsilon_j - \epsilon_a - \epsilon_b)} \right.$$
$$\left. + \frac{V_{piac}\left[V_{abij}(V_{qbjc} - 2V_{qbcj}) + V_{abji}(V_{qbcj} - 2V_{qbjc})\right]}{(\omega + \epsilon_i - \epsilon_a - \epsilon_c)(\epsilon_i + \epsilon_j - \epsilon_a - \epsilon_b)} \right\}, \tag{C.19}$$

$$D3_{pq}(\omega) = \sum_{a,b,c} \sum_{i,j} \left\{ \frac{V_{pcja}\left[V_{jicb}(V_{qiba} - 2V_{qiab}) + V_{jibc}(V_{qiab} - 2V_{qiba})\right]}{(\omega + \epsilon_i - \epsilon_a - \epsilon_b)(\epsilon_j + \epsilon_i - \epsilon_b - \epsilon_c)} \right.$$
$$\left. + \frac{V_{pcaj}\left[V_{jicb}(4V_{qiab} - 2V_{qiba}) + V_{jibc}(V_{qiba} - 2V_{qiab})\right]}{(\omega + \epsilon_i - \epsilon_a - \epsilon_b)(\epsilon_j + \epsilon_i - \epsilon_b - \epsilon_c)} \right\}, \tag{C.20}$$

$$D4_{pq}(\omega) = \sum_{a,b} \sum_{i,j,k} \left\{ \frac{V_{pakj}\left[V_{jiab}(4V_{qikb} - 2V_{qibk}) + V_{jiba}(V_{qibk} - 2V_{qikb})\right]}{(\omega + \epsilon_a - \epsilon_j - \epsilon_k)(\epsilon_i + \epsilon_j - \epsilon_a - \epsilon_b)} \right.$$

$$+\frac{V_{pajk}\left[V_{jiab}\left(V_{qibk}-2V_{qikb}\right)+V_{jiba}\left(V_{qikb}-2V_{qibk}\right)\right]}{(\omega+\epsilon_a-\epsilon_j-\epsilon_k)(\epsilon_i+\epsilon_j-\epsilon_a-\epsilon_b)}\Bigg\}, \tag{C.21}$$

$$D5_{pq}(\omega)=\sum_{a,b}\sum_{i,j,k}\left\{\frac{V_{pibk}\left[V_{jiab}\left(V_{qajk}-2V_{qakj}\right)+V_{jiba}\left(V_{qakj}-2V_{qajk}\right)\right]}{(\omega+\epsilon_a-\epsilon_j-\epsilon_k)(\epsilon_i+\epsilon_j-\epsilon_a-\epsilon_b)}\right.$$

$$+\frac{V_{pikb}\left[V_{jiab}\left(4V_{qakj}-2V_{qajk}\right)+V_{jiba}\left(V_{qajk}-2V_{qakj}\right)\right]}{(\omega+\epsilon_a-\epsilon_j-\epsilon_k)(\epsilon_i+\epsilon_j-\epsilon_a-\epsilon_b)}\Bigg\}, \tag{C.22}$$

$$D6_{pq}(\omega)=-\sum_{a,b}\sum_{i,j,k}\left\{\frac{V_{paki}\left[V_{ibaj}\left(4V_{qbkj}-2V_{qbjk}\right)+V_{ibja}\left(V_{qbjk}-2V_{qbkj}\right)\right]}{(\omega+\epsilon_a-\epsilon_i-\epsilon_k)(\omega+\epsilon_b-\epsilon_j-\epsilon_k)}\right.$$

$$+\frac{V_{paik}\left[V_{ibaj}\left(V_{qbjk}-2V_{qbkj}\right)+V_{ibja}\left(V_{qbkj}-2V_{qbjk}\right)\right]}{(\omega+\epsilon_a-\epsilon_i-\epsilon_k)(\omega+\epsilon_b-\epsilon_j-\epsilon_k)}\Bigg\}. \tag{C.23}$$

For $p=q$ the following equalities hold

$$A3=A4;\ A5=A6;\quad C2=C3;\ C4=C5;\quad D2=D3;\ D4=D5. \tag{C.24}$$

Formulae for the renormalization

a)
Geometric parameter

$$A=-(C2+C3+C4+C5+D2+D3+D4+D5)/\Sigma^{(2)} \tag{C.25}$$

(eq. 4.56 of ref. [6] and eq. (2.56) of the text).
Effective self-energy

$$\Sigma^{\text{eff}}=\Sigma^{(2)}+(1+A)^{-1}\Sigma^{(3)} \tag{C.26}$$

(eq. 4.56 of ref. [6] and eq. (2.57) of the text).

b)
Geometric parameters (see difussion following eq. (2.57))

$$G1=-(C4+C5+D4+D5)/B1 \tag{C.27}$$

(eq. 17 of ref. [17], eq. 4.60b of ref. [6]);

$$G2=-(C2+C3+D2+D3)/B2 \tag{C.28}$$

(eq. 20 of ref. [17], eq. 4.60b of ref. [6]).
Effective self-energy

$$\Sigma^{\mathrm{eff}} = \Sigma^{(2)} + (1 + G1)^{-1}(C4 + C5 + C6 + D4 + D5 + D6)$$
$$+ (1 + G2)^{-1}(C1 + C2 + C3 + D1 + D2 + D3) + \sum_{I=1}^{6} AI \qquad \text{(C.29)}$$

(eq. 21 of ref. [17]).

c)
Geometric parameter

$$A = \frac{[G1(C4 + C5 + C6 + D4 + D5 + D6) + G2(C1 + C2 + C3 + D1 + D2 + D3)]}{\sum_{I=1}^{6} (CI + DI)} \qquad \text{(C.30)}$$

(eq. 4.60a of ref. [6]) with G1 und G2 from eqs. (C.27) and C.28).
Effective self-energy

$$\Sigma^{\mathrm{eff}} = \Sigma^{(2)} + (1 + A)^{-1}\Sigma^{(3)}. \qquad \text{(C.31)}$$

References

[1] A.A. Abrikosov, L.P. Gorkov and I.E. Dzyaloshinski, Methods of Quantum Field Theory in Statistical Physics (Prentice-Hall, Englewood Cliffs, NJ, 1963).
[2] A.B. Migdal, Theory of Finite Fermi Systems (Wiley–Interscience, New York, 1967).
[3] R.D. Mattuck, A. Guide to Feynman Diagrams in the Many-Body Problem (McGraw-Hill, New York, 1967).
[4] A.L. Fetter and I.D. Walecka, Quantum Theory of Many-Particle Systems (McGraw-Hill, New York, 1971).
[5] G. Csanak, H.S. Taylor and R. Yaris, in: Advances in Atomic and Molecular Physics, vol. 7, eds. D.R. Bates and I. Esterman (Academic Press, New York, 1971).
[6] L.S. Cederbaum and W. Domcke, in: Advances in Chemical Physics, vol.36, eds. I. Prigogine and S.A. Rice (Wiley, New York, 1977) p. 205.
[7] M.F. Herman, K.F. Freed and D.L. Yeager, in: Advances in Chemical Physics, vol. 48, eds. I. Prigogine and S.A. Rice (Wiley, New York, 1981) p. 1.
[8] Y. Öhrn and G. Born, in: Advances in Quantum Chemistry, vol. 13, ed. P.O. Löwdin (Academic Press, New York, 1981) p. 1.
[9] D.J. Rowe, Rev. Mod. Phys. 40 (1968) 153.
[10] T. Shibuya and V. McKoy, Phys. Rev. A2 (1970) 2208.
[11] J. Simons and W.D. Smith, J. Chem. Phys. 58 (173) 4899.
[12] G.D. Purvis and Y. Öhrn, Chem. Phys. Lett. 33 (1975) 396.
[13] P. Jörgensen and J. Simons, J. Chem. Phys. 63 (1975) 5302.
[14] M.F. Hermann, D.L. Yeager and K.F. Freed, Chem. Phys. 29 (1978) 77.
[15] B.T. Pickup and O. Goscinski, Mol. Phys. 26 (1973) 1013.
[16] G.D. Purvis and Y. Öhrn, J. Chem. Phys. 60 (1974) 4063.

[17] L.S. Cederbaum, J. Phys. B 8 (1975) 290.
[18] O. Walter and J. Schirmer, J. Phys. B 14 (1981) 3805.
[19] J. Schirmer, L.S. Cederbaum and O. Walter, Phys. Rev. A28 (1983) 1237.
[20] J. Schirmer and L.S. Cederbaum, J. Phys. B 11 (1978) 1889.
[21] J. Schirmer, Phys. Rev. A26 (1982) 2395.
[22] J.D. Doll and W.P. Reinhardt, J. Chem. Phys. 57 (1972) 1169.
[23] P.W. Langhoff and A.J. Hernandez, Chem. Phys. Lett. 49 (1977) 361.
[24] P.W. Langhoff, S.R. Langhoff, T.N. Rescigno, J. Schirmer, L.S. Cederbaum, W. Domcke and W. von Niessen, Chem. Phys. 58 (1981) 71.
[25] S. Ethofer and P. Schuck, Z. Phys. 228 (1969) 264.
[26] J. Winter, Nucl. Phys. A 194 (1972) 535.
[27] L.S. Cederbaum, Theor. Chim. Acta 31 (1973) 239.
[28] W. von Niessen, G.H.F. Diercksen and L.S. Cederbaum, J. Chem. Phys. 67 (1977) 4124, and references therein.
[29] L. Åsbrink, W. von Niessen and G. Bieri, J. Electron Spectr. 21 (1980) 93.
W. von Niessen, G. Bieri and L. Åsbrink, ibid. 21 (1980) 175.
G. Bieri, L. Åsbrink and W. von Niessen, ibid. 23 (1981) 281.
L. Åsbrink, A. Svensson, W. von Niessen and G. Bieri, ibid. 24 (1981) 293.
W. von Niessen, L. Åsbrink, G. Bieri and A. Svensson, ibid. 26 (1982) 173.
G. Bieri, L. Åsbrink and W. von Niessen, ibid. 27 (1982) 129.
W. von Niessen, L.S. Cederbaum, J. Schirmer, G.H.F. Diercksen and W.P. Kraemer, ibid. 28 (1982) 45.
[30] G.H.F. Diercksen and W.P. Kraemer, MUNICH, Molecular Program System, Reference Manual, Special Technical Report, Max Planck Institut für Physik und Astrophysik, Munich, to be published.
G.H.F. Diercksen, Theoret. Chim. Acta 33 (1974) 1.
[31] D.M. Silver, Comput. Phys. Commun. 14 (1978) 71, 81.
S. Wilson, ibid. 14 (1978) 91.
[32] G.H.F. Diercksen, private communication.
[33] M. Yoshimine, IBM Corp. Technical Report RJ 555 (1969), San Jose.
G.H.F. Diercksen, Theoret. Chim. Acta 33 (1974) 1.
[34] G.H.F. Diercksen, N.E. Grüner and J. Oddershede, Comput. Phys. Commun. 30 (1983) 349.
[35] J. Oddershede, Advan. Quantum Chem. 11 (1978) 275.
[36] G.H.F. Diercksen and W. von Niessen, in preparation.
[37] O. Walter, L.S. Cederbaum and J. Schirmer, J. Math. Phys. to be published.
O. Walter, Thesis, University of Heidelberg (1983).
[38] E.R. Davidson, J. Comput. Phys. 17 (1975) 87.
[39] J. Schirmer, L.S. Cederbaum, W. Domcke and W. von Niessen, Chem. Phys. 26 (1977) 149.
[40] L.S. Cederbaum, J. Schirmer, W. Domcke and W. von Niessen, Intern. J. Quantum Chem. 14 (1978) 593.
[41] L.S. Cederbaum, W. Domcke, J. Schirmer, W. von Niessen, G.H.F. Diercksen and W.P. Kraemer, J. Chem. Phys. 69 (1978) 1591.
[42] J. Baker and B.T. Pickup, Mol. Phys. 49 (1983) 651.
J. Baker, Chem. Phys. Lett. 101 (1983) 136.
[43] E.A. Nylleraas and B. Undheim. Z. Phys. 65 (1930) 759.
[44] P.Ö. Löwdin, J. Mol. Spectr. 10 (1963) 12.
[45] E.U. Condon and G.H. Shortley, The Theory of Atomic Spectra (Cambridge Univ. Press, Cambridge, 1967) section II, p. 11.
[46] F.B. Hildebrand, Introduction to Numerical Analysis (McGraw-Hill, New York, 1974).
[47] I. Cacelli, R. Moccia and V. Carravetta, Chem. Phys. Lett. 70 (1979) 569.
[48] M. Jaszunski, B.T. Pickup and R. McWeeny, Chem. Phys. Lett. 90 (1982) 167.
[49] O. Walter, W. von Niessen, J. Schirmer and L.S. Cederbaum, unpublished results.
O. Walter, Thesis, Heidelberg (1983).
[50] M. Berman and U. Kaldor, J. Phys. B 14 (1981) 3993.
[51] A. Klonover and U. Kaldor, J. Phys. B 12 (1979) 3797.
[52] M. Berman, O. Walter and L.S. Cederbaum, Phys. Rev. Lett. 50 (1983) 1979.

[53] M.C. Böhm and R. Gleiter, Theoret. Chim. Acta 57 (1980) 315; Chem. Phys. 64 (1982) 183.
[54] M.C. Böhm, Z. Naturforsch. 37a (1982) 1193; Ber. Bunsenges. Phys. Chem. 86 (1982) 56.
[55] S. Krummacher, V. Schmidt and F. Wuilleumier, J. Phys. B 13 (1980) 3993.
S. Krummacher, V. Schmidt, F. Wuillemier, J.M. Bizau and D. Ederer, ibid. 16 (1983) 1733.
[56] K. Siegbahn, C. Nordling, G. Johansson, J. Hedman, P.F. Hedén, K. Hamrin, U. Gelius, T. Bergmark, L.O. Werme, R. Manne and Y. Baer, ESCA Applied to Free Molecules (North-Holland, Amsterdam, 1971).
[57] J.L. Gardner and J.A.R. Samson, J. Electron Spectr. 2 (1973) 259, 8 (1976) 35; J. Chem. Phys. 62 (1975) 1447.
[58] U. Gelius, E. Basilier, S. Svensson, T. Bergmark and K. Siegbahn, J. Electron Spectr. 2 (1974) 405.
[59] A.W. Potts and T.A. Williams, J. Electron Spectr. 3 (1974) 3.
[60] M.S. Banna and D.A. Shirley, J. Electron Spectr. 8 (1976) 255.
[61] L. Åsbrink and C. Fridh, Phys. Scripta 9 (1974) 338.
L. Åsbrink, C. Fridh, E. Lindholm and C. Codling, ibid. 10 (1974) 183.
[62] B. Nilsson, R. Nyholm, A. Berendtsson, J. Hedman and C. Nordling, J. Electron Spectr. 9 (1976) 337; Phys. Scripta 16 (1977) 383.
[63] P.S. Bagus and E.K. Viinikka, Phys. Rev. A5 (1977) 1486.
[64] See, for example, J. Schirmer, W. Domcke, L.S. Cederbaum and W. von Niessen, J. Phys. B11 (1978) 1901.
L.S. Cederbaum, W. Domcke, J. Schirmer, W. von Niessen, G.H.F. Diercksen and W.P. Kraemer, J. Chem. Phys. 69 (1978) 1591.
L.S. Cederbaum, J. Schirmer, W. Domcke and W. von Niessen, J. Phys. B10 (1977) L549.
R. Arneberg, J. Müller and R. Manne, Chem. Phys. 64 (1982) 249.
J. Müller, R. Arneberg, H. Ågren, R. Manne, P.A. Malmquist, S. Svensson and U. Gelius, J. Chem. Phys. 77 (1982) 4895.
[65] L.S. Cederbaum, W. Domcke, J. Schirmer and W. von Niessen, Phys. Scripta 21 (1980) 481.
[66] G. Wendin, in: Structure and Bonding, vol. 45, eds. M.J. Clark et al. (Springer, Berlin, 1981), and references therein.
[67] L.S. Cederbaum and W. von Niessen, J. Chem. Phys. 62 (1975) 3824.
[68] J. Schirmer and O. Walter, Chem. Phys. 78 (1983) 201.
[69] C. Salez and A. Veillard, Theoret. Chim. Acta 11 (1968) 441.
[70] M.F. Herman, D.L. Yeager, K.F. Freed and V. McKoy, Chem. Phys. Lett. 46 (1977) 1.
[71] S.K. Shih, W. Butscher, R.J. Buenker and S. Peyerimhoff, Chem. Phys. 29 (1978) 241.
[72] D.P. Chong and S.R. Langhoff, Chem. Phys. Lett. 59 (1978) 397.
[73] W.C. Ermler and A.D. McLean, J. Chem. Phys. 73 (1980) 2297.
[74] D.P. Chong and S.R. Langhoff, Chem. Phys. 67 (1982) 153.
[75] M.F. Herman, K.F. Freed and D.L. Yeager, Chem. Phys. 32 (1978) 437.
[76] J. Simons and W.D. Smith, J. Chem. Phys. 58 (1973) 4899.
P. Jörgensen and J. Simons, ibid. 63 (1975) 5302.
[77] G.B. Bacskay and N.S. Hush, Chem. Phys. 16 (1976) 219.
[78] J.C. Lorquet and M. Desouter, Chem. Phys. Lett. 16 (1972) 136.
[79] M. Okuda and N. Jonathan, J. Electron Spectr. 3 (1974) 19.
[80] E.W. Thulstrup and A. Andersen, J. Phys. B 8 (1975) 965.
[81] D.C. Cartwright and T.H. Dunning, J. Phys. B 8 (1975) L100.
[82] I.H. Hillier and J. Kendrick, J. Electron Spectr. 8 (1976) 239.
[83] N. Kosugi, H. Kuroda and S. Iwata, Chem. Phys. 39 (1979) 337.
[84] W. von Niessen, private communication.
[85] D.W. Turner, C. Baker, A.D. Baker and C.R. Brundle, Molecular Photoelectron Spectroscopy (Wiley-Interscience, New York, 1970).
[86] N.M. Hugenholtz, Physica 23 (1957) 481.
[87] B.N. Parlett, The Symmetric Eigenvalue Problem (Prentice Hall, Englewood Cliffs, 1980).
[88] E.R. Davidson, The World of Quantum Chemistry, Proc. First Intern. Congr. on Quantum Chem., eds. R. Daudel and B. Pullman (Reidel, Dordrecht, 1974).
[89] S.R. Langhoff and E.R. Davidson, Intern. J. Quantum Chem. 8 (1974) 61.
[90] E.R. Davidson and D.W. Silver, Chem. Phys. Lett. 52 (1977) 403.

[91] P.E.M. Siegbahn, Chem. Phys. Lett. 55 (1978) 386.
[92] A. Veillard, Theoret. Chim. Acta 12 (1968) 405.
[93] S. Huzinaga, J. Chem. Phys. 42 (1965) 1293.
[94] C. Fridh, L. Åsbrink, B.Ö. Jonsson and E. Lindholm, Intern. J. Mass. Spectrom. Ion Phys. 9 (1972) 485.
[95] R. Gleiter, E. Heilbronner and V. Hornung, Helv. Chim. Acta 55 (1970) 255.
[96] W. von Niessen, W.P. Kraemer and G.H.F. Diercksen, Chem. Phys. 41 (1979) 113.
[97] J. Almlöf, B. Roos, U. Wahlgren and H. Johansen, J. Electron Spectr. 2 (1973) 51.
[98] M.F. Guest, I.H. Hillier, A.A. McDowell and M. Berry, Mol. Phys. 41 (1980) 519.
[99] G. Jonkers, S.M. Van Der Kerk and C.A. De Lange, Chem. Phys. 70 (1982) 69.
[100] W. von Niessen and L.S. Cederbaum, Mol. Phys. 43 (1981) 897.
[101] G.W. Bogges, J.D. Allen, Jr. and G.K. Schweitzer, J. Electron Spectr. 2 (1973) 467.
[102] B.G. Cocksey, J.H.D. Eland and C.J. Danby, J. Chem. Soc. Faraday Trans. II 69 (1973) 1558.
[103] J. Berkowitz, J. Chem. Phys. 61 (1974) 407.
[104] A.F. Orchard and N.V. Richardson, J. Electron Spectr. 6 (1975) 61.
[105] G.M. Bancroft, D.J. Bristow and L.L. Coatsworth, Chem. Phys. Lett. 82 (1981) 344.
[106] S. Huzinaga, J. Chem. Phys. 66 (1977) 4245.
[107] A.J.H. Wachters, J. Chem. Phys. 52 (1970) 1033.
[108] P.J. Hay, J. Chem. Phys. 66 (1977) 4377.
[109] H. Hotop and W.C. Lineberger, J. Phys. Chem. Ref. Data 4 (1975) 539.
[110] J.L. Franklin and P.W. Harald, Annual Review of Physical Chemistry, Vol. 25, ed. H. Eyring (Palo Alto, CA, Annual Reviews).
[111] P.A. Schulz, R.D. Mead, P.L. Jones and W.C. Lineberger, J. Chem. Phys. 77 (1982) 1153.
[112] F. Sasaki and M. Yoshimine, Phys. Rev. A9 (1974) 17.
[113] M. Zeitz, S.D. Peyerimhoff and R.J. Buenker, Chem. Phys. Lett. 64 (1979) 243.
[114] J. Simons, Theor. Chem. Advan. Prosp. 3 (1978) 1.
[115] L.S. Cederbaum, W. Domcke and W. von Niessen, J. Phys. B 10 (1977) 2963.
[116] J.V. Ortiz B. and Y. Öhrn, J. Chem. Phys. 72 (1980) 5744.
[117] L.S. Cederbaum, K. Schönhammer and W. von Niessen, Phys. Rev. A15 (1977) 833.
[118] D. Feldmann, Z. Naturforsch. 25a (1970) 621.
[119] J.D. Carette and L. Kerwin, Can. J. Phys. 39 (1961) 1300.
[120] S.L. Bennell, J.L. Margrave and J.L. Franklin, J. Chem. Phys. 61 (1974) 1647.
[121] S.E. Novick, P.C. Engelking, P.L. Jones, J.H. Futrell and W.C. Lineberger, J. Chem. Phys. 70 (1979) 2652.
[122] R.J. Celotta, R.A. Bennett and J.L. Hall, J. Chem. Phys. 60 (1974) 1740.
[123] L.S. Cederbaum, W. Domcke and W. von Niessen, Mol. Phys. 33 (1977) 1399.
[124] See e.g. Y. Yoshioka and K.D. Jordan, Chem. Phys. 56 (1981) 303, and references contained therein.